Fluorescence microscopy for Cdc42 quantification in *Saccharomyces Cerevisiae*

Gregory van Beek

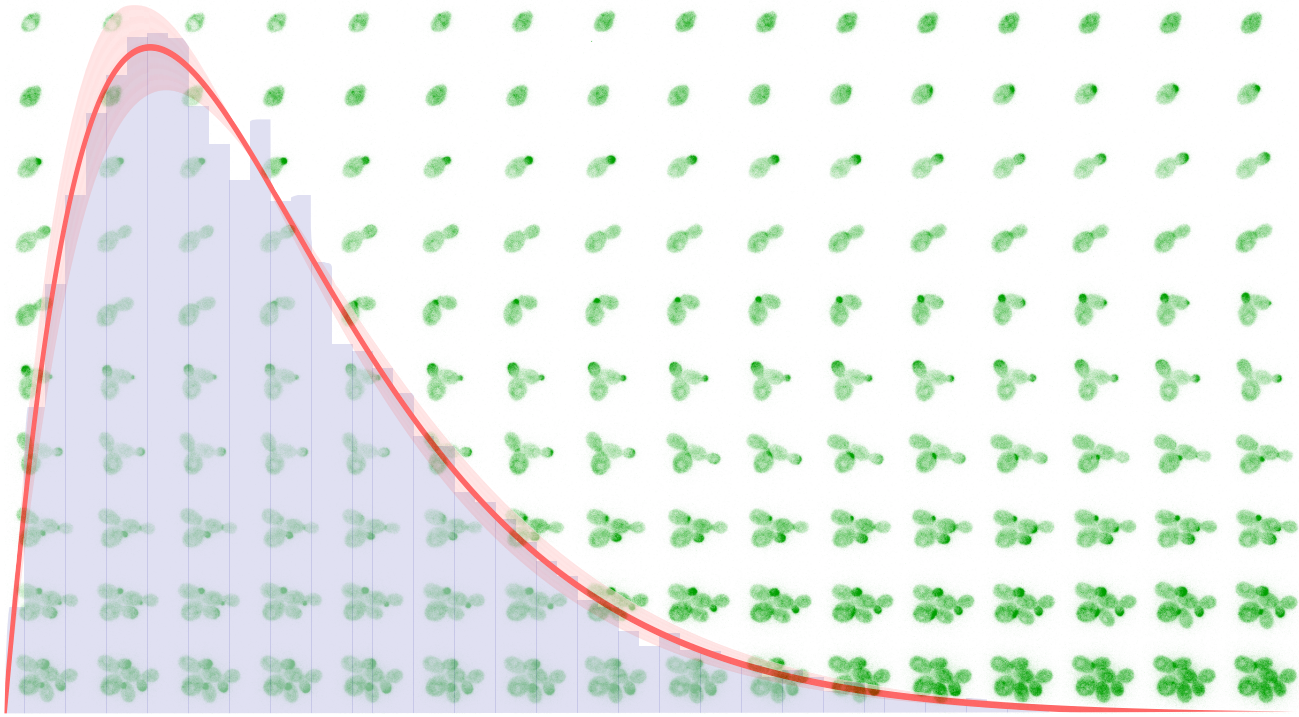

Fluorescence microscopy for Cdc42 quantification in *Saccharomyces Cerevisiae*

by

Gregory van Beek

In partial fullfillment of the requirements for the Degree of

Master of Science

in Biomedical Engineering

At the Delft University of Technology

To be defended on Friday November 15, 2019

Supervisor	Dr. Reza Ranjbar Choubeh
Thesis Committee	Dr. Ir. Liedewij Laan Dr. Reza Ranjbar Choubeh Prof. Dr. Bernd Rieger

Abstract

In budding yeast, a certain concentration of the GTPase Cdc42 is optimal for cell division. This optimal concentration depends on the phenotype and genetic background of the cells. Due to bet hedging, the Cdc42 concentration is different between cells in a population and it is expected that the concentration, measured for many cells, is gamma distributed. This study describes a method for determining the concentration of Cdc42 proteins depending on the phenotype of individual cells. Fluorescence microscopy images were analyzed using custom designed software for tracking single cells and detecting budding and polarization events, based on existing segmentation software. This allows for estimating the cell volume and determining the concentration distribution based on the fluorescence intensity. The estimated cell volume is larger than was expected which is proven to be caused by segmentation errors. The intensity is shown to scale linearly with the number of fluorescent sources and using this result, the distribution for the Cdc42 concentration and copy number can be determined. For calculating the absolute concentration and copy number values, a constant still needs to be determined. To assess the reliability of the obtained results, validation measurements should be performed, for example by using different galactose concentrations to control the Cdc42 production by means of a galactose promoter or by using different genetic backgrounds. Based on the results, this method shows a possible way of determining the budding and polarization events and measuring the protein concentration for individual cells.

Acknowledgements

My choice to do my graduation project at the Laan Lab was not a very obvious one given my background in Medical Physics. I knew close to nothing about biology and how to work with living cells. The only reason I am able to finish this graduation project is due to an incredible team where everyone was always eager to help out with any problems and questions that I had, how silly they might have been sometimes.

First of all, I want to express my sincere gratitude to Reza for his infinite patience and support throughout the project and his critical view on my work. I lost count on how many draft versions of my thesis I have sent, and each time I was increasingly amazed that you found the energy and the courage to read it again and to point out all the mistakes, vague sentences and spelling errors (and goodness knows how many are still left unnoticed). I also want to thank Liedewij for allowing me to do my graduation project in her group and inviting me to visit the Dutch BioPhysics conference to present my poster. Also, I want to thank Liedewij and Reza for the many ideas that we discussed during the meetings to get the most out of my project.

Before I started here, my experience in a biological laboratory was basically non-existent and many of the techniques required for my project I learned from Ramon. With his seemingly limitless knowledge about everything to do with biology, he has been an exceptionally valuable help. Also, many thanks go to Christine for her much needed help with the microscope and to Els and Enzo for their help with the BioTek. I want to thank Werner and Leila for their ideas and advice for my project and to Miranda for explaining the process of the constructing the strains that I used. Finally, I also want to thank Jeremie for showing me how to work with the microscope and to have enough trust in me to let me use it.

Of course, I am grateful to the whole team for the amazing time I had in the lab and also for the times outside the lab with the laboutings, dinners and the enormous quantity of cake and Cuban, Iranian, German and Portuguese sweets.

At last I want to thank my parents who have been an incredible support for me, not only during this project, but during my complete study. To remember me not to give up during times when I could not even hope to ever finish this study.

Contents

List of Figures

List of Tables

List of abbreviations

Abbreviation	
AD-test	Anderson-Darling test
Cdc	Cell Division Cycle
CDK	Cyclin-Dependent Kinase
ConA	Concanavalin A
CSM	Complete Supplement Mixture
GAP	GTPase-Activating Protein
GDI	GDP Dissociation Inhibitor
GEF	Guanine nucleotide Exchange Factor
GFP	Green Fluorescent Protein
Lat	Latrunculin
MAT	Mating Type
mNG	mNeonGreen
OD600	Optical Density at 600 nm wavelength
PAK	p21-Activated Kinase
qq-plot	Quantile-Quantile plot
SDM	Spinning Disc Microscope
SNR	Signal to Noise Ratio
Ura	Uracil
WT	Wild Type

Introduction

Cell division is crucial for reproduction and maintaining homeostasis in all Eukaryotes. It requires a large and complex network of proteins that have to localize (in a process called cell polarization) and interact properly at specific time points in the cell cycle. The Cell Division Cycle 42 protein, or Cdc42, is a highly conserved protein in most Eukaryotes that is regarded as one of the master controllers of cell polarization [Adams et al., 1990] [Chiou et al., 2017] [Martin, 2015]. In some mammals (including humans) it is thought that Cdc42 plays a role in certain diseases and the development of specific cancer types. Deregulation, depending on type of tissue either overexpression or inhibition, of Cdc42 has been shown to be one of the main causes for uncontrolled proliferation and increased survival rates of tumor cells [Vega and Ridley, 2008] and it is thought to play a role in the increased metabolism of tumor cells [Stengel and Zheng, 2011]. Cdc42 is also suspected to play a role in the aging of hematopoietic stem cells that are necessary for the development of blood- and certain immune cells. Elevated activity of Cdc42 might induce a faster aging of these stem cells which is related to a number of diseases in humans [Florian et al., 2012] [Yang et al., 2007] [Geiger and Zheng, 2013]. A study involving elderly people has been performed that shows a correlation between Cdc42 activity and general aging in humans [Kerber et al., 2009].

Cdc42 was first discovered in *Saccharomyces Cerevisiae* (budding yeast). The amino acid sequence of Cdc42 in *S. Cerevisiae* is about 80% identical with the Cdc42 ortholog in humans [Chiou et al., 2017]. Since *S. Cerevisiae* is a relative simple organism to study (it has a relatively short doubling time, its genetic manipulation is easy and some of the cellular processes are similar to those in humans), it is extensively used as a model organism for a variety of cellular studies [Munemitsu et al., 1990] [Johnson, 1999]. For these reasons, and because it is the first Eukaryote for which the entire genome was sequenced, budding yeast is widely used for cell polarization studies.

The cell cycle of *S. Cerevisiae* follows four major phases, as shown in figure 1. This shows the localization of Cdc42 (green) during the cell cycle and the orientation of the actin cables and patches (red). Apical growth means that the cell growth is primarily oriented towards the bud and isotropic growth is where the bud mainly grows in diameter until mitosis. After mitosis, both the mother and the daughter cell show a bud scar (magenta) at the site of division [Bi and Park, 2012]. A single location for the next cell division is determined at the end of the G1 phase and is mainly defined by eight landmark proteins. In haploid cells (cells with a single set of chromosomes), this single position for division is chosen next to the bud scar since the landmark proteins from the previous cell cycle are still present during the G1 phase near this area [Goryachev and Leda, 2017] [Moseley and Goode, 2006]. These landmark proteins are involved in a protein network that recruits Cdc42 towards the site of budding [Woods et al., 2016].

The doubling time of Wild Type (WT) *S. Cerevisiae* cells is about 80 to 90 minutes (although this can vary in different environments) [Moran et al., 2010]. The exact time depends partly on the genetic background of a cell as DNA mutations and/or deletions can alter the proteins and the protein production rate and hence alter the phenotype of the cell [Smith et al., 2013] [Yamamoto et al., 2010]. For example, a decrease in production rate of Cdc42 can result in a lowered concentration which increases the polarization and doubling times [de Bruin, unpublished results]. Besides genetics, also epigenetics plays a role in the phenotypic behavior of the cell [Gruenert and Cozens, 1991]. An epigenetic trait can be defined as "a stably heritable phenotype resulting from changes in a chromosome without alterations in the DNA sequence" [Berger et al., 2009]. For example, genetically identical cells can have different Cdc42 transcrip-

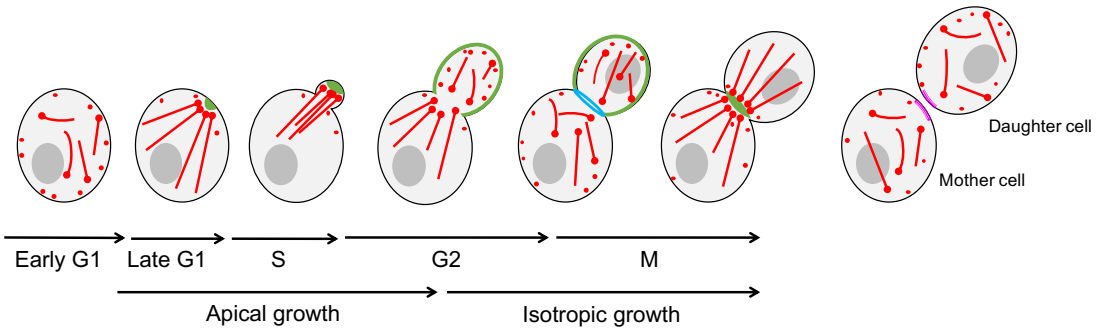

Figure 1: Cell cycle of *S. Cerevisiae*. Cdc42 is shown in green and the red lines and dots represent actin (cables as lines and patches as dots). In early M-phase, a contractile ring (shown in blue), constructed from actin-filaments and -myosin, forms that helps in cell division. This leaves a division scar in both the mother and the daughter cell, as is shown in magenta in the last figure. In late G1 phase, a Cdc42 patch occurs that orientates the actin cables and patches towards the future bud site. The cell growth is mainly in the direction of the bud. In G2 phase Cdc42 distributes itself over the surface of the bud to enhance isotropic growth [Pruyne and Bretscher, 2000]. In the beginning of the M phase, the actin cables and patches are disorientated and a ring forms that contracts to divide the cells after which it disassembles. After this disassembly of the ring, actin cables reorientate to help forming a new cell wall [Karpova et al., 1998][Bi and Park, 2012] [Howell and Lew, 2012][Chiou et al., 2017].

tion rates. Moreover, the daughter cells are likely to inherit the Cdc42 transcription rate of their mother cell and so the trait of having a certain transcription rate can be passed on to subsequent generations without genetic alterations. A change in a chromosome is caused by certain molecules that can modify the transcription and translation rate of genes. This requires non-coding RNA (ncRNA) or binding of certain molecules to histones or to some DNA nucleotides.

The phenotype of cells is determined by both genetic and epigenetic processes, but none of these processes are yet fully understood. Most proteins are involved in a highly interactive network. Changes in the epigenetics that influences the expression rate of a single gene or a mutation in the DNA coding for this gene can therefore have an influence not only on the protein the gene is coding for, but can influence a large part of the network where the protein is part of. Therefore, many studies are done towards better understanding the interaction of proteins. However, not many studies have been focussing on epigenetic processes in combination with different genetic backgrounds, especially not in combination with Cdc42 and polarization. Recently, a theoretical model showed that a population of cells can adapt their Cdc42 concentration to increase their fitness by using the stochastic behavior of protein production [Daalman, unpublished results]. It also shows that after only a few generations, the average protein concentration shifted towards an optimal concentration, indicating that the trait of a having a specific Cdc42 concentration that results in a high population fitness is inherited by the daughter cells. In only a few generations, genetic effects could not have a major effect on the protein concentration (genetic mutations typically need many generations to influence the phenotype), thus the shift in concentration is expected to be caused by epigenetics. Since this model is not yet experimentally confirmed, the main research question of this thesis is *how can the distribution of Cdc42 proteins in Saccharomyces Cerevisiae in different genetic backgrounds be experimentally determined?*

The first part of this thesis is a literature study which is mainly focused on the protein network for cell polarization in *S. Cerevisiae* and the influence of epigenetic interactions on this network. The second part focusses on the experimental validation of a technique for estimating the protein concentration in cells based on fluorescence imaging and custom made software to automatically determine relevant characteristics of the yeast cells.

Literature Review

Bud site selection and protein localization

Cdc42 is a highly conserved G-protein that belongs to the Rho family of GTPases. This is a group of enzymes that control cell polarization and polymerization of the actin cytoskeleton. GTPases can be catalyzed in a hydrolysis reaction in which the protein turns a bound GTP molecule into a GDP molecule by losing a phosphate group. Due to this hydrolysis reaction, the protein undergoes a conformational change that inactivates the protein. This is usually referred to as an on/off switch behavior of these proteins. Changing the state from inactive (GDP-bound) to active (GTP-bound) is regulated by Guanine nucleotide Exchange Factors (GEF). Hydrolysis of Cdc42-GTP is catalyzed by GTPase-Activating Proteins (GAP). Both states of Cdc42 are important for stable polarization and budding, but especially the GTP-bound Cdc42 is actively polarized by a network starting with the landmark proteins.

Cell polarization is important for bud emergence and for the development of daughter cells. Most of the processes and proteins involved in polarization are regulated by the effector proteins of Cdc42 (figure 2). Wherever a location with high concentration of Cdc42 is established (and maintained) is likely to become the site of cell division. This means that, during the cell cycle, an inhomogeneous distribution of proteins occurs that is polarized towards the division site. In wild type (WT) cells this location is not chosen randomly, but is determined by landmark proteins (figure 2).

There are eight known landmark proteins. Four of these landmark proteins are primarily for diploid cells. These cells have chromosomes from both mating types, denoted as MAT$\boldsymbol{a}/\alpha$. These cells bud in a bipolar manner which means that a bud can emerge in two distinct locations, typically denoted as proximal and distal. Proximal polarization is polarization near the bud scar and distal polarization is on the opposite site of the bud scar. The landmark proteins involved are Bud8 (which is primarily for distal polarization), Bud9 (primarily for proximal polarization) and Rax1 which requires Rax2 (the latter helps maintaining the bud site) [Bi and Park, 2012]. In the case of axial budding in haploid cells, a single site of polarization (typically the proximal site) is determined by the other four landmark proteins. These are Bud3 (which can also be a GEF for Cdc42 in early phase of G1 [Kang et al., 2014]) and Bud4 (which helps in organization of the septin ring [Sanders and Herskowitz, 1996]) which together interact to localize Axl1 and Axl2 [Kang et al., 2014]. Haploid cells have chromosomes from a single mating type and can therefore be either MAT$\boldsymbol{a}$ or MATα [Pillus and Rine, 1989]. The landmark proteins primarily accumulate at the bud neck of the mother cell and are distributed to both the mother and the daughter cell during cell division [Schenkman et al., 2002]. As a consequence, after cell division the landmark proteins still have a relative high concentration near the previous budding site. Since the mother cell typically polarize right after cell division, the next polarization usually occurs near the preceding division site [Tong et al., 2007]. Although the daughter cells typically need more time before their first cell division, they also show the next division site near their birth scar [Chant and Pringle, 1995] [Kozminski and Park, 2010] [Moran et al., 2019]. So, landmark proteins seem to play a role in determining both the number of budding sites and the polarization at these sites, but they do not arrange the actual localization of Cdc42. Instead, they rely on a network of other proteins that recruit Cdc42.

The landmark proteins localize the protein Bud5 (see figure 2). This is a GEF for the Ras-like GTPase Rsr1 and, like Cdc42, Rsr1 can switch between an active and inactive form. The active

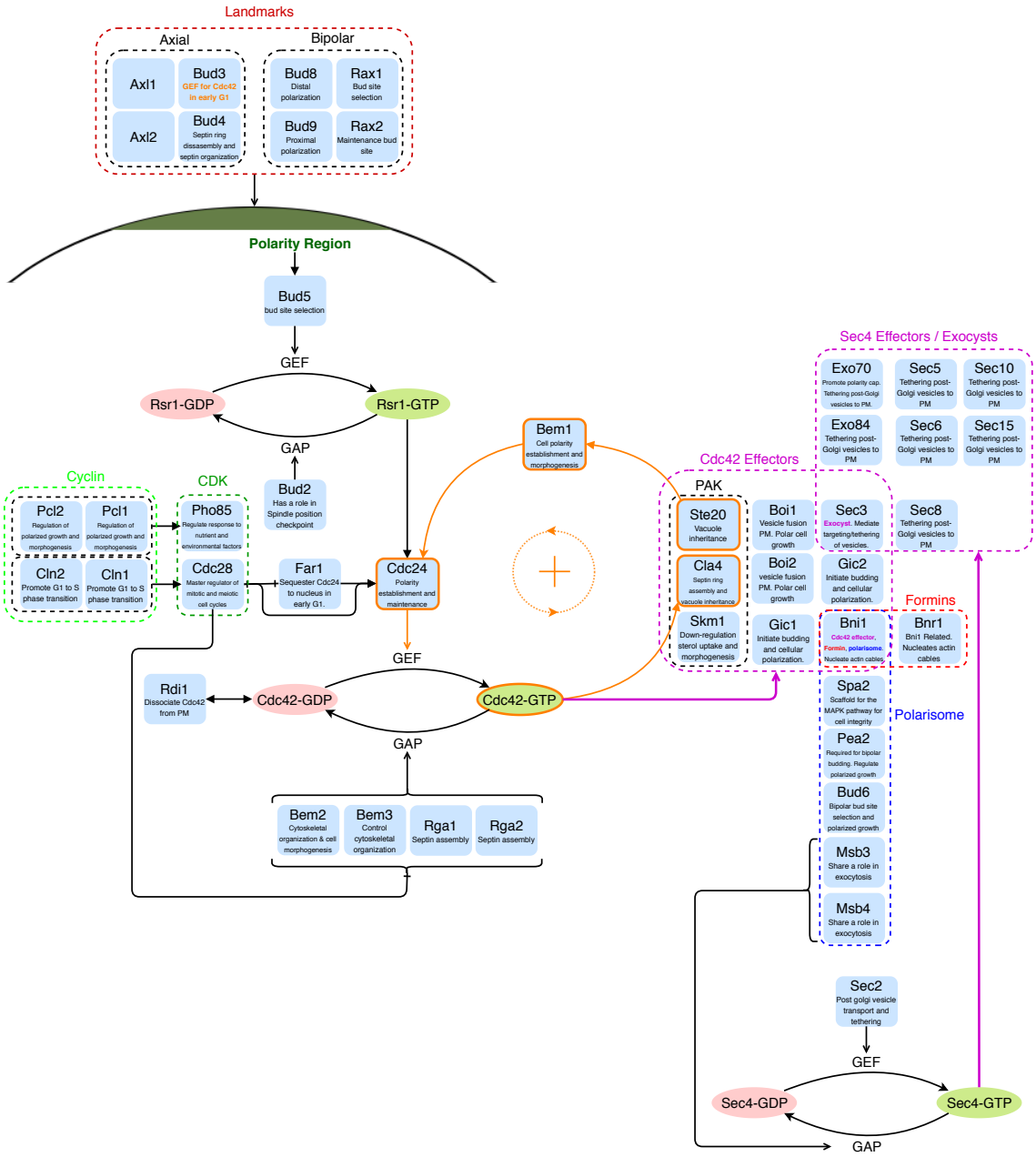

Figure 2: Overview of the most important proteins discussed. Most proteins have a brief description of some of their other functions. GTPases are drawn as ellipses. Proteins that belong to a certain group are nested by dashed lines. Proteins that are shown in orange belong to the PAK-Bem1-GEF positive feedback loop. The polarization pathway starts on the top left with the landmark proteins [Moran et al., 2019] [Bi and Park, 2012], [Howell and Lew, 2012], [Chiou et al., 2017].

Rsr1-GTP binds to Cdc24, which acts as a GEF for Cdc42. Deletion of Rsr1 and/or Bud5 results in division sites that are randomly chosen, most likely because Cdc42 does not have a link anymore with any of the landmark proteins in late G1 phase and onward. This random bud site localization is often referred to as symmetry breaking [Martin, 2015] [Wedlich-Soldner and Li, 2003]. One of the Cdc42 effector proteins, the PAK kinase Cla4, is required for polarization in Rsr1Δ cells as one study found that Cla4 is necessary for symmetry breaking [Kozubowski et al., 2008].

Cdc42 is thought to have a role in bud site selection as well since overexpression, by means of a galactose promoter, showed abnormalities in bud site selection, but this overexpression was not lethal to the cell [Johnson and Pringle, 1990]. This was later substantiated by other studies, for example by overexpressing Cdc42 by locking it in its GTP-bound state, which showed

random bud site selection as well [Howell and Lew, 2012]. However, they noticed that their Cdc42 overexpression is lethal. Another study, which describes a temperature sensitive *cdc42*-mutant, found that this mutant shows random polarization at the permissive temperature, leading the authors to conclude that Cdc42 is involved in bud site selection [Miller and Johnson, 1997]. At the restrictive temperature, these mutant cells do not bud as they show a phenotype that indicates a loss of Cdc42 function which resulted in large cells with no buds. Even though the proposed role of Cdc42 in bud site selection, its effect is not strong enough to prevent symmetry breaking in Rsr1Δ or Bud5Δ cells.

Cdc24 activates Cdc42 and is known to be involved in the PAK-Bem1-GEF positive feedback loop. Cdc24 and the landmark Bud3 are the only known GEF's for Cdc42 (see figure 2) [Kang et al., 2014]. Its deletion is lethal since Cdc24Δ cells are shown not to be able to form buds. Only hyperactivation of Cdc42 can rescue Cdc24Δ, apparently because the lack of the positive feedback loop is then compensated for [Caviston et al., 2002]. Hyperactivation of both Cdc24 and Cdc42 is lethal [Ziman and Johnson, 1994]. Cdc24 is redistributed from the nucleus to the cytosol at bud emergence by activation of the protein Cdc28 (a Cyclin Dependent Kinase (CDK)). Once in the cytosol it can be localized by Rsr1-GTP. Cdc28 also inhibits Cdc42 GAP proteins and therefore helps in two ways in the activation of Cdc42 (figure 2) [Gulli et al., 2000] [Toenjes et al., 1999] [O'Shea and Herskowitz, 2000].

Earlier was noted that the landmark protein Bud3 also function as a direct GEF for Cdc42, especially in early G1 [Kang et al., 2014]. Based on the results of this study and also of more recent research, a positive feedback mechanism between Bud3, Bud5 and Rsr1, that localizes Cdc42 in early G1, is proposed [Kang et al., 2014] [Martin, 2015]. However, this is not sufficient for bud formation since the sole deletion of Cdc24 is lethal. In late G1 and onward, other positive feedback loops might take over that includes Cdc24 which might explain why only Bud3 as the Cdc42 GEF is not enough for complete cell polarization. Since Rsr1 and Bem1 can bind together and both also bind to Cdc24, there may exist a connection between the PAK-Bem1-GEF loop and the proposed feedback by Rsr1 [Martin, 2015].

Not only landmark proteins are still localized at the previous bud site after cell division, also proteins that might inhibit polarization are still localized, for example the Cdc42 GAP proteins (see figure 2). Some studies found that Rga1Δ cells tend to bud *at* the same location of the previous bud [Tong et al., 2007] [Lee et al., 2015]. In contrast, WT cells typically form the new bud *next* to the previous budding site which is convenient for the cells as the daughter cell from the previous cell cycle might be in the way for the new bud. Therefore, it is proposed that GAP proteins might play a role in determining the exact localization of proteins involved in bud emergence. The GAP proteins counteract the Cdc42 activation at the site of future budding since there is a competition between the GAP and GEF proteins. Indeed, in cells where (some of) the GAP proteins are deleted, the polarity cap is much broader than normal, indicating that the GAP proteins have a role in localizing Cdc42 to a very specific location [Klünder et al., 2013] [Okada et al., 2013] [Woods et al., 2016].

Cdc42 is thus localized using a pathway of landmark proteins, Bud5, the GTPase Rsr1 and the Cdc42 GEF Cdc24. The latter is also involved a positive feedback cycle that increases the Cdc42-GTP concentration at the polarity region. Some of the Cdc42 effector proteins are involved in positive feedback loops to promote its own activation. Examples are the PAK kinases, but also Bni1 is involved in activating Cdc42 by nucleating actin cables (this will be discussed in the section Actin dependent pathway). GAP proteins regulate the Cdc42-GTP concentration and probably help in the timing of polarization events.

Positive feedback loops

At the end of G1 phase, when a small cluster of Cdc42 starts to accumulate, the concentration of active Cdc42 has to be increased to ensure proper polarization and bud formation. One of the most important and best understood methods of Cdc42 amplification is by the PAK-Bem1-GEF positive feedback loop [Bose et al., 2001] [Bi and Park, 2012]. The Cdc42 effector proteins Cla4 and Ste20, which are part of the PAK group proteins, bind to the Cdc42 GEF Cdc24 using the scaffold protein Bem1 (See figure 2 orange outlined proteins). This activates more Cdc42 at the

polarity site, promoting the formation of this PAK-Bem1-GEF complex, hence creating a positive feedback loop [Gulli et al., 2000] [Martin, 2015]. The kinase Cla4 is not required for cytokinesis after early stages of bud emergence and for localizing actin to the polarity cap [Weiss et al., 2000]. This might indicate that its main function is to help in localizing Cdc42 which is confirmed by the deletion of Cla4 which results in a decreased efficiency of the Cdc42-GTP polarization [Gulli et al., 2000]. This study also found that overexpression of Cla4 causes cells to be unable to polarize Cdc42 since it promotes phosphorylation of Cdc24. Cdc24 phosphorylation might function as an inhibitory pathway as will be discussed in the section Negative feedback loops. Bem1Δ is not lethal as long as actin cable are still functional [Smith et al., 2013]. It was thought that the role of Bem1 is to bind the PAK, GEF and Cdc42 together and to stimulate polarization and phosphorylation of Cdc24 [Zheng et al., 1995] [Bose et al., 2001]. But another study found that the function of Bem1 in this feedback loop seems to be only to bind the PAKs to the Cdc42 GEF, since Bem1Δ cells in which Cla4 and Cdc24 are artificially bound, behave like WT cells [Kozubowski et al., 2008].

The Bem1-mediated feedback loop might play a role in establishing a single polarity cap [Klünder et al., 2013] [Howell et al., 2012]. Even though landmark proteins promote Cdc42 to localize near the previous budding site, there might still arise multiple small clusters of Cdc42 along the membrane because of the stochastic nature of protein diffusion in the cell. Each of the possible clusters can grow significantly using the positive feedback and each of these feedback loops require the localization of certain proteins, like for example Bem1. Since only a limited number of these proteins are available in the cell, a competition is created where eventually one winner comes out that has enough of the required proteins localized to ensure proper polarization. However, when the positive feedback is disrupted, a single cluster is still polarized, indicating that determining a single polarity region does not depend only on the PAK-Bem1-GEF positive feedback loop. The negative feedback mechanism by the GAP proteins might be involved as the final deciding factor [Kuo et al., 2014].

Besides Cla4, the PAK kinase Ste20 also plays a role in the PAK-Bem1-GEF feedback cycle. It is one of the proteins involved in the mating pheromone response and its role as a PAK is similar to that of Cla4. It was shown that it can also phosphorylate Cdc24, although its effect is weaker than that of Cla4 with Cdc24 [Bose et al., 2001]. Ste20 polarization does not require localization of CDK proteins, unlike other Cdc42 effector proteins and therefore Ste20 can polarize faster. The sole deletion of Ste20 is not lethal, indicating that it is not required for the PAK-Bem1-GEF positive feedback loop unlike Cla4. The synthetic deletion of Ste20 and Cla4 prevent the cells from maintaining a septin ring, inhibiting cell division [Cvrckova et al., 1995].

The PAK-Bem1-GEF feedback is not the only positive feedback loop. Also, a feedback loop mediated by actin might help in enhancing Cdc42 concentration near the polarity cap [Wedlich-Soldner et al., 2003]. Actin cables are necessary for guiding exocytotic vesicles, which can carry Cdc42 as cargo on their membranes. Since actin cables are nucleated by the Cdc42 effector protein Bni1, a positive feedback can be arranged [Pruyne et al., 2004]. Cdc42 can be dissociated from the cell membrane by endocytosis [Karpova et al., 1998]. When the vesicles are recycled, they are transported back to the membrane along the actin cables which are located near the polarity region [Moseley and Goode, 2006]. This process will be discussed in more detail in section 'Actin dependent pathway'.

The PAK-Bem1-GEF feedback cycle is important in proper polarization of Cdc42. However, disruption of the feedback loop by Bem1Δ or deletion of the PAKs still allow the cells to polarize and forming buds, although the polarization rate is severely reduced [Smith et al., 2013] [Kozubowski et al., 2008] [Wedlich-Soldner et al., 2004]. The recycling pathway of actin, which might also be regarded a positive feedback loop, might be enough for cells to polarize (discussed in the next section). The role of the Bem1 mediated feedback cycle is therefore mainly to speed up and stabilize the polarization process.

Cdc42 recycling pathways

Landmark proteins localize Cdc42 and the PAK-Bem1-GEF feedback loop ensures local activation. But Cdc42 is not stably fixed to the membrane at the polarity cap but it is able to diffuse

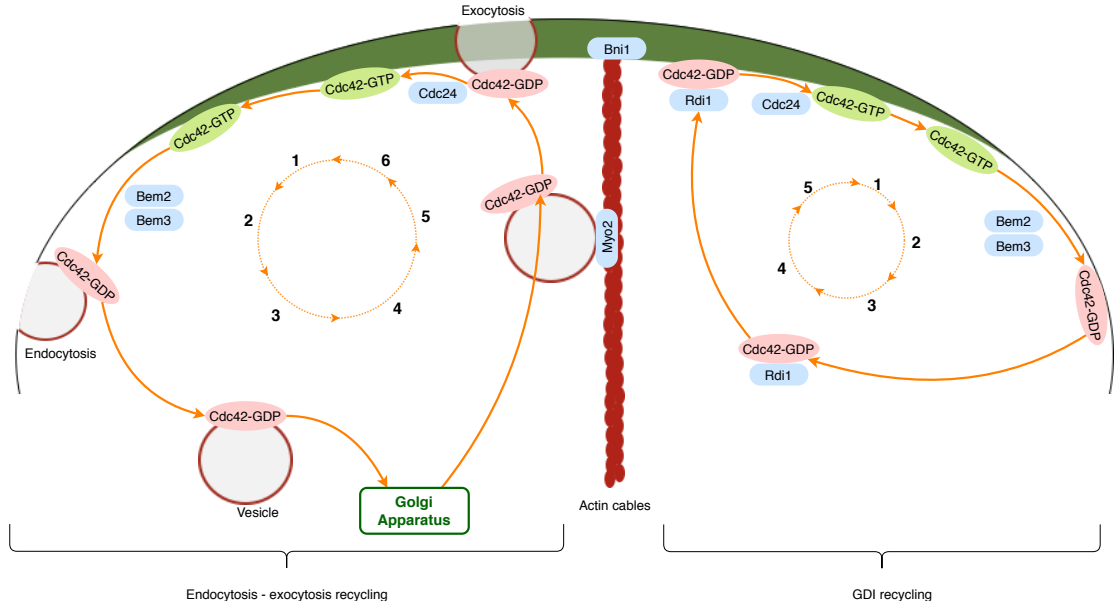

Figure 3: Overview of two recycling pathways. **Left** is the endocytosis - exocytosis pathway. (1) Cdc42 diffuses away from the polarity region, (2) gets deactivated by GAP proteins and (3) gets carried away from the membrane on an endocytotic vesicle. (4) The vesicles are transported from the Golgi apparatus to the actin cables which are nucleated by the Cdc42 effector protein Bni1. (5) The vesicles are carried along the actin cables back to the polarity region where (6) Cdc42 is released and activated by Cdc24 [Tcheperegine et al., 2005]. **Right** the GDI pathway is shown where again (1) Cdc42 diffuses away from the polarity cap and (2) gets hydrolyzed by the GAP proteins. It then (3) binds to the GDI Rdi1 which allows Cdc42-GDP to dissolve in the cytosol. (4) Once it reaches the polarity region, (5) the Cdc42 gets activated by the localized Cdc24 which promotes the dissociation of Cdc42 from the Rdi1 [Klünder et al., 2013] [Martin, 2015].

away. Therefore, some mechanisms must exist to recycle Cdc42 back to the polarity region. There are at least three recycling pathways proposed.

The first proposed recycling pathway is diffusion of Cdc42 along the membrane to the polarity site. At the polarity region, Cdc42-GDP is activated to Cdc42-GTP by the local concentration of Cdc24. Therefore, a low concentration of Cdc42-GDP is present at the polarity region and Cdc42-GDP will diffuse towards the polarity region. If the diffusion rate of Cdc42-GTP is slower than that of Cdc42-GDP, the active Cdc42 diffuse slower away from the polarity cap than inactive Cdc42 diffuses towards the polarity cap. This creates a net influx of Cdc42 towards the polarity cap [Martin, 2015]. But, the diffusion rate for Cdc42 is estimated to be around 0.4 μm^{-2} for both Cdc42-GTP and Cdc42-GDP [Marco et al., 2007]. In this case, there would be no net influx but actually Cdc42 would diffuse away from the high concentration polarity region, counteracting polarization. It is thought that this diffusion is therefore not a key mechanism in Cdc42 polarization [Howell and Lew, 2012].

Therefore, other ways of recycling have to be present. Another possible recycling pathway is using the protein Rdi1. The Cdc42-Rdi1 complex can detach from the membrane to the cytosol in which the diffusion rate is higher [Koch et al., 1997]. Rdi1, a Rho GDP Dissociation Inhibitor (GDI) which binds preferably to Cdc42-GDP, keeps Cdc42 dissolved in the cytosol and possibly increases the exchange rate of Cdc42 from the membrane and the cytosol [Woods et al., 2016] [Martin, 2015]. This allows Cdc42 to diffuse through the cytosol (see right part figure 3). However, one study found that both Cdc42-GTP and Cdc42-GDP can bind to Rdi1, but that the affinity of Cdc42-GDP is higher (more then 10-fold) than that of the GTP bound form [Johnson et al., 2009]. This indicates that the Rdi1 pathway is depended on hydrolyzes by GAP proteins.

The Rdi1 recycling pathway is faster than membrane diffusion and this route might explain how Cdc42 can be localized in significant levels to ensure polarization. This is shown by modelling in which only the PAK-Bem1-GEF feedback and the Rdi1 pathway were enough to get a single Cdc42 cluster [Klünder et al., 2013]. Rdi1Δ cells with normal GAP levels and cells in which Rdi1 is overexpressed are still able to polarize [Klünder et al., 2013] [Slaughter et al., 2009], although overexpression can cause some morphological changes [Tcheperegine et al., 2005]. When,

in Rdi1Δ cells, the GAP levels are reduced the cells are not viable anymore [Woods et al., 2016]. A possible explanation given in this study is that in Rdi1Δ cells the fast Cdc42 recycling pathway mediated by the GDI is blocked. But the presence of GAP proteins limits the number of Cdc42-GTP copies and therefore also reduces the Cdc42-GTP efflux from the high concentration polarity region. Since the Rdi1-mediated recycling is most likely not the only recycling pathway, other, slower recycling pathways might be enough to ensure polarization. However, when also the GAP function is reduced, for example in Rdi1ΔBem2Δ cells, Cdc42 is not effectively hydrolyzed to its inactive form. Relatively large quantities of Cdc42-GTP might then diffuse away from the polarity region and, without the fast Rdi1-mediated recycling pathway, this Cdc42 is not returned to the polarity cap quickly enough to prevent loss of polarization. Indeed, using models they found that cells with Rdi1Δ and with reduced GAP levels were more sensitive to higher exchange rates of Cdc42-GTP compared with Rdi1Δ with normal GAP levels [Woods et al., 2016].

Finally, a third way for Cdc42 recycling is with actin cables, besides their possible role as a positive feedback mechanism. This actin mediated recycling is important mainly during the later stages of cell polarization and might explain why in Rdi1Δ cells there is still polarization [Martin, 2015] [Ayscough et al., 1997] [Woods et al., 2016] [Slaughter et al., 2009]. This will be described in the next section.

Initial localization of Cdc42 and stabilizing its polarization can be ensured by different mechanisms, but the most potent of these are transportation of Cdc42 through the cytosol using Rdi1 and vesicle trafficking by endocytosis and exocytosis with Cdc42 as cargo along actin cables.

Actin dependent pathway

Actin cables are involved in one of the major recycling pathways in yeast cells and are necessary for the shape of the cell. They consist of actin subunits (globular- or G-actin) that bind in a head-to-tail like manner into two, 37nm long protofilaments. These bind together in a helix shape to form filamentous- or F-actin.

F-actin has two structurally different ends where one is a slow growing pointed end and another fast-growing barbed end [Mishra et al., 2014]. Assembly of actin is performed in a process called nucleation. In budding yeast, actin nucleation is promoted by formins, which consists of the Cdc42 effector protein Bni1 and the related protein Bnr1 (see figure 2) [Pruyne et al., 2004] [Chen et al., 2012]. Bni1 is mainly responsible for actin cable polarization to the bud cortex and Bnr1 primarily polarizes the actin cables toward the mother bud neck [Pruyne et al., 2004]. Besides being an effector protein of Cdc42, Bni1 belongs also to the polarisome proteins (figure 2). These polarisome proteins control the cell shape of the daughter cell during polarization [Tcheperegine et al., 2005].

Individual deletion of each of the formins is not lethal [Evangelista et al., 2002], although Bni1Δ causes severe morphological defects in the bud. However, Bni1ΔBnr1Δ cells are not able to polarize [Kamei et al., 1998]. Two tropomyosin proteins, the major isoform Tpm1 and the minor isoform Tpm2, stabilize the actin cables after nucleation. Tpm2 is about six times less abundant than Tpm1 and the sole deletion of Tpm2 does not seem to have any influence on the cells in any aspect (e.g. growth rate, mating efficiency, morphology etc.) [Drees et al., 1995]. Deletion of Tpm1 on the other end, has significant consequences since these cells are not able to bud and grow in a more spherical manner, indicating that actin cables are either completely lost or their function is severely disrupted [Liu and Bretscher, 1992]. Moreover, synthetic deletion of both tropomyosins is lethal, indicating that stabilization of actin cables is essential [Drees et al., 1995] [Pruyne et al., 1998].

To study the influence of actin cables, it might be necessary to inhibit the formation of actin cables. This can be done by deletion of the formins or the tropomyosins. However, these proteins have more functions then just nucleation or stabilization of actin cables, for example Bni1 has also a direct interaction with Cdc42, Bud6 and the actin-binding protein profilin [Evangelista et al., 1997]. Deletion of the actin nucleating and stabilizing proteins might therefore have more consequences then only inhibition of actin cables. An alternative method of actin cables inhibition is using the toxin Latrunculin, that originally was found in sponges, which binds to the actin subunits and thereby destabilize actin cables. This toxin exists in the two

different, but chemically very similar, variants Latrunculin A (LatA) and the somewhat less potent Latrunculin B (LatB) [Ayscough et al., 1997]. Actin structures can be stained with a fluorescent dye (typically rhodamine-phalloidin). When adding Latrunculin to the cells the fluorescence of the dye disappeared within five minutes, indicating inhibition of the assembly of actin [Ayscough et al., 1997] [Karpova et al., 1998]. This toxin does leave other structures of the cytoskeleton intact. Adding LatB inhibits only actin cables, but leaving the actin patches mostly intact, unlike LatA which inhibits both actin cables and patches [Irazoqui et al., 2005]. This study also shows that LatB causes some dispersion of Cdc42 from the polarity region which is not seen in LatA treated cells. This might be due to the still intact actin patches in LatB treatment. The location of these actin patches is thought to be the main site of endocytosis [Kaksonen et al., 2003]. After treatment with LatA or LatB the yeast cells are not able to bud or show significant bud defects. However, the effects of LatA treatment are reversible as washing the cells with fresh growth medium (without toxins) after LatA treatment allows the cells to nucleate actin cables and patches within 1 hour after washing [Ayscough et al., 1997].

The actin cables are thought to transport Bem3 to the polarization site, since LatA treatment prevented recruitment of Bem3 to the polarity cap [Knaus et al., 2007]. But, both Cdc42 and Bem1 do not require actin cables for polarization since in LatA treated cells these proteins could still polarize normally [Yamamoto et al., 2010]. However, another study claims that actin is required for Cdc42 polarization [Wedlich-Soldner et al., 2004]. They also found that Bem1Δ cells treated with LatA are not able to form any polarization of Cdc42. Finally, one other study claims that results found with Latrunculin treated cells just reflect a stress response that occur upon deletion of actin cables due to the added toxin and therefore questions some results found by other studies regarding Latrunculin treatment [Woods et al., 2016].

If localized Cdc42 diffuses away from the polarity region, it can be transported away from the membrane by endocytosis [Karpova et al., 1998]. An endocytotic vesicle carries substances from outside the cell inwards and, as the cell membrane invaginate to create a vesicle, it can carry Cdc42 along with it as cargo (see left part figure 3) [Irazoqui et al., 2005] [Huckaba et al., 2004]. This process is mainly regulated by actin patches [Kaksonen et al., 2003]. The patches are polarized by Cdc42 and, although the exact mechanism is not entirely clear, it is thought that either some Cdc42 effector proteins or GAP proteins may be involved [Adams and Pringle, 1984]. Also, tropomyosin proteins seem to play a role in patch localization, since the disruption of the function of Tpm1 and Tpm2 affects the localization of actin patches [Pruyne et al., 1998]. After separation of the endocytotic vesicle from the membrane, the vesicles are transported to the Golgi-apparatus, from which they can be transported back to the membrane by exocytosis [Moseley and Goode, 2006]. However, the exact mechanism by which this is controlled is not well understood yet. Initially it was thought that actin cables and actin patches were spatially coupled [Karpova et al., 1998], but later this was questioned as another study found that endocytosis and exocytosis are segregated from each other [Slaughter et al., 2013].

As mentioned before, Cdc42 is required for localizing actin cables near the polarity site using Bni1. In turn, these actin cables are necessary for Cdc42 localization as Cdc42 is delivered by the cables as cargo on exocytotic vesicles [Wedlich-Soldner et al., 2003] [Wedlich-Soldner et al., 2004] [Harris and Tepass, 2010] [Bi and Park, 2012]. This creates a positive feedback loop which stimulates actin cable localization (figure 3). Actin cables function as guidelines that direct vesicles for exocytosis and in this way helps in localizing Cdc42 [Ayscough et al., 1997] [Mishra et al., 2014] [Karpova et al., 1998] [Walworth et al., 1992] [Okada et al., 2013]. Exocytotic vesicles are controlled by the Rab-GTPase Sec4. The effector proteins of Sec4, the eight exocysts proteins, tethers the exocytotic vesicles to the membrane prior to vesicle-membrane fusion (see figure 2) [Liu and Novick, 2014] [France et al., 2006].

Exocytosis thus may help in increasing the Cdc42 concentration at the polarity region. However, it is also proposed that exocytosis may dilute Cdc42 concentration instead of increasing it since the vesicles fuse with the cell membrane and therefore increasing the surface area of the cell [Watson et al., 2014]. This increase in surface area is more prominent than the increase in Cdc42 proteins since the concentration of Cdc42 on the vesicles is typically lower than the concentration near the polarity site. It is thought that therefore this exocytosis mediated recycling might be to partly compensate the dilution of Cdc42 proteins, which would be more prominent in the case of exocytosis where Cdc42 would not be carried on the exocytotic vesicles.

The exocytotic vesicles cannot directly bind to the actin cables, but instead they need a mediator which is the protein Myo2, a type V myosin motor. This Myo2 protein is a critical component for Cdc42 polarization, since the inhibition of the function of Myo2 causes a significant lower number of cells that are able to polarize [Irazoqui et al., 2005].

Actin cables are nucleated by Bni1 and Bnr1 and stabilized by Tpm1 and Tpm2. Bni1 and Bnr1 are necessary for proper bud morphology and Tpm1 is required for developing a bud. Actin is involved in a recycling pathway by endocytosis and exocytosis that are controlled by actin patches and actin cables, respectively, but it is still not entirely clear to what extent this recycling is required for Cdc42 polarization [Martin, 2015]. Nevertheless, Cdc42 is involved in polarization of both actin cables (by Bni1 and Bnr1) and patches. This might indicate a relation between endocytosis and exocytosis by Cdc42.

Negative feedback loops

Some studies found that Cdc42 is polarized in an oscillatory pattern that was observed in Rsr1Δ cells [Howell et al., 2012] [Kuo et al., 2014] and another study found small displacements in the polarity region before it settles at the final budding site location [Ozbudak et al., 2005]. This might indicate the existence of some negative, inhibitory, feedbacks as these effects cannot solely be explained by positive feedback loops. These negative feedback loops compete with the positive feedbacks. Negative feedbacks regarding Cdc24 phosphorylation, GAP proteins, polarized endocytosis by actin cables and septins are discussed next.

A possible negative feedback might be caused by Cdc24 phosphorylation [Moran et al., 2019]. Quantification of the Cdc24 activity showed that phosphorylated Cdc24 is less active, by a factor of two, compared with unphosphorylated Cdc24 [Kuo et al., 2014]. A mutant in which all the phophorylation sites are blocked, so that Cdc24 is nonphophorylatable, showed hyperactivation of its function as a Cdc42 GEF. Over 30 different phosphorylation sites were identified in Cdc24 by one study, although initially they did not find any functional relevance for these sites [Wai et al., 2009]. This is the main reason that some studies doubt the relevance of Cdc24 phosphorylation as a negative feedback [Bose et al., 2001] [Kozubowski et al., 2008] [Wai et al., 2009]. Nevertheless, phosphorylation is recently repeatedly brought in connection with a negative feedback in budding yeast [Gulli et al., 2000] [Howell et al., 2012] [Kuo et al., 2014].These studies propose a feedback with most of the polarity network proteins that can bind to Cdc24, like Cla4 (and also by Ste20, but this seems to phosphorylate Cdc24 only weakly), Bem1 and Cdc42 [Gulli et al., 2000] [Bose et al., 2001]. At the polarity region, Cdc24 activates Cdc42 and the Cdc42-GTP effector protein Cla4 phosphorylates Cdc24, inhibiting its function as a Cdc42 GEF so that it cannot activate more Cdc42 proteins [Kuo et al., 2014].

Evidence for a feedback mechanism by Cdc24 phosphorylation was intially found by overexpressing Cla4, which hyperphosphorylated Cdc24. This caused depolarized cell growth and reduced the activation of Cdc42, possibly by detaching Cdc24 from Bem1 [Gulli et al., 2000]. The authors of this paper argue that phosphorylation might be necessary for switching from apical growth to isotropic growth or for ending polarized growth. However, another study found that phosphorylated Cdc24 does not detach from Bem1 and that hyperphosphorylation of Cdc24 by Cla4 overexpression is actually favorable for polarized cell growth [Bose et al., 2001]. This would create a feedback in a positive manner rather than in a negative. A difference in the method by both studies is that the latter used less overexpression of Cla4 compared with [Gulli et al., 2000], which might also indicate that overexpression of Cla4 might have more effects on the polarity network than only Cdc24 phosphorylation.

Phosphorylation of Cdc24 is not the only proposed negative feedback. For example, one study found that, in cells where the landmark proteins are not functional anymore in the polarity network, the polarity region shows small displacements before it settles and forms a bud [Ozbudak et al., 2005]. They checked the role of Cdc42 GAP proteins and found that the deletion of these proteins reduced the mobility of the polarity region. A possible mechanism for this feedback might be the polarized delivery of GAP proteins to the polarity region by endocytotic vesicles. However, by overexpressing the GAP proteins, the mobility did not increase, leading the authors to conclude that GAP proteins are not the only inhibiting factor. Also, they noticed

that when the cells were treated with LatA, the cells show less mobile polarity caps as well. Therefore, they argued that actin cables might be involved in a negative feedback, due to protein dispersal, parallel to the actin positive feedback mechanism by endocytosis/exocytosis. Possible mechanisms for an actin mediated negative feedback is delivery of GAP proteins by exocytosis to the polarity cap, or by dispersing the proteins in the polarity cap by fusing an exocytotic vesicle with the membrane at the polarity cap (which was also mentioned in the section Actin dependent pathway).

The polarity region needs a high concentration of active Cdc42 since Cdc42-GTP interacts with its downstream effector proteins. The GAP proteins catalyze a hydrolysis reaction in Cdc42 which initially suppresses polarization as it inhibits the interaction with the effector proteins. This might explain that the deletion of GAP proteins show morphological deformation of the buds, even though these deletions are still viable [Rodrıguez-Pachón et al., 2002]. A combined deletion of two or three of these GAP proteins is also viable, but the morphological changes are then emphasized [Rodrıguez-Pachón et al., 2002] [Stevenson et al., 1995]. Overexpression of Bem2 cause weak growth defects, but Bem3 overexpression is toxic as the cells cannot maintain a polarization region [Knaus et al., 2007]. It was found that in Bem1Δ cells, the growth rate significantly decreases as Cdc42 is not activated by the Bem1-mediated positive feedback loop. But the growth rate can partly increase again when one of the GAP proteins (for example Bem3) is deleted as well and it increases even more (almost to WT level) when two GAPs (for example Bem2 and bem3) are deleted [Smeets, 2017. Unpublished results]. This shows that GAP proteins have an inhibitory role in the Cdc42 polarization network, which is also evident from the fact that they are necessary for maintaining a stable polarity region [Chen et al., 1997] [Howell et al., 2012] [Kuo et al., 2014]. As mentioned earlier, it is suggested that GAP proteins help in localizing Cdc42 to a narrow polarity region as it prevents GEF proteins to activate Cdc42 in a broader patch on the membrane [Lee et al., 2015] [Tong et al., 2007]. Also, GAP proteins might promote binding of Cdc42 to Rdi1 since Cdc42-GDP have a higher Rdi1 affinity than Cdc42-GTP [Slaughter et al., 2009].

Finally, one other inhibitory process that regulate Cdc42 concentration near the polarity cap is organized by septins. These are cytoskeletal proteins that help form actin filaments [Howell et al., 2012]. Septins are localized by Cdc42 which initially forms a solid region of septins near the polarity region. Influenced by exocytosis, the septin region is hollowed to form a ring-like structure in which Cdc42 and its effector proteins are trapped [Okada et al., 2013]. This decreases the net efflux of proteins away from the polarity region. This study also shows that these septins suppresses the Cdc42 cluster and that septins and actin cables have a mutual inhibitory influence on each other, thereby regulating the Cdc42 polarization. It is also suggested that septins play a role in the oscillatory behavior of the polarity cap [Howell et al., 2012]. The timing of localization of septins coincides with a decrease in oscillation amplitude, leading to the proposal that septins might be involved in dampening of the oscillations.

There are still some discrepancies about which of these processes are the most influential for polarization [Perez and Rincón, 2010]. For example, several studies claim that the Cdc42 effector protein Cla4, which is promoted by Cdc28, mainly regulates the phosphorylation of Cdc24 in a negative manner, for example [Gulli et al., 2000]. Other studies claim a feedback in a positive manner with Cla4 and Cdc24 using Bem1 [Bose et al., 2001] [Kozubowski et al., 2008]. But another study counteracts these statements as they find that Cdc24 phosphorylation does not have a big influence on the regulation of Cdc42. [Wai et al., 2009]. Yet another paper claim that mainly the phosphorylation of Cdc42 GAP proteins control Cdc42 activity, for example [Knaus et al., 2007]. It is still an open question about the exact mechanisms behind these processes and what the connection between them exactly is. But, in general, studies agree that negative feedback mechanisms are necessary to make the cells somewhat robust for differences in polarity protein concentrations, to reduce polarity factor accumulation and to ensure fast competition between multiple polarity clusters [Howell et al., 2012] [Kuo et al., 2014].

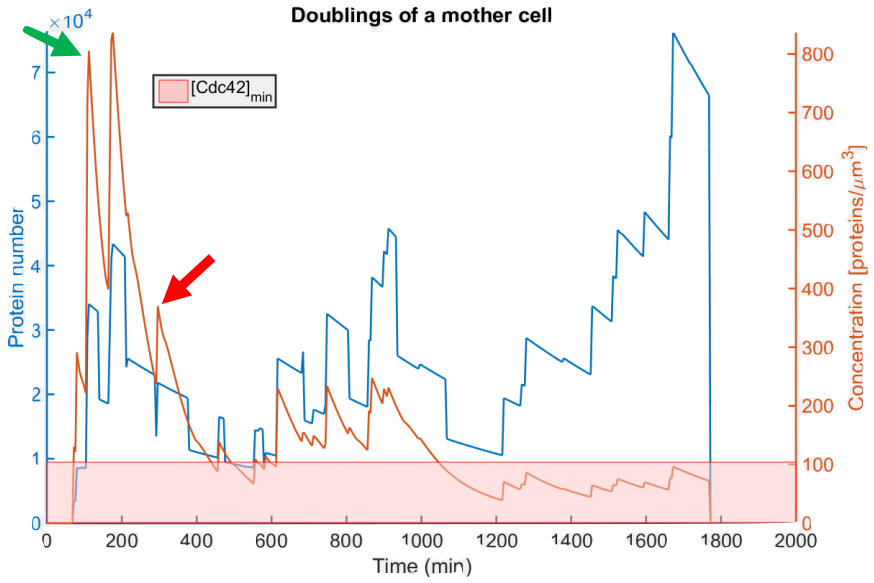

Figure 4: Protein copy number (blue line) and concentration (red line) as a function of time for a Bem1Δ mother cell during multiple cell divisions under the assumption of a constant membrane growth. The red line initially shows a large increase due to protein translation. Small drops indicate degradation, but the degradation rate is typically smaller than the translation rate. After about 180 minutes the cell divides (indicated by the green arrow), donating a part of its proteins to the daughter cell, hence the protein concentration shows a sudden drop. The cell recovers from this as the concentration quickly increases again. This means the cell is viable. After another cell division at 300 minutes (indicated with the red arrow), the protein concentration drops again, but this time the cell is not able to recover the protein concentration quickly enough before the next cell division (note that translation is stochastic, so this inability to recover is pure by chance). The protein concentration briefly drops below a threshold concentration that is minimally required for the cell to grow. The cell tries to recover from it by translating new proteins after cell division (hence the small increases after each division), but it does not manage to increase the concentration enough to account for multiple subsequent cell divisions. The cell is now in a dying state. When, after about 1000 minutes, the cell permanently drops below the threshold value, it is not able to divide anymore and dies. The protein copy number (blue line) typically increases as the cell grows (the net result is a decrease of protein concentration). Extreme cell growth can be an indication of the inability to divide, in which the cells increase their membrane area due to delivery of lipids, but the membrane area does not decrease after some time since the cell does not divide and the membrane is not donated to the daughter cell. [Daalman, unpublished results]

Transgenerational epigenetic inheritance

A possible strategy for a population of organisms to survive in different environments, is to allow each cell to have a slightly different phenotype [Bar-Even et al., 2006] [Kussell and Leibler, 2005]. Organisms that are best adapted for a specific environment will give rise to the most offspring. But when the environment changes, other phenotypes might be better suited. If there are multiple phenotypes present, the chances of survival of the population in this new environment increases because a few cells might already have a phenotype that matches the requirements for survival in this new environment. To put it differently, by sustaining multiple phenotypes in a population the overall population fitness increases [Levy et al., 2012] [Acar et al., 2008]. This phenomenon is often called 'bet hedging' [Xue and Leibler, 2016].

Given an environment, cells in a population have a specific average protein concentration, but there will exist some variance in the concentration of proteins between cells in a population. This variance is mainly caused by the stochastic nature of protein production (transcription and translation) and degradation [Ozbudak et al., 2002]. If a cell has a relative high protein concentration compared with other cells, the offspring of this cell is expected to have, on average, a high concentration as well. The concentration can be inherited by subsequent generations. This is called transgenerational epigenetic inheritance [Xue and Leibler, 2016] [Heard and Martienssen, 2014]. For example, cells with a higher concentration of Cdc42 yield, on average, more offspring compared to cells with low concentrations Cdc42. Within a few generations, the cells with low Cdc42 concentrations will become scarce in the population, causing the average Cdc42 distribution of the entire population to shift to higher concentrations. In the case of Cdc42, overexpression can be harmful for the cell, as is discussed earlier. In a specific environment a certain concentration will thus be optimal, but there will be some spread around this concentration due to stochasticity

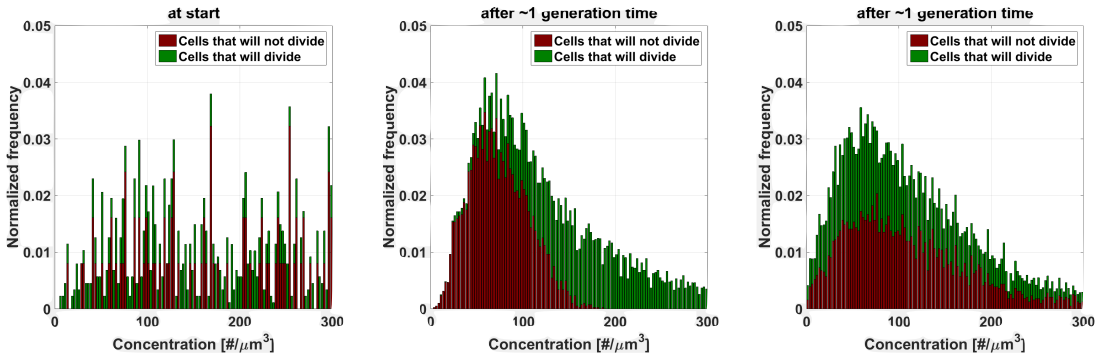

Figure 5: Simulation for protein concentration for viable cells (green) and dying cells (red) in a Bem1Δ background. **Left:** Starting condition. The protein concentration of a population of cells is randomly distributed for both viable and dying cells. **Middle:** For important proteins (e.g. Cdc42) after one generation, the protein distribution has adopted a gamma distribution. The cells have more copies of Cdc42 due to a higher translation rate than degradation rate. For viable cells, the distribution is more skewed towards the higher concentrations compared with the dying cells. The dying cells also show more cells with very low concentrations relative to the viable cells. The distribution is determined regardless of the phase of the cell cycle each cell was in. **Right:** Similar to the middle figure, but in this case the protein concentration is plotted for an unimportant protein. Unimportant in this simulation means a hypothetical protein that is very similar to Cdc42 but does not influence cell division in any way. In case of this unimportant protein the distributions for viable and dying cells are similar [Daalman, unpublished results].

[Acar et al., 2008].

The epigenome of an organism is determined by certain molecules that have a direct or indirect effect on gene expression. In general, this is controlled by either marking the DNA or histones with molecules, typically methyl, acetyl or phosphor groups or by the protein ubiquitin [Berger, 2002]. Methylation is adding a methyl group to the CPG islands (locations on the DNA where a guanine nucleotide directly follows on cytosine nucleotide), but this process does not seem to be present in *S. Cerevisiae* [Huang et al., 2013] [Capuano et al., 2014]. Acetylation ([Grunstein, 1997]), phosphorylation ([Baker et al., 2010]), ubiquitination ([Sun and Allis, 2002]) and histone methylation ([Krogan et al., 2003], [Nagy et al., 2002]) all work on histones and are present in budding yeast. By binding to the tails of the histones, these molecules can change the way how DNA folds around the histones. If DNA is bound tighter, the genes around the histones are less likely to be expressed. For example, the process of acetylation binds an acetyl group to the N-terminus of a histone, thereby decreasing the positive charge of the histone, making the negatively charged DNA less attracted to the histones and thus the DNA is less tightly wrapped around the histone. This increases the chances that local genes are expressed. Deacetylation reverses this process [Weinert et al., 2014].

Model for protein concentrations

The central dogma of biology states that a gene is transcribed from the DNA to mRNA using RNA polymerase, after which the genetic code on the mRNA is translated using ribosomes to a chain of amino acids that forms the protein. Both mRNA and proteins degrade after a certain time defined by their half-life. Transcription, translation and degradation are stochastic processes and therefore the concentration of proteins is not constant during the cell cycle [Blake et al., 2003] [Elowitz et al., 2002]. Moreover, during cell division some of the proteins from the mother cell are donated to the daughter cell, causing the concentration to decrease in the mother cell. As a consequence, after cell division both the mother cell and the daughter cell have to translate proteins at a rate that creates enough proteins to buffer a decrease in protein concentration during the next cell division.

Due to the stochastic nature of protein synthesis and degradation, it might happen that the cell is not able to increase its protein concentration to a level that can compensate for the concentration decrease. After cell division, the concentration is then so low that the cell cannot synthesize enough proteins for proper polarization prior to the next cell division, causing the cell to die. This indicates that there is a certain minimum threshold concentration that the cell has to reach to ensure proper polarization and cell division. If the protein concentration stays below

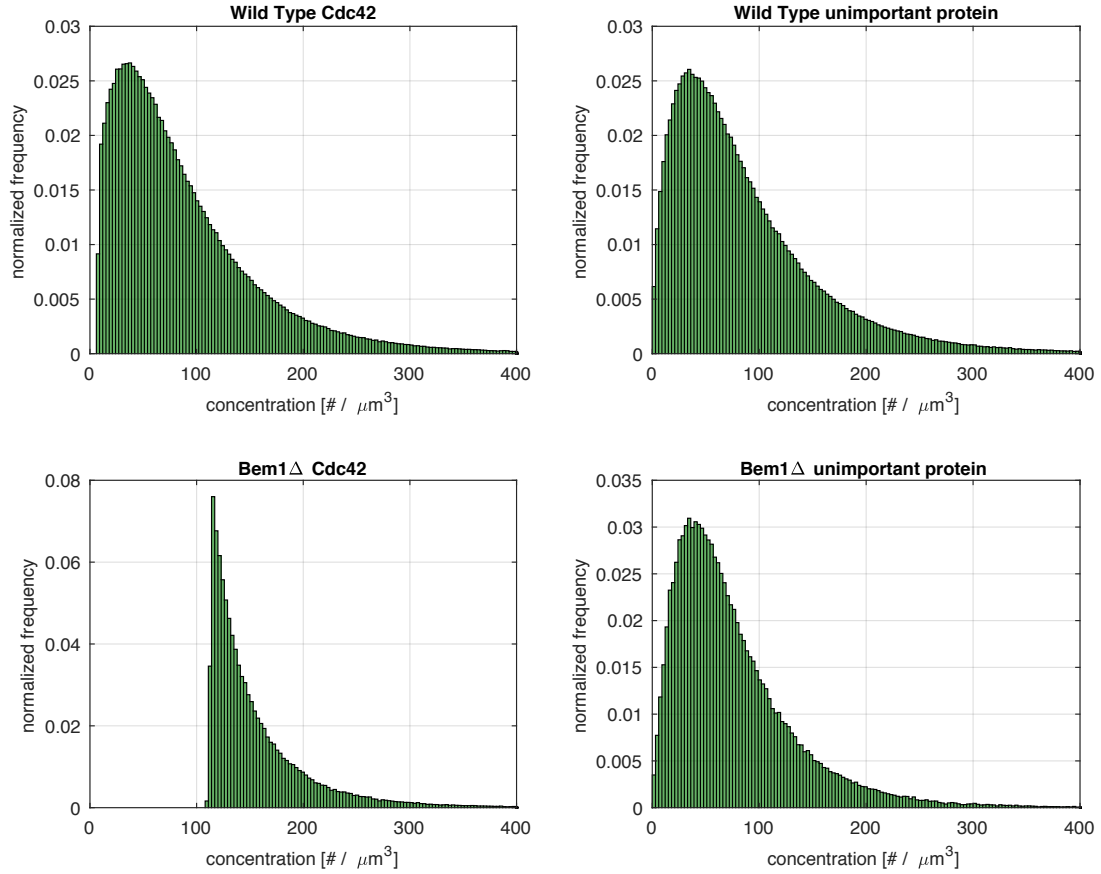

Figure 6: Simulation for Cdc42 concentration during polarization. **Top left**: Distribution of Cdc42 proteins in WT cells. Similar to the middle graph in figure 5. The difference is that the distribution is determined at the time of budding (so all cells were in the same phase, i.e. late G1 / beginning of S-phase) and more cells are used in this distribution ($> 10^5$), hence a smoother distribution. All measured cells were able to polarize and bud, so this graph only represents viable cells. Note that there is a threshold concentration as there are no cells with very low concentrations. **Top right**: Similar conditions as the top left graph, but this distribution is for an unimportant hypothetical protein that is similar to Cdc42, but has no influence on cell division. Note that now there is no threshold concentration present. **Bottom left**: Cdc42 protein distribution in the same conditions as the top left graph, but now in a Bem1Δ background. The threshold value has shifted to a higher concentration as the cells require more Cdc42 in order to compensate for the inhibition of the positive feedback loop for Cdc42. **Bottom right**: Protein distribution of the same unimportant protein as in the top right graph, but in the Bem1Δ background. This protein has no threshold concentration, similar to the WT background.

this threshold concentration for too long, the cell is said to be in a dying state.

This is illustrated in a simulation of a single cell using Cdc42 in a Bem1Δ background shown in figure 4. In this simulation, the Bem1Δ mother cell is initially viable and has a high enough Cdc42 concentration for polarization and budding. After about 180 minutes the cell divides which causes a drop in protein concentration (green arrow), but the cell is able to fully recover from this since the concentration increases to a level that is similar as before cell division (second peak in the concentration). However, after 300 minutes the protein concentration drops again due to a new cell division, but this time the cell does not recover the concentration to sufficient levels (red arrow). This eventually results in a protein concentration below the threshold value, causing the cell to die. Note that the cell can recover from a concentration below the threshold as long as the concentration is not too low, and it is not below the threshold for an extended period of time.

The threshold concentration is depending on the genetic background. In, for example, Bem1Δ cells the threshold for Cdc42 is expected to be higher than in WT (the cells need a higher Cdc42 concentration to bud). In Bem1Δ cells the Bem1-mediated feedback loop is inhibited and therefore Cdc42 is not effectively enriched at the polarity cap. A decrease in Cdc42 concentration has then a higher chance to be lethal in the Bem1Δ background than in WT. In Bem1ΔBem3Δ, the threshold is expected to have a value somewhere between that of Bem1Δ and WT cells

since in Bem1ΔBem3Δ cells less Cdc42 is deactivated. Regardless of the genetic background, on average a higher Cdc42 concentration is expected in cells that survive compared with cells that do not survive.

A theoretical model for the distribution of protein concentration has been described before [Friedman et al., 2006]. The authors assume that proteins are translated in bursts, meaning that a single mRNA strand translates multiple proteins. Next, they assume that the lifetime of a mRNA strand is much shorter than that of the proteins it encodes so that any fluctuations in mRNA levels can be neglected. Using these assumptions, they were able to prove that the protein concentrations follow a gamma distribution in which the most important parameters are the number of bursts per cell cycle and the number of proteins translated per burst.

The gamma distribution of protein concentration is confirmed using a computer model [Daalman, unpublished results]. An example of the distribution determined with this model is show in figure 5 where the concentration is shown for Cdc42 (middle graph) and a hypothetical protein very similar to Cdc42, but that has no influence on cell division (right graph). These distributions are made for a population of Bem1Δ cells as these have a greater change to be in a dying state compared with WT cells, allowing measuring enough dying cells to make the distribution. This model showed that the distribution of protein concentration is slightly different for cells that have a high translation rate and/or low degradation rate (viable cells) compared with cells that have a relatively low translation rate and/or high degradation rate (dying cells) (see middle graph of figure 5). This difference only holds for essential proteins that are necessary for proper cell division, like Cdc42. Less important proteins have a distribution that is similar for viable and dying cells (see right graph of figure 5).

The results shown in figure 5 are based on a model for Bem1Δ cells, but this distribution is different for different genetic backgrounds (e.g. WT or Bem1ΔBem3Δ). An example is given in figure 6. In the left column the Cdc42 concentration at the time of polarization is given for both WT cells and Bem1Δ cells. The right column shows the same measurements, but now for a hypothetical protein that is similar to Cdc42, but unimportant for cell division (the same unimportant protein as was described for figure 5). Since the distribution is determined for cells at the time of polarization all the cells are viable in this case. For Cdc42, there is a threshold concentration that the cell requires for budding. This threshold concentration is significantly higher in the Bem1Δ background compared with the WT cells[1]. In the simulation it was also observed that the growth rate of the population is slower in the Bem1Δ background relative to the WT background. Only the cells that divide contribute to population growth. Since in Bem1Δ less cells divide due to this increased threshold concentration (less cells have a high enough Cdc42 concentration), the population growth rate will be slower compared with a population of WT cells. This agrees with experimental results, as the doubling time of WT cells is shorter than that of Bem1Δ cells [Laan et al., 2015]. When unimportant proteins are considered, there is no threshold concentration and thus the concentration of this proteins does not influence whether a cell is viable or not and does also not have an impact on the growth rate of the cells.

According to the model, an order of magnitude of 10.000 cells need to be measured in order to see the characteristics of the gamma distribution. However, when more information about the cell is known, for example the number of proteins during polarization and the cell volume, it is empirically determined that an order of magnitude of 100 cells might be sufficient to have the characteristic gamma distribution. When the cells are measured during the same stage of the cell cycle, there is less variance in the protein concentration due to cell growth and protein production between the different stages in the cell cycle. Measured differences in the protein concentration are than likely to be caused by the natural variance in concentration between cells. This is also apparent in the bottom left graph of figure 6, where measurements were done during polarization. The graph shows a clearer threshold concentration and a steeper drop-off at the higher concentrations compared with the middle graph of figure 5 where all cells were measured regardless of which part of the cell cycle the cells were in.

To give an indication about protein copy numbers in budding yeast, some studies have tried

[1]The bottom left graph is similar to the middle graph in figure 5, the only difference being that in figure 6 the distribution is determined at time of polarization. Therefore the threshold concentration is more pronounced compared with the threshold in figure 5 where also cells are included that, for example, just went through cell division, causing them to have a low Cdc42 concentration at the moment of measurement.

to specify the proteome abundance in cells. It has been estimated that the copy number of most proteins ranges between $1 \cdot 10^3$ and $1 \cdot 10^4$ copies per cell, but extremes as low as 3 copies and up to almost $1 \cdot 10^6$ copies of a single protein have been measured[Ghaemmaghami et al., 2003] [Ho et al., 2018]. Multiple studies quantified the number of copies of specifically the Cdc42 protein and found results ranging from $3.5 \cdot 10^3$ up to almost $13 \cdot 10^3$ copies of Cdc42 per cell, for example [Lawless et al., 2016] [Lahtvee et al., 2017] [Kulak et al., 2014]. Although most studies give an exact number of copies, there are still significant differences between studies. This is discussed in more detail in other studies that show some discrepancies between different methods and results [Milo, 2013].

Recently, a meta analysis was performed to quantify the copy number of all proteins present in budding yeast based on the results of many different studies [Ho et al., 2018]. They looked at the correlation between results of different studies and compared this with the methods they used (e.g. fluorescent labeling, mass spectroscopy and immunoblot analysis) and noticed that the results from studies using fluorescent labeling (typically with Green Fluorescent Proteins (GFP)) correlate best with each other. This indicates that fluorescent labeling might be a reliable method for protein quantification studies. For measuring cells experimentally using this method, two common techniques can be applied. When there is no interest in the state of the cell cycle, flow cytometry techniques can be used to measure fluorescence of many cells in a single experiment. With this technique, a distribution is expected as shown in the middle graph of figure 5. When more information is required, fluorescence microscopy is better suited. This allows for measuring the temporal behavior of the cells, allowing measuring the phenotype of the cell during multiple cell cycles. With automated data analysis, the time of polarization can be determined, and the appropriate fluorescent intensity can be measured. Moreover, with fluorescence microscopy, the cell can be measured at different focal planes, allowing a three-dimensional reconstruction of the shape of the cell (for example see [Lai et al., 2018]). Using this information, the volume, and therefore also the protein concentration, can be estimated. A major drawback of this method is the relative low number of cells that can be measured in each experiment (tens of cells) relative to flow cytometry techniques (order of magnitude of 100.000 cells or more). However, with the right experimental parameters (e.g. concentration of cells in the solution that is measured, sample preparation and microscope settings), more than 30 to 40 cells per measurement might be possible. Since less cells are expected to be needed for a proper distribution in fluorescence microscopy, this method is still a reasonable approach for showing the distribution and also this technique allows for more information to be obtained of the cells (e.g. protein concentration changes as a function of cell cycle or three dimensional reconstruction of the cell for determining the protein concentration). However, a drawback of quantifying proteins based on fluorescent labeling is when the copy number is low such that the fluorescence intensity is in the same order of magnitude as the background intensity. In this case fluorescence intensity might not be a reliable method [Ho et al., 2018]. For Cdc42 this is expected not to be a concern as the copy number is in the order of many thousands of proteins throughout the cell cycle which should result a fluorescence intensity that yields a relative high Signal to Noise Ratio (SNR).

Fluorescence imaging can lead to a better understanding of the temporal behavior of budding yeast cells [Cookson et al., 2009]. This study was able to determine the production rate, cell volume as a function of the cell cycle and concentration, based on a stable fluorescent protein. However, the authors did not look how the production rate and concentration looked for a native protein of budding yeast. But, their results indicate that fluorescence imaging might be a suitable method for determining protein concentration. When Cdc42 is tagged with a fluorescent protein, it allows for imaging the dynamics of Cdc42 over time as is shown in [Cookson et al., 2009]. Besides measuring the cell volume and concentration of Cdc42, different stages of the cell cycle can be differentiated, allowing to make a distinction between cell volume and concentration in different stages of the cell cycle. Using fluorescence microscopy, the phenotype of the cells can be visualized and cells that do not divide can be separated from cells that do undergo cell division. This allows for validating the hypothesis that cells that do not divide have, on average, a lower Cdc42 concentration compared with cells that do divide.

Materials and Methods

Yeast strains and growth media

YMB007
Haploid WT, Mating type α.
[Pgal1]Cdc42:mNeonGreen^{sw}, URA3 selection marker.
The yeast cells are grown in Complete Supplement Mixture with Uracil dropout (CSM-Ura) with 2% raffinose and varying galactose concentrations (depending on the measurements, typically 0.0%, 0.1% or 2.0%). Cells were stored at -80°C in 80% glycerol and 0.0% galactose CSM-Ura in a cells:glycerol ratio of 2:1.

Growth curves

Growth curve measurements were performed with the BioTek EPOCH2 96-well plate reader. The cells were incubated at 30°C overnight in 2.0% galactose concentration after recovering them from -80°C. The cells were then washed in different galactose concentrations (0.1% or 2.0%) and grown for 8 more hours before putting the cells in a 96-well plate. To minimize evaporation of the media, the surroundings of the wells are filled with water and the plate is sealed using parafilm. During the measurement the temperature was set to 30°C and 1°C gradient to prevent condensation on the lid of the 96-well imaging plate. Between measurements, both linear shaking (731 cycles per minute with 2 mm amplitude for 3.5 minutes) and orbital shaking (548 cycles per minute with 2 mm amplitude for 3.5 minutes) was used to prevent precipitation of the cells. An absorbance measurement was performed every 8.5 minutes at a wavelength of 600 nm (denoted as OD_{600}) for a total measurement time of > 60 hours. For each sample a background measurement is performed with the same media, but without cells and this background is subtracted from the measurements using cells.

For determining the growth rate, the base 2 logarithm is calculated from the OD_{600} values to determine the log phase. The slope of the log phase corresponds with the growth rate which is the inverse of the doubling time.

Microscopy

Microscopy images were made using a confocal Spinning Disc Microscope (SDM) with an Olympus IX81 microscope stand. A 100x magnification, NA=1.4 oil objective from Olympus was used together with a Yokogawa CSU X1 spinning disc scanner unit with 50 μm diameter pinholes. IMMOIL-F30CC immersion oil type F from Olympus is used which has a refractive index of $n = 1.518$. For detection an Electron Multiplication (EM) CCD Andor iXon X3 DU897 was used which was set at a gain value of 200 and an exposure time of 200 ms. A 491 nm laser, set to a power output of 3mW, was used for illumination of the mNeonGreen (mNG) proteins. The excitation peak of mNG proteins is at 506 nm and at the wavelength of the used laser, the excitation efficiency is reduced to just over 68%. To ensure only the fluorescence light of the mNG proteins was captured in the camera, a bandpass filter (525 nm$\pm$25 nm) was applied.

For preparation of the sample, the cells were recovered from -80°C from a 0.0% galactose concentration and incubated overnight at 30°C in the desired galactose concentration. The cells

were checked if they were still in log phase and were then diluted to an appropriate concentration and sonicated for 15 minutes at 40 kHz using a Branson m1800 sonicator. For imaging, a 96-well imaging plate was used that was coated with Concanavalin A (ConA), a lectin to which the carbohydrates on the membrane of the cells can bind to, for immobilizing the cells on the surface of the imaging plate. The redundant ConA in the wells was removed after 30 minutes after which 100 μL of each sample were added to the wells. The 96-well plate was then put in a centrifuge at 700 rpm for 7 minutes to spin down the cells to the imaging glass coated with the ConA to stick them to the imaging plate surface.

Only cells were imaged that were well separated from each other (i.e. not more than 3 cells in the same image and the cells are not clustered together) and that did not have any daughter cells yet (to make the image analysis easier). For each of the imaged cells, a brightfield image was taken and a z-stack of fluorescence images was made of 9 or 11 different focal planes in steps of 1μm. Cells were imaged in a time interval of 3 minutes for a total of 8 hour measuring time. During imaging the cells were incubated at 30^{o}C.

Software Cell Segmentation

For analysis of the imaged cells, software was developed based on an existing cell segmentation program[2]. The cell segmentation software uses neural networks to identify cells in brightfield or fluorescence images from the SDM (for the rest of the software described here, only the fluorescence images are used). Custom functionality was added to handle large sequences of images. Furthermore, an easy way of storing results from the segmentation for further analysis is added and background noise and illumination correction can be applied. Noise is subtracted from the images and these images are then divided by the normalized background illumination. Most importantly, the software is able to automatically detect when a cell is budding and estimate the timepoint at which the cell polarizes, including determining the corresponding pixel intensities. Budding is detected by checking, each time when a new cell is found, whether the new cell has fluorescence (to lower the chances that segmentation errors are recognized as buds), that it is within close proximity of the potential mother cell (Pythagorean distance is used) and that the area of the bud is smaller than that of the mother cell. This proved to be about 70% accurate (35 false positive budding recognitions, 4 false negatives and 4 missed cells during segmentation out of in total 138 segmentations). Most false positive recognitions are caused by situations where, in the first image, there are two cells close together. The budding event of one cell can then be ascribed to the other cell.

The timepoint of polarization is determined by calculating the coefficient of variance using the pixel intensities. The coefficient of variance is defined as the ratio between the standard deviation and the mean intensity in the cell [Lai et al., 2018]. Before the images are segmented using the software, the sum of all slices is determined using ImageJ, where each slice corresponds to one focal plane (i.e. one of the 9 or 11 z-stack slices from the SDM).

For determining the cell volume, z-stack images are used of a cell at a specific timepoint in its cell cycle. Only a few focal planes will be within the volume of the cell, whilst the remaining planes are focused above or below the cell. To discard the images that do not have a part of the cell in focus, constraints have been applied that determine the area of the segmented part (focal planes that are not within the volume of the cell have a low signal to noise ratio which causes missegmentation, typically resulting in a large area), the intensity, ratio between the major and minor axis and the difference between the area and intensity between two neighboring focal planes. For each cell, the intensity and the volume are stored so that the concentration and the protein copy number can be determined.

The workflow and pseudocodes of the segmentation and recognition software is presented in the appendix Pseudocodes.

[2] https://github.com/alexxijielu/yeast_segmentation

Results

Growth Curve Measurements

For the experiments discussed in this chapter, the YMB007 strain is used which has a galactose promoter placed before the *cdc42* gene. This allows for controlling the transcription rate of the gene by using different galactose concentrations. By measuring the growth rate of a population of cells, the growth rate of individual cells during microscopy can be validated to check whether they grow as expected. When they grow slower, this might indicate, for example, a stressed cell or deficiencies in the growth media. Also when the cells have to acclimate to a new environment, for example after preparation, the doubling time can temporarily be prolonged.

Figure 7 shows the growth curves for the YMB007 strain using OD_{600} values (blue curve) and the $\log_2(OD_{600})$ (orange curves). For each curve, the average is taken from 10 measurements. The growth rate is determined during log phase where the cells have an excess of nutrients to rapidly grow and divide. This phase is indicated with black lines in figure 7. As the population grows and nutrients become scarce, the growth rate decreases and the cells eventually enter a stationary phase where the growth rate goes towards zero.

For the used strain, it is expected that a 0.1% galactose concentration should have an average doubling time that is about equal to the growth rate for WT cells. Depending on the media, the doubling time is about 80 to 100 minutes in Yeast extract Peptone Dextrose (YPD) and 140 minutes in synthetic media [Sherman, 2002] [Moran et al., 2010] [Blansjaar, unpublished results] [de Bruin, unpublished results]. For the yeast cells grown in 2.0% galactose concentration in synthetic media, the average growth rate is measured to be to $g_{2.0\%} = 0.44\text{h}^{-1}$, which corresponds to a doubling time of 135 minutes. For 0.1% galactose, the growth rate is $g_{0.1\%} = 0.41\text{h}^{-1}$, corresponding to a 146 minutes doubling time. Both are around the expected 140 minutes for cells grown in synthetic media. The growth rate for YMB007 cells grown in 2.0% galactose is on average more than 10 minutes faster compared to the growth rate in 0.1% galactose, which implies a higher concentration of Cdc42 in cells grown in 2.0% galactose media. For measuring in 0.0% galactose, the cells were grown in 0.0% overnight before the measurement was started. As the cells are not able to transcribe Cdc42 without the galactose, the population does not show any growth as is expected.

The cells behave as expected under different galactose concentrations. The microscopy measurements are performed using 0.1% galactose, thus on average a doubling time is expected of about 146 minutes.

Microscopy

In the strains used in the following experiments, Cdc42 proteins are tagged with mNG. This allows Cdc42 to be visualized by exciting the mNG proteins at a wavelength of around 506 nm and imaging the fluorescence at a wavelength of 517 nm. The goal is to make time lapse movies for individual cells, check if they grow a bud and determine the fluorescence intensity during polarization. Knowing the fluorescence intensity could potentially allow for quantification of the amount of proteins present in the cells. Using this information, the model for protein concentration (as explained in the literature review) can be experimentally investigated.

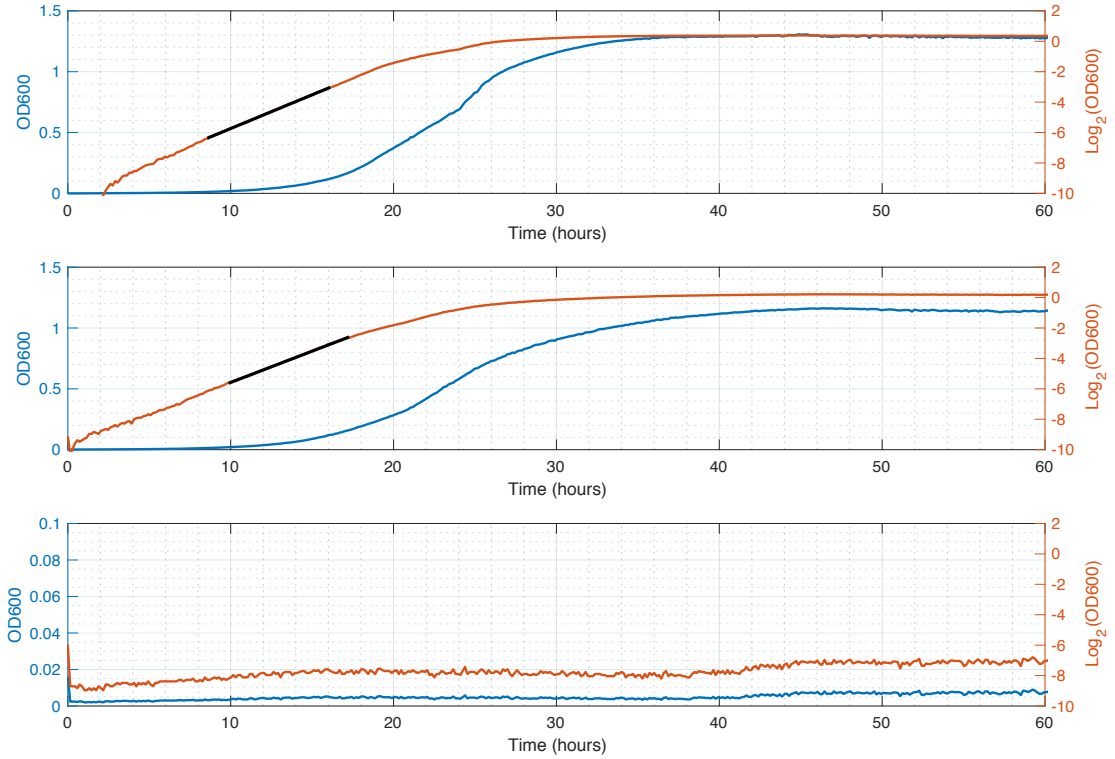

Figure 7: Growth curves for YMB007 strain in CSM-Ura (blue line) and the growth curves plotted using a $\log_2$ scale (orange line). The black line indicates the linear part during log phase that is used for determining the growth rate. **Top**: 2.0% galactose. **Middle**: 0.1% galactose. **Bottom**: 0.0% galactose (note the different scale on the blue y-axis relative to the other graphs).

Fluorescence imaging of the cell cycle

To indicate the different stages of Cdc42 polarization using fluorescence imaging, a montage is shown in figure 8 for a cell grown in CSM-Ura with 0.1% galactose. At 69 minutes after start of the measurement the cell is still in G1-phase. Around 84 minutes the cell proceed towards late G1 phase and it start to polarize Cdc42. After onset of polarization it takes the cell 15 minutes enter the S phase indicated by the development of a bud at the polarity cap. The bud then continues its isotropic growth throughout G2 phase while the Cdc42 is polarized at the bud cortex. The bud cortex polarization eventually diminishes at 156 minutes after which the Cdc42 polarizes at the bud neck at 180 minutes until mitosis.

The microscopy images show a normal behavior of the cells in terms of polarization and budding. At the start of the microscopy measurements, the doubling time is often observed to be longer than what would be expected based on the growth curve measurements (180 minutes in this particular example compared to 146 minutes on average as determined with the growth curve measurements). Since the cells typically need to adjust to new media and the new environment (e.g. recover from the preparation of the imaging plate including a temperature shock from sonication where the cells are put in ice to prevent overheating and spinning down of the cells in the ConA), the initial phase of the measurement shows a longer doubling time. After a while, the doubling time typically goes towards the doubling time that is measured during the growth curve measurements.

Relation between average pixel intensity and number of fluorescent sources

Under the assumption that each Cdc42 protein is tagged with a mNG protein, it is expected that the total fluorescence increases linearly as more Cdc42 proteins are present in the cell. By measuring the total intensity from the fluorescent proteins, the number of Cdc42 proteins can then potentially then be calculated. The question is, when this fluorescence intensity is captured

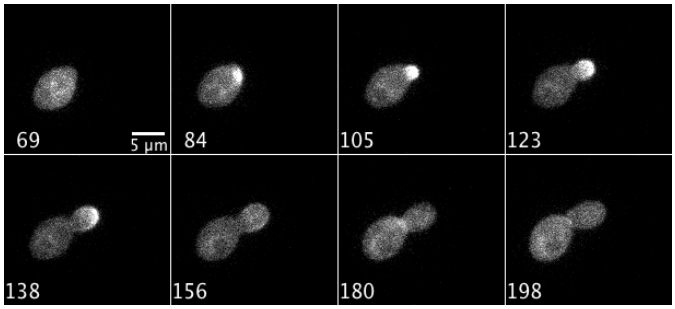

Figure 8: Montage of one cell cycle of a cell grown in 0.1% galactose concentration in synthetic media. Time points represent minutes after start of the measurement.

by the camera and translated to pixel intensities in an image, if the number of fluorescent sources (e.g. mNG proteins) scales linearly with the pixel intensity in the image?

To assess this question, fluorescent beads are used that contain multiple fluorescent dyes (Tetraspeck T14792 Fluorescent Microspheres Size Kit). For this experiment, the green fluorescent dye is used which has an excitation peak at 505 nm and an emission peak at 515 nm in 0.5 μm diameter beads. The settings for the microscope were identical to the settings as described in the Materials and Methods chapter. Different number of beads were imaged, ranging from one bead to over 100 beads in a single image. For each measurement, the average intensity over the entire image is determined. The results and the 99.9% confidence intervals of a linear fit are plotted in the left graph of figure 9. For each image, the background noise is estimated and subtracted from the image and an illumination correction is applied.

To check whether the relation between the number of flourescent sources and the pixel intensity is actually linear, a t-test is performed with the null hypothesis that the slope of the linear fit is equal to zero (i.e. no dependency between the variables) with the alternative hypothesis that the slope is unequal to zero. Based on the t-test ($F_{(1,16)} = 180.3, p < 0.001$) the null hypothesis was rejected and the fitted linear regression is statistically significant. A residual plot is made to show that the error made by the linear fit is stochastic (see right graph figure 9). The residuals are determined by the difference between the data points and linear regression line. As there is no clear relation between the residuals (the residuals seem to be randomly distributed), it is assumed that all information is captured in the linear line (i.e. a higher order equation is not needed to fully describe the data).

This shows that the relation between the number of fluorescent sources and the pixel intensity is linear. However, this only holds when the camera sensor is not under- or overexposed and the SNR is not too small so that the noise is dominating the image. Also, in the case of fluorescent proteins, the sources might overlap in the axial direction. The proteins are much smaller than the resolution of the microscope, so proteins might be on top of each other in the same focal plane of the microscope. The protein on top can than block part of the light from the proteins beneath it, resulting in an underestimation of protein count.

In general, it is assumed that this blocking of the fluorescence light by other proteins does not significantly influence the measurements and that the intensity scales linearly with the number of fluorescent sources (e.g. mNG proteins).

Fluorescence intensity changes during the cell cycle

With the previous results, it is shown that the relation between the number of fluorescent sources and the pixel intensity is linear. This might allow for determining changes in the Cdc42 concentration by measuring the intensity changes as a function of cell cycle. A number of cells are chosen that start as single cells (i.e. no other cells are close by to make analysis easier and more reliable) that polarizes after a few minutes and form multiple daughter cells. This is done so that multiple cell cycles can be measured of a single cell. The cells are prepared and the microscope is set as explained in the Materials and Methods section.

A representative measurement is shown in figure 10. The graph shows the total intensity

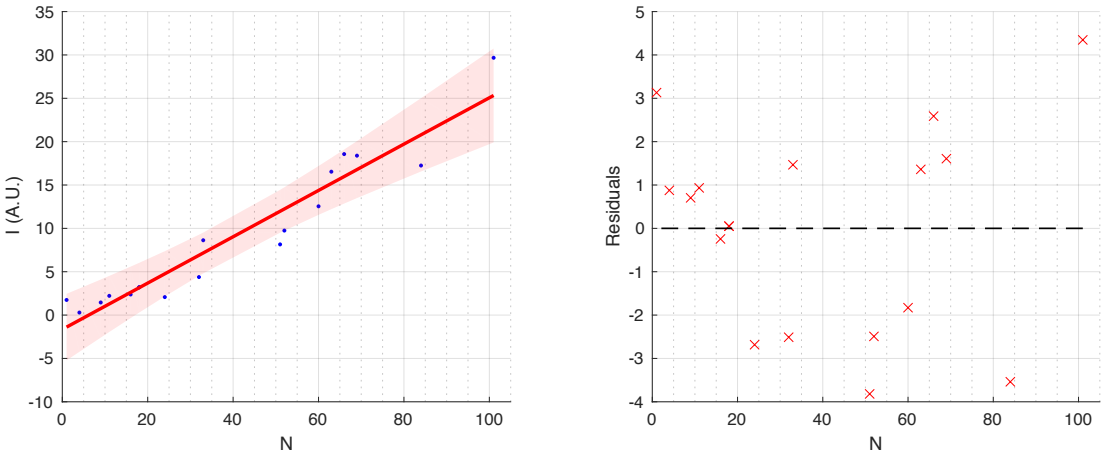

Figure 9: **Left**: Average pixel intensity for different quantities of fluorescent beads. The red line indicates a linear fit together with the 99.9% confidence interval (shaded area). The y-axis is the average pixel from the whole image with noise subtraction and correction for the background illumination. **Right**: Residual plot for the linear fit in the left figure. The residual values represent the difference between the data value and the fitted line. The residual plot shows random behavior, which implies that the variance in the intensity is independent of N (homoscedasticity). This indicates that the model is a good representation of the data.

of the cell (intensity summed over all focal planes). The blue line represents the mother cell (yellow outlined in the montage) and the red line shows the first daughter cell after start of the experiment (red outlined in the montage). The green line shows the summed intensity of the mother and daughter cell. The vertical lines indicate some recognizable events in the cell cycle of the mother cell. The first polarization is seen just after 20 minutes after start of the measurement. The cell is polarized for about 18 minutes when the first signs of bud development is observed at 42 minutes after start of the measurement. Note that the red line starts a little later, as the segmentation software does not immediately recognize the new bud as an individual cell. More figures of different cells are shown in appendix Fluorescence intensity changes during the cell cycle - figures.

The mother cell shows a constant increase in the fluorescence intensity, especially in the beginning of the measurement, which is expected to be caused by an increase in number of proteins. When after 42 minutes the first bud develops, the intensity of the mother cell drops since the polarity cap is located in the bud which at this point not recognized as part of the mother cell anymore. This indicates that many proteins are present near the polarity region. The bud shows a rapid increase in intensity because of polarization in the bud cortex and the rapid growth of the bud. At 96 minutes in the measurement the polarity cap in the bud cortex withdraws and the cell enters M phase of the cell cycle. The bud is now also isotropically growing which is slower than the apical growth in the beginning of the bud development, causing the intensity increase to slow down until cell division at 126 minutes. When the intensity of the bud is added to the mother cell, the total intensity keeps increasing, suggesting a continued production of Cdc42 during budding. The increase in intensity in a cell is seen in 90% (54 out of 60 cells) of the segmented cells.

The mother cell is tracked for one and a half cell cycle after the first cell division, showing a repetitive trend in the intensity (i.e. a constant increase in intensity and a drop during budding). This is also visible in the plots in appendix Fluorescence intensity changes during the cell cycle - figures. The rate of increase does seem to slow down as the cell progresses through multiple cell cycles, which might indicate that the cell is less able to synthesize new proteins after a few cell cycles. Yeast cells are estimated to have a life span of more than 20 cell divisions [Kaeberlein et al., 2005]. It might be that the cell has gone through multiple cell cycles already before start of the measurement and that the increase in Cdc42 is slowed down as the cell is getting near the end of its life cycle. But since it is not known how many daughter cells this cell has produced, this can not be concluded from this measurement. Also, this slowing down in intensity increase is less apparent in the plots in appendix Fluorescence intensity changes during the cell cycle - figures and in the other measured cells, which might therefore be a phenotype of

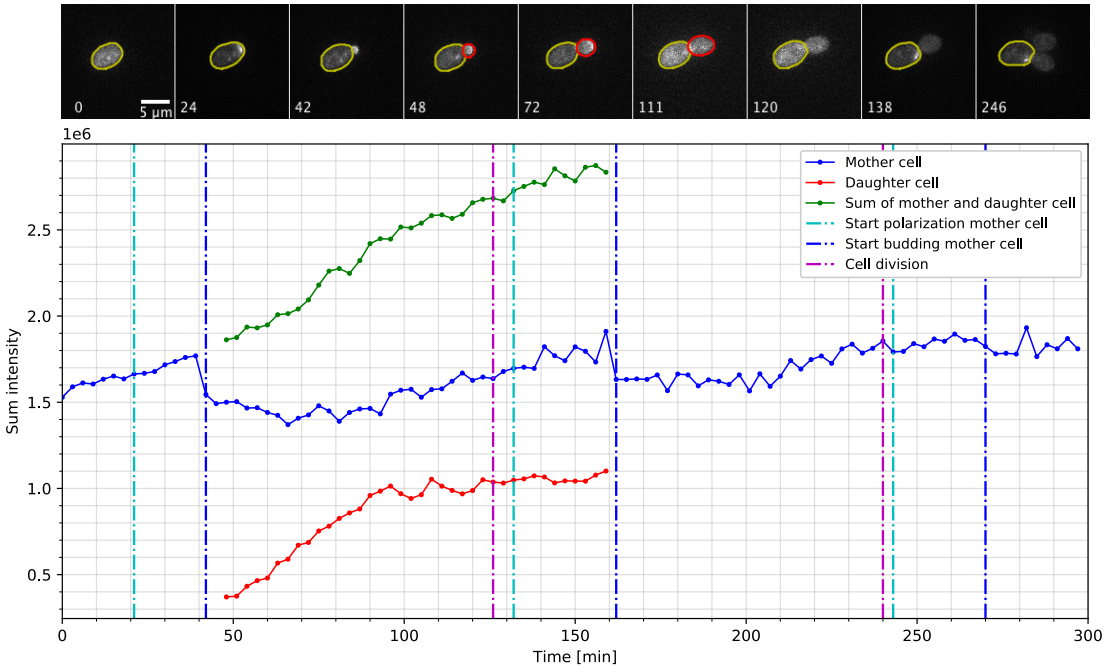

Figure 10: **Top**: Montage of the cell that is measured in the graph below. The timepoints in minutes in the images correspond to the timepoints in the graph. **Bottom**: Summed intensity from the cell. The blue points correspond to the mother cell that is yellow outlined in the montage. The bud that is red outlined in the montage correspond to the red points. The green line is the sum of the mother and daughter cell. Vertical lines are shown to indicate characteristic events in the cell cycle of the mother cell. This graph represents a single cell, but similar behavior is observed in 90% of the cells (54/60 cells)

this particular cell.

A similar repetitive trend in fluorescence is also observed in [Cookson et al., 2009]. This study looked at a stable fluorescent protein which had a constant production rate. The mNG proteins measured in figure 10 are bound to Cdc42, which degrades in about 8 hours and its production rate might change during the cell cycle [Christiano et al., 2014]. This may cause the fluctuations in fluorescence not to be as consistent as the fluorescence shown in [Cookson et al., 2009].

If the linear scaling factor between the number of mNG molecules and the measured intensity is known, the increase in intensity might allow for estimating the production rate of Cdc42 during the cell cycle. These results show that the cell intensity changes during the cell cycle and that the changes in fluorescence intensity can be explained using the known stages of Cdc42 polarization in cell polarization.

Estimating protein concentration

The summed intensity that is measured so far does not provide enough information to make a proper estimation of the total copy number of Cdc42 in the cell. For this, the volume of the cell needs to be known. As mentioned in the Materials and Methods section, the fluorescence from the cells is measured by taking either 9 or 11 different images, each focused on a slice 1 μm apart from each other. The used 9 or 11 different focal planes are empirically determined to be optimal, considering the effects of photobleaching and signal to noise ratio (more planes can be used, but then the exposure time and/or laser power have to be decreased to prevent photobleaching). Of the focal planes, typically 4 or 5 of these actually capture a part of the cell whilst the other focal planes are either just above or just below the cell. Since not all cells are perfectly positioned in the same z-plane of the objective, slightly more than 6 focal planes have to be imaged, hence the choice for 9 or 11 focal planes. Since the focal planes only capture a fraction of the entire volume of a cell, a large part of the cell is not imaged. The question discussed in this section is therefore if the concentration can still be determined based on the measurements done with a limited number of focal planes?

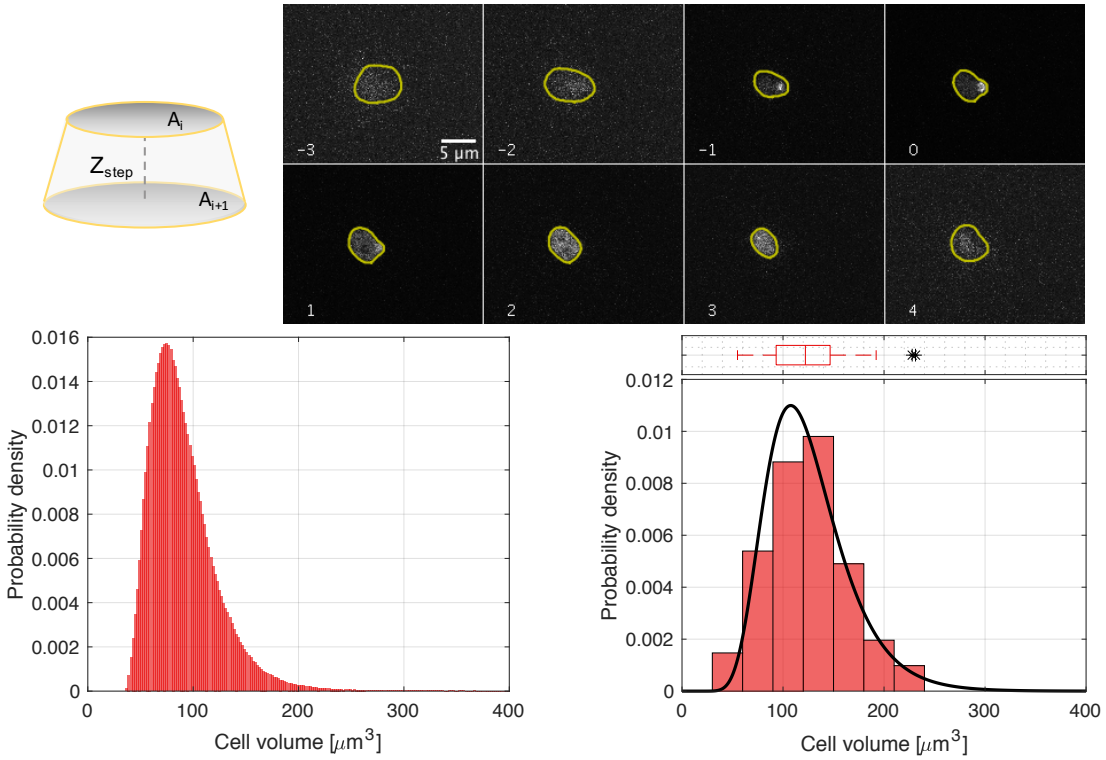

Figure 11: **Top left**: Schematic representation for the calculation of the cell volume. The top and bottom surface represent two subsequent focal planes with an area A_i and A_{i+1}, separated by a distance equal to the z-step set in the microscope (see Materials and Methods chapter). **Top right**: Montage of a cell during polarization with the different focal planes that were recognized by the segmentation software. The frame that was used for focussing is defined as frame 0 and the other frames are each 1 μm apart. **Bottom left**: Cell volume as determined by simulations for WT cells. Mean volume is $\overline{V} = 91 \pm 35$ μm^3. **Bottom right**: Experimentally determined cell volume as measured by the segmentation software together with a box and whisker plot. Mean volume is $\overline{V} = 125 \pm 39$ μm^3. A lognormal distribution is fitted over the data with mean $\mu = 4.78$ and standard deviation $\sigma = 0.32$ for the natural logarithm of the measured concentrations.

Estimating cell volume

The depth of focus of a single imaging plane of the spinning disc microscope can be estimated using the equation

$$\Delta z = \frac{\lambda}{4n\left(1 - \sqrt{1 - \left(\frac{\mathrm{NA}}{n}\right)^2}\right)} \tag{1}$$

[Young et al., 1993] where λ is the wavelength of the light used (peak emission wavelength of mNG $\lambda = 517$ nm), n the refractive index of the media between the sample and the objective lens (in this case immersion oil with $n = 1.518$) and NA is the numerical aperture of the objective (NA=1.4). This results in a depth of focus of Δz =0.139 μm per focal plane. When 6 focal planes are imaged of a cell, less than 1 μm of the cell in the z-direction is measured, which is less 20% of the diameter of a typical healthy cell. The measured intensity increases somewhat when fluorescence from out-of-focus planes are considered as well. This out-of-focus light is partly described by the axial resolution of the microscope (resolution along the z-direction) which is typically smaller than 0.5 μm for spinning disc microscopes [Schulz et al., 2013]. But the intensity of the light is slightly dimmed when it is captured from an out-of-focus plane compared when the same light when would be captured from an in-focus plane. Therefore, the fluorescence from the out-of-focus planes cannot be used for reliable estimating the concentration. To be able to calculate the protein copy number and concentration, the volume of the cell should be determined.

To estimate the volume of the cell, images of the different focal planes at single time point are used. Here the onset of polarization is chosen. The images of all the focal planes at this time point are segmented and the area and mean intensity of the cell in each of the images are

determined. Typically, three or four focal planes are above and below the cell and hence do not have any part of the cell in focus. These focal planes are therefore ignored. As shown in the montage in figure 11, where frame -3,-2 and 4 do not have the cell in focus, the area is relative large and the intensity low (low SNR). A threshold for the area and average intensity is set such that those frames are ignored when the volume is calculated.

The frames where a part of the cell is visible are used for estimating the volume of the cell. This is done by assuming the volume between two focal planes can be represented by a frustum. The top and base of the frustum are the segmented areas of two subsequent frames. The volume can then be estimated using

$$V_i = \frac{1}{3} z_{step} \left(A_i + A_{i+1} + \sqrt{A_i A_{i+1}} \right) \tag{2}$$

(see top left of figure 11 for a schematic representation). In this equation, V_i is the volume between two subsequent frames separated by a distance z_{step}. For the segmented area A of the cell, the number of pixels in the cell are counted and multiplied with the physical area of a single pixel ($A_{pixel} = 0.16^2 \mu\text{m}^2$). The total volume of the cell is the sum of all the individual volumes V_i.

The bottom right histogram in figure 11 shows the results when this estimation is implemented for over 100 cells. The cells were all measured while they were in G1 phase. The average cell volume is 125 $\pm$ 39 μm^3. This is about 37% more compared with the volume that is expected based on the simulation (bottom left histogram in figure 11, average cell volume is 91 $\pm$ 35 μm^3[Daalman, unpublished results]) and also more than expected based on literature [Johnston et al., 1979] [Moran et al., 2010].The box and whisker plot determined for the cell volume gives a median value of 121 μm^3 with box width that ranges from 93 μm^3 to 146 μm^3. If the cells are assumed to be an ellipsoid, the length of the major and minor axis (typically between 2 and 3 μm) indicate that the volumes of the cells are in the range that matches with the simulation and the literature and not with the measured volumes by the segmentation software. Therefore, it is proposed that the biggest contribution to the error in the average cell volume, as determined by the software, is due to the uncertainty in the segmentation.

Because of the irregular shape of the cells during polarization and the low SNR at the edges of the cell, the segmentation is not accurate, causing wrong estimates of the cell volume. A possible solution is using brightfield images for the volume estimation instead of the fluorescence images. The downside of this method is that fluorescence imaging has to be done separately after measuring the brightfield z-stack with the same focal planes to later be able to match the fluorescence intensity with the measured volume. This method is discussed further for fluorescent beads in section Validating volume calculation.

The cell volume is expected to be lognormal distributed [Bryan et al., 2010]. The cells measured in this article for determining the distribution were not selected according the state of their cell cycle they were in during measuring. The distribution thus reflects the volume of all cell cycles, whereas the volumes shown here are all from early G1 phase of the cell cycle. The authors do show that the cell volume increases during the cell cycle and that the volume during G1 (during which the measurements shown here are also made), is about 70 μm^3.

To check whether the distribution of the measured data is similar to the distributions found in literature, a chi-square (χ^2) tests has been performed to test the goodness-of-fit of the lognormal distribution. Other distributions have been tested as well for comparison. The results are shown in figure 19 and table 2 in appendix Distribution fits. For some of the distributions, the Anderson-Darling (AD-) test is determined as verification. The null hypothesis used for these tests is the probability that the distribution of the observed data is not statistically different from the expected distribution. A low p-value (≤ 0.05) means that there is enough evidence to reject the null hypothesis and that the distribution of the data is statistically different from the expected distribution. According to the χ^2-test, for all the considered distributions the null hypothesis cannot be rejected. Partly based on the qq-plots, the gamma, Nakagami and lognormal distributions seem to fit the data best. Figure 11 shows the fitted lognormal distribution (mean value $e^{4.78} = 119.2$ μm^3) for the measured data, based on literature and the qq-plots.

Using more data and better segmentation it is expected that the measured cell volume show a lognormal distribution with a mean value around 70 μm^3, based on literature and the measured

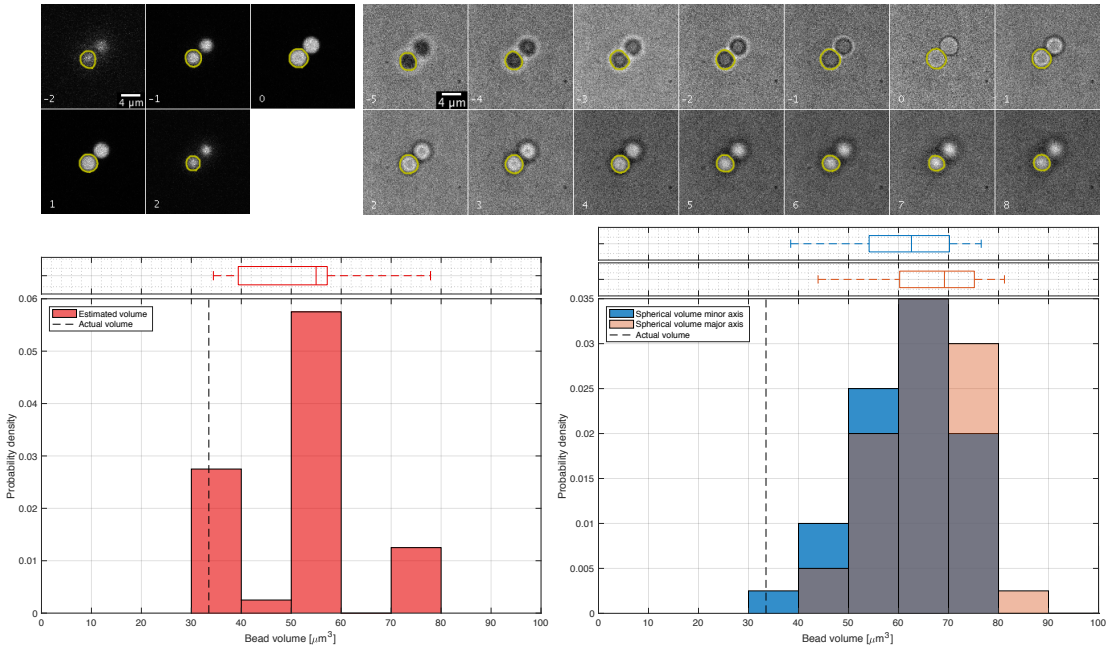

Figure 12: **Top left**: Montage of spherical beads with a radius of 2 μm (which corresponds to a volume of 33.5μm^3) using fluorescence imaging. The yellow outline is determined using the same segmentation software used for the cells. Note that only a few frames are shown. The other frames did not have a segmented area since the bead was completely out of focus. **Top right**: Montage of the same beads in brightfield imaging. The camera settings were the same as for the fluorescence imaging. **Bottom left**: Histogram for the bead volume using the segmentation shown by the yellow outline. For the calculation, the fluorescence images are used since the brightfield images yield too little contrast for accurately determine the area of the beads in the focal planes. **Bottom right**: Histogram for the volume of the same beads determined in the left histogram. The same software is used, but instead of interpolating the segmented areas, the volume is determined using the fact that the beads are spherical. The volume is determined twice where either the radius in the z-direction is determined using the minor axis of the segmented area or the major axis.

lengths of the axes of the cells. More data is also expected to result in the rejection of the null hypothesis for some of the tested distributions.

Validating volume calculation

The cell volume calculated in the previous section yields a volume that is bigger than was expected based on the radius of the cells and also based on literature and simulations. This is most likely due to segmentation errors where the software primarily segments an area that is bigger than the actual size of the cell in that focal plane. To quantify the error made by the software, beads containing a fluorescent dye (similar beads as used in section Relation between average pixel intensity and number of fluorescent sources) were imaged using the same settings as for imaging cells. The beads are spherical and have a radius of 2 μm which yields a volume of 33.5 μm^3. Segmentation is also performed with the same software as used for the cells of which the results are shown in top left montage in figure 12. The volume is determined by interpolating the segmented area in each frame. This shows that the outline by the segmentation is consistently larger than the imaged part of the beads in the focal plane (for example, note the small dark ring between the yellow outline and the bright part that represents the bead). This is especially notable for focal planes near the upper or lower boundaries of the bead, see for example image -2 or 2 in the montage for the fluorescence images in figure 12. Similar effects are expected to be present in the cells, resulting in volumes larger than expected. The bead volumes, determined similarly as the cell volumes, result in a mean volume of 51 $\pm$13 μm^3 (based on 42 beads) which is an increase of $> 50\%$ compared to the real volume (see the bottom left histogram in figure 12).

An alternative method for determining the volume is based on measuring the major and minor axis lengths. By assuming a specific shape for the objects, the volume can be calculated using these lengths. For the beads the shape is known to be spherical. The shape of the cells is not known exactly, but a common representation are ellipsoids (for example see

[Cookson et al., 2009]). The minor and major axis lengths are determined based on the segmentation of the beads. The average radius of the minor axis is $R_{minor} = 2.46 \pm 0.18$ μm and for the major axis the radius is $R_{major} = 2.54 \pm 0.19$ μm. The measured radius has an error of about 25% relative to the actual radius of the beads. However, when the volume is calculated based on spherical shape, the volume yields a similar result as the volume from the interpolating method (see the bottom right histogram in figure 12). The volume is calculated twice, one where the volume is determined using the equation $\frac{4}{3}\pi R_{major}R_{minor}^2$ (blue histogram), yielding a mean volume of 64 ± 15 μm^3, and another using $\frac{4}{3}\pi R_{minor}R_{major}^2$ (orange histogram), resulting in a mean volume of 70 ± 16 μm^3. Since the volume scales by a power three of the radius, a relatively small error in the measured radius yield a significant error in the volume calculation. The measured radius comes with another uncertainty since it is typically not known whether center plane of the object is imaged. If the center plane of the object is missed, the estimated radius is smaller than the actual radius. This is primarily a concern when individual z-stack images are considered, but by taking the sum of the intensities of all focal planes this problem can be omitted.

To see whether imaging in brightfield decreases the errors in determining the volume, the same beads where imaged using brightfield together with the same camera settings and the same focal planes (an example is shown in the top right montage in figure 12). The first noticeable problem is that all segmentation areas are very similar due to the low contrast with the background, even for focal planes where the bead is almost completely out of focus (for example the first image in the brightfield montage). For this reason, the segmentation of brightfield images are thought not to be a good measure for determining the volume. Another disadvantage of using z-stack brightfield images for cells is that they have to be generated separately from the z-stack fluorescence images. This increases the measuring time of each cell, decreasing the number of cells that can be measured or decreasing the temporal resolution (to allow for the extra time of generating the brightfield images).

The relative large uncertainty is due to the erratic segmentation, especially when the SNR is poor, for example as in the frame -2 in top right montage of figure 12. Based on the measurement using the beads, the method of interpolation and the method of assuming a shape and using the minor and major axis lengths do not significantly differ from each other. But, if the software can be optimized, the interpolation method might yield a more accurate results, especially when using different genetic backgrounds where the cells can grow in different shapes, for example due to stress a response. The brightfield images do not yield an accurate result due to the low contrast with the background noise, which is primarily notable when the beads are out of focus.

Therefore, determining the cell volume should be done using fluorescence images instead of the brightfield images and optimization of the software is expected to be able to result in a significant improvement of the determined volumes.

Defining a timepoint for determining the concentration

The intensity preferably needs to be determined at a specific timepoint of the cell cycle, so that less cells need to be measured to distinguish the distribution of the protein concentration and copy number (as discussed in section Model for protein concentrations in the Literature Review chapter). An easy recognizable timepoint is the Cdc42 polarization, but this makes estimating the concentration difficult. To explain this, first consider the situation where the cell is not polarized and the Cdc42 proteins are assumed to be homogeneously distributed throughout the cell. The concentration of the individual focal planes is then similar to the concentration in the entire cell. Thus, the ratio between the average intensity and the volume of the focal planes can be used to determine the concentration of the entire cell. However, when the concentration needs to be determined during polarization, the concentration in the focal planes is not necessarily similar to the intensity of the entire cell. An explanation for this is schematically visualized on the bottom left side of figure 13. In this figure, darker colors represent low fluorescence intensity, and the brighter colors, for example in the polarity cap on the top right of right cell, represent a high intensity. The focal planes where no polarization is present have a low average intensity as most Cdc42 proteins are located near the polarity cap. The intensity measured in these focal planes yield an underestimation of the actual concentration in the entire cell. Typically, only one or

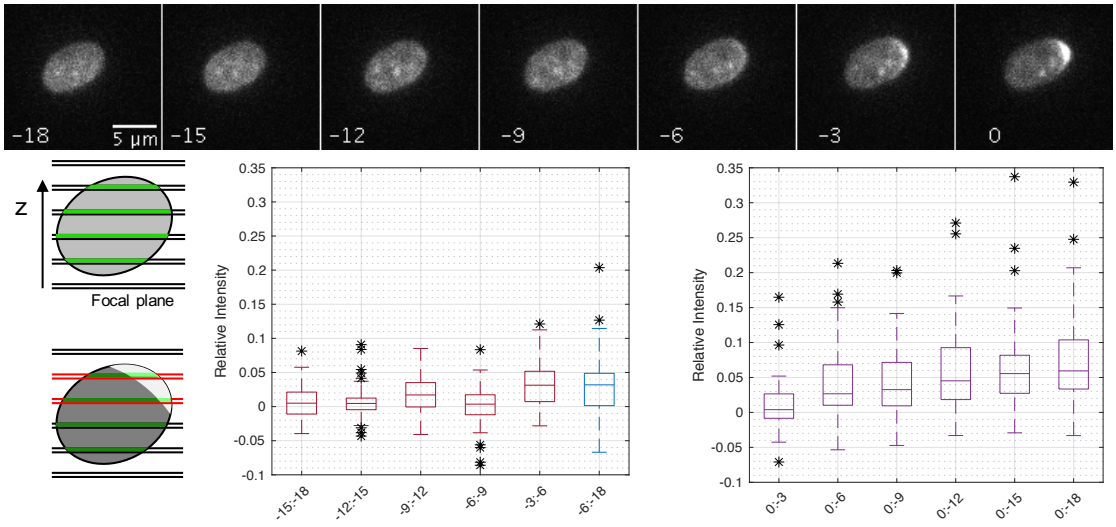

Figure 13: **Top**: Montage of an example measurement. The numbers represent the time before polarization is recognized by the software (defined as time point 0) and corresponds to the label in the boxplots below. **Bottom left**: Schematic representation of a cell with different focal planes of the microscope. The brightness of the grey and green colors corresponds with brightness as what would be seen in the images. The green and grey represent the fluorescence intensity that is respectively captured or missed by the microscope due to the finite width of the focal planes. The red focal planes indicate the planes that capture the polarity cap. **Bottom middle**: Box and whisker plot for the relative difference in intensity for subsequent frames. The labels correspond to the different frames before polarization (red box and whisker plots), for example as is shown in the montage on top. The final blue box and whisker plot represent the relative difference between timepoint -6 (right before polarization) and timepoint -18. **Bottom right**: Box and whisker plots for the relative difference between timepoint 0 and all previous frames. The black asterisks indicate outlier data, which is defined as a difference that is more than 1.5 times the width of the box above or below the box. About 40 cells are used for each box and whisker plot. The differences are determined such that a positive difference indicates an increase in intensity. For the labels, for example 0:-3 means the intensity of frame 0 minus the intensity of frame -3 divided by frame 0 (see also equation 3).

two focal planes capture the polarity cap (see for example the montage in figure 11). This means that a non-negligible part of the intensity of the polarity cap is not captured in the images, but instead is present in the part of the cell between the focal planes that is not measured (in the figure shown as the grey parts). This causes the focal planes that capture a part of the polarity cap to underestimate the concentration as well. The average intensity measured over all the focal planes during polarization therefore yield a too low concentration for the entire cell.

This might be solved by considering the polarity cap and the rest of the cell separately. However, this is coming with two problems. First, the segmentation of the polarity cap is not accurate, as the polarity cap is highly dynamic and does not have clear boundaries. Then the intensity needs to be interpolated over different focal planes to account for the parts of the cell that are not imaged. secondly, the local concentration of proteins in the polarity cap is relatively high. This means that within a single focal plane, many proteins might be present that are stacked up, so that the emitted light from one protein can be (partly) blocked by another protein. When the density of proteins is high, this effect might result in a measured intensity that is too low compared to the actual intensity emitted by all proteins. This would result in an unreliable measurement of the concentration.

An alternative method is by determining the concentration not during polarization, but just before the polarity cap occurs. However, the results from section Fluorescence intensity changes during the cell cycle hints that there is a slow increase in Cdc42 copy number until budding (see figure 10). This means that the calculated concentration is depended on when the intensity is measured. Also, there is some variability in the recognition of the polarization events by the software. This means that polarization can be assigned two or three timepoints (i.e. 6 to 9 minutes) after the polarization is visually observed. The question is what the difference is in the intensity between a time point right before polarization and during polarization to estimate the error made by using this approach. To approach this question, the summed intensities are determined from the frame where polarization is present and up to six frames before. Next, the relative difference in intensity between the subsequent frames is determined by using the

equation

$$\mathrm{d}I = \frac{I_i - I_{i-1}}{I_i} \tag{3}$$

where I_i is the summed intensity in frame i. The time point during polarization is defined as $i = 0$ (see the labels in the montage in figure 13) and a positive value indicates an increase in intensity. The results are shown as box and whisker plots in figure 13 where 40 cells are used to estimate the differences.

The middle graph shows the difference between all subsequent frames (red boxplots) and the difference between frame -6 and -18 (blue plot, largest difference for the considered frames where no polarization is present). The median between the values are all smaller than 3%. Only the difference between frame -3 and -6 is slightly larger since polarization starts around this time. The right graph shows the difference of all frames with respect to the frame where polarization is recognized. This shows that the difference in intensity increases as frames further back in time relative to frame 0 are compared, indicating an increase in intensity as the cell progresses towards polarization. This is in agreement with the results showed in figure 10. The measurements that result in large differences, shown as outliers in the box and whisker plots, are confirmed to be mostly caused by wrongly tracking of a cell causing the segmentation to jump from one cell to another and therefore measuring wrong intensities.

The relative difference in intensity between subsequent frames is typically not more than 5%. The variability in the recognition of the polarization event is therefore expected not to yield a large variance in the measured concentration. Using a timepoint before polarization should not matter as long as a fixed timepoint is defined for all cells to get an honest comparison between measurements. Some of the differences are significantly larger than the median values (up to 30%), but this is mainly due to segmentation errors and not due to a large fluctuation in intensity. With improvements of the software the number of outliers is expected to be reduced.

Protein concentration based on fluorescence intensity

Under the assumption that Cdc42 is homogeneously distributed in the cell, the Cdc42 concentration can be estimated by using the intensity measured in the focal planes before polarization. The volume of the part of the cells that is within a focal plane can be determined by measuring the area of the cell in the x-,y-direction (the area of the cell that is outlined using the segmentation software, see for example the montage in figure 11) and the known depth of the focal plane as calculated using equation 1. Using the volume of the cell V_{cell} and the volume of the focal planes $V_{focalplane}$ and the assumption that the fluorescent proteins are homogeneously distributed in the cell, the concentration C [$\mu\mathrm{m}^{-3}$] of the intensity in the cell can be determined by

$$C = \frac{N}{V_{cell}} = \frac{\alpha I}{V_{focalplane}} \tag{4}$$

where N is the Cdc42 copy number, which is linearly depended on the average of the measured fluorescence intensity I with a scaling factor α. This linear relation is assumed to hold for fluorescent proteins based on the experiment explained in section Relation between average pixel intensity and number of fluorescent sources.

In the top row of figure 14 the Cdc42 concentration and copy number are shown based on simulations [Daalman, unpublished results]. The concentration is determined using the simulated Cdc42 copy number and volume of the cell. The bottom left graph shows the experimentally determined concentration, based on 68 cells, by using the right part of equation 4. The concentration is determined from the measured intensity (for experimental setup and parameters of the microscope, see section Materials and Methods) and volume of the focal planes. Assuming a homogeneous distribution of Cdc42, the average concentration in the cell is determined by calculating the concentration of each individual focal plane by dividing the intensity by the volume of the focal plane. This is then averaged to get the concentration of the cell. The results for the concentration are scaled by the scaling factor α because this factor is not known. Since this scaling factor is expected to be constant for all cells, the distribution should look the same as is shown here (expect for some potential scaling along the x-axis). When the concentration is multiplied by α, the mean concentration would shift to different values that are expected to

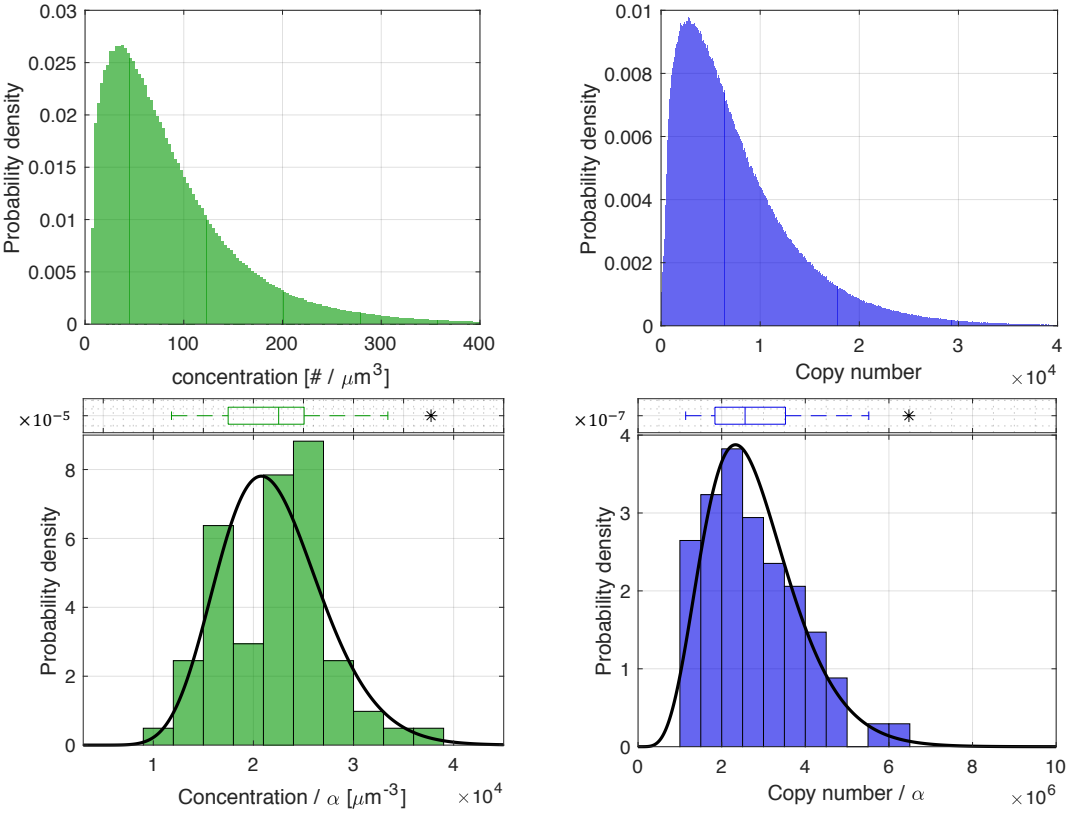

Figure 14: **Top left**: Ccd42 concentration based on a simulation of WT cells as determined during polarization. **Top right**: Cdc42 copy number based on a simulation of WT cells during polarization.**Bottom left**:Concentration based on the fluorescence intensities measured in the cells with a mean concentration $\overline{C} = 2.20 \cdot 10^4 \pm 5.19 \cdot 10^3$ μm^{-3}. A gamma distribution has been fitted with shape parameter $m = 17.72$ and scaling parameter $\theta = 1243$. **Bottom right**: Cdc42 copy number determined using the volume and the concentration of the cells with a mean value of $\overline{N} = 2.77{\cdot}10^6 \pm 1.13{\cdot}10^6$. The fitted gamma distribution has a shape parameter $m = 6.29$ and a scale parameter $\theta = 4.41 \cdot 10^5$.

represent the actual Cdc42 concentration. The simulation for the concentration is gamma distributed, which was expected based on a mathematical model [Friedman et al., 2006]. For the experimental results several distributions are plotted (see figure 20 and table 3 in the appendix Distribution fits). The null hypothesis is that the data distribution is not statistically different from the expected distribution and a high p-value (> 0.05) indicates that there is not enough evidence to reject the null hypothesis (the same as is used for the cell volume distribution). Due to the bimodal characteristic none of the distributions seem to have a proper fit, indicating that the data does not follow the proposed distributions, but only the loglogistic and lognormal have a p-value small enough to reject the null hypothesis. The poor fits are also apparent in the qq-plots where the lower bin count around $2 \cdot 10^4$ μm^{-3} is visible as a deviation from the diagonal line. The bottom left histogram in figure 14 shows a gamma distribution that is heuristically fitted over the data based on the expected distribution and the qq-plots. But, like as is discussed for the cell volume histogram, the limited number of datapoints used for determining the distribution might conceal the actual distribution.

When the scaling factor α is known and Cdc42 is homogeneously distributed, the actual copy number of Cdc42 can be determined using

$$N = \frac{V_{cell}}{V_{focalplane}} (\alpha I) \tag{5}$$

where the term $\frac{V_{cell}}{V_{focalplane}}$ can be regarded as an interpolation term to get the copy number in the entire cell based on the copy number determined in all the focal planes. When the concentration is determined based on the fluorescence intensity in the focal planes, this equation can be reduced to $N = V_{cell} \cdot C_{focalplane}$. The distribution of the Cdc42 copy number divided

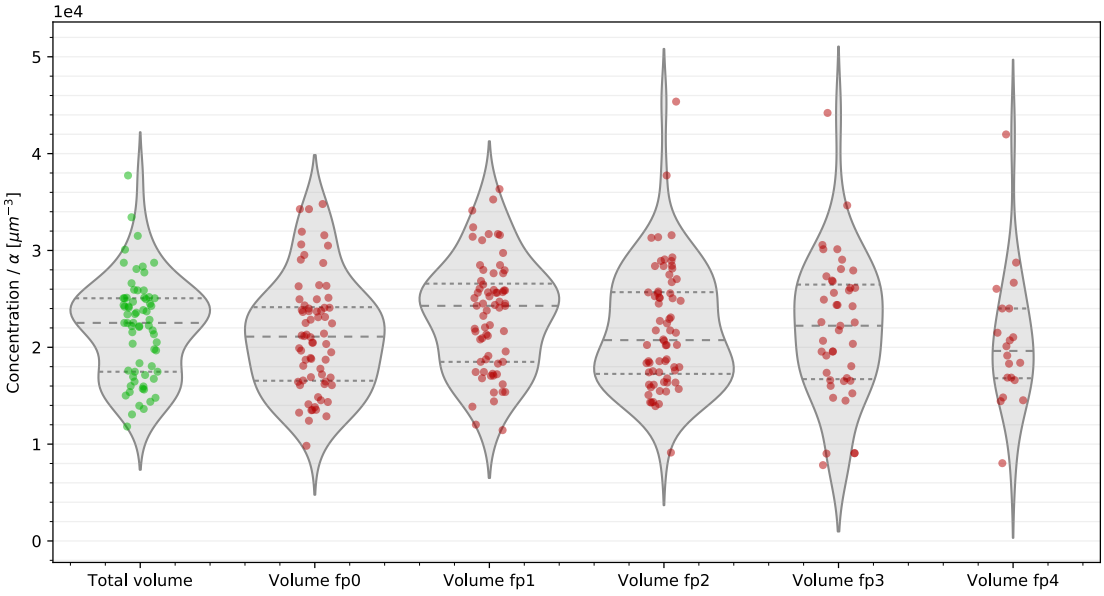

Figure 15: Violin plots for the Cdc42 concentration in the cells. The left, green, plot shows the concentration for the all focal planes in a cell and is equivalent to the bottom left histogram shown in figure 14. The scatter plot represents the measured concentration of individual cells. The horizontal dashed and dotted lines indicate the median value and the 25^{th} and 75^{th} percentile, respectively. The grey area represents the smoothed outline of the histogram of the data. (Note that the shape of the grey area correspond to the shape of the bottom left histogram in figure 14). The red plots represent the concentration measured for the same cells, but based on individual focal planes rather than the entire measured volume. The first focal plane (abbreviated in the figure to 'fp') in a cell is defined as 0 and the subsequent focal planes are numbered in ascending order. Note that the latter two violin plots have less data points (43 and 20, respectively compared to 68 for the other plots) as not all cells have more than 3 focal planes.

by the scaling factor is shown in bottom right graph in figure 14. The copy number of Cdc42 ($\overline{N} = 2.77 \cdot 10^6$) is three orders of magnitude larger as what is expected based on simulation (top right graph, mean copy number is 7752) and literature [Lawless et al., 2016] [Lahtvee et al., 2017] [Kulak et al., 2014].Based on these results and the current experimental setup and microscope settings (e.g. exposure time, gain, laser power), the scaling factor α is expected to be in the order of magnitude of 10^{-3}. This would mean that a signal is amplified by about 1000 times, but actual calibration measurements have to be performed in order to validate this hypothesis. (Possibilities in measuring this factor are described in the Future Work section). The fitted gamma distribution is based on the results from the χ^2-test and the qq-plots (see figure 21 and table 4 in appendix Distribution fits).

Using the described approach, the distribution for the protein concentration can be determined, despite the unknown scaling factor α. Based on the results discussed here, the α factor is in the order of magnitude of 10^{-3}. When the cell volume and the concentrations are known, the Cdc42 copy number can be calculated which might be used as a validating test since the copy number of Cdc42 has been studied before as is discussed in Model for protein concentrations section of the Literature Review chapter.

Table 1: Values for the median and 25^{th} and 75^{th} percentile concentrations for the Cdc42 concentration in different focal planes (abbreviated as 'fp') as determined from figure 15.

Concentration / α [μm^{-3}]	**Total**	fp0	fp1	fp2	fp3	fp4	**std**
Number of cells	*68*	*68*	*68*	*68*	*43*	*20*	
25th Percentile	17475	16545	18496	17254	16170	16803	749
Median	22520	21099	24282	20739	22227	19625	1483
75th Percentile	25063	24143	26572	25691	26474	24007	1017

Validating the assumption of a homogeneously distributed concentration

The concentration in the cell was determined in the previous subsection by calculating the average of the concentrations of all focal planes. This has the advantage of averaging out the concentration over multiple measurements which compensates for possible deviations in the measured intensity and/or area in individual focal planes. Since the concentration is determined before the onset of polarization, it is assumed that the Cdc42 concentration is homogeneously distributed throughout the cell. It therefore should not matter if the concentration is determined by considering all the focal planes, or when just a single focal plane is used. This can be used for checking to what extend the different focal planes of a cell agree in terms of concentration.

When the concentration is determined for a specific focal plane, the distribution is expected to be similar to the concentration distribution for another focal plane. This is shown in the violin plots in figure 15. The green left plot, labeled 'total volume', is used as a reference where the concentration is determined by considering all focal planes. This plot is equivalent to the bottom left histogram shown in figure 14. The volume that is calculated using the first focal plane that has a part of the cell in focus is defined as Focal Plane 0 (fp0). All subsequent focal planes are numbered in ascending order. Not all cells have more than three focal planes, so the number of measurements for the last plot is less than in the other plots. The median concentrations of all the focal planes seem to correlate with each other within the limits of the interquartile range (indicated with the dotted lines in each graph) (see also table 1). This indicates that the concentration, calculated for individual focal planes, agree with each other and that the assumption that Cdc42 is homogeneously distributed is reasonable.

Before the onset of polarization, the assumption that the Cdc42 concentration is homogeneously distributed throughout the cell is considered to be valid based on the obtained results. When the concentration is determined with all focal planes, the calculation is expected to be the most accurate as this method is less sensitive for missegmentation or miscalculation of the concentration in a single focal plane. However, if desired a single focal plane can be used for estimating the Cdc42 concentration. In this case it is recommended that a plane is chosen that images the cell near its center since the largest cross section area will be imaged and the SNR is expected to be highest of all focal planes.

Conclusion and Discussion

The results show a possible solution for protein quantification based on fluorescence imaging. The advantage of using fluorescence microscopy over other methods for determining the concentration and protein copy number is that with this technique cells can be selected based on their phenotype. This work discussed the results from segmentation software that is developed for automatically detecting and tracking cells over time periods of many hours based on fluorescence imaging. This allows for measuring certain parameters of the cell like the fluorescence intensity, shape of the cell, its volume and the timepoints of budding and polarization events.

Another possible method for protein quantification based on fluorescence intensity is by imaging flow cytometry which has the advantage of being able to image many cells in a single experiment [Newman et al., 2006], but with this method it is not possible to track single cells over time. Using flow cytometry does also not allow for controlling at which timepoint in the cell cycle the cells are measured. During a single experiment all timepoints are likely to be present and in the results discussed here it was shown that the Cdc42 intensity fluctuates throughout the cell cycle. Because the fluctuations in intensity are expected to become insignificant when many cells are measured, flow cytometry is still a suitable approach for determining protein concentration. But the proposed method using fluorescence microscopy allows for more control and more information can be extracted, for example the cell volume and temporal information about the different stages of the cell cycle.

Fluorescent labeling might influence the copy number of the tagged protein as a part of the protein is blocked by the fluorescent protein. This effect was observed in a meta analysis that looked at the results from protein quantification studies using fluorescent labeling, typically with GFP. They noticed that in about 12% of the proteins present in budding yeast there is a difference in the copy number of proteins labeled with a fluorescent tag and other methods, for example mass spectroscopy [Ho et al., 2018]. But it is not known if tagging with other fluorescent proteins, for example mNG, also influences the Cdc42 copy number in the cell.

One of the steps in the discussed method is determining the cell volume which did not prove accurate enough for reliably determining the concentration. An alternative method for measuring the cell size is by using cell analyzers, as for example is used in [Bryan et al., 2010]. But this method does not allow for measuring the cell size in between or after microscopy imaging as the cells need to be recovered from the imaging plate to be placed in the cell analyzer. Also, since microscopy uses a low concentration of cells that are bound to the surface of the imaging plate, recovering enough cells for cell analyzers is not possible. Another alternative is by simply assuming that the cell shape represents an ellipsoid of which the volume can be calculated using the length of the major and minor axis, both which can be determined with the discussed method.

For segmenting the cells from fluorescence microscopy images, the neural networks method proves to be a reliable approach. But, images with a low SNR are not always segmented properly since the software tends to outline an area that is bigger than the area of the cell in that frame. This gives a significant error in calculating the cell volume since this is calculated by interpolating the segmented areas from all the focal planes. This was expected based on the results from the z-stack images from the cells and was later confirmed using fluorescent beads where again the segmented area is consistently too large. Using brightfield images did not improve the outlined area due to the low contrast with the background. Brightfield images should therefore not be used for determining the cell volumes.

In order to quantify proteins based on fluorescence intensity, the relation between the number of fluorescent sources and the intensity is determined. This relation is shown to be linear as

determined by measuring the average intensity of 1 to over 100 fluorescent beads. The measurement was performed for beads that were well separated from each other over the entire image, something that is not true for the proteins. In a single focal plane, many proteins are present (order of magnitude of 100 proteins) which might overlap in the z-direction, blocking the light from other proteins causing this light not to be captured by the camera. Despite the possible overlap it is assumed that this effect does not play a significant role and that the linear relation holds when imaging many fluorescent proteins that are close together.

This measurement also showed that the background illumination from the microscope is not homogeneous. The illumination shows vignetting where in the corners of the image the illumination is less than half of the intensity compared with the illumination in center of the image. Therefore, a background correction is applied by dividing the images by the normalized background illumination that was measured using a homogeneous fluorescent microscope slide for calibration. However, the correction for the images taken with the beads or cells proved not to be properly corrected. Other corrections have to be implemented for proper illumination correction. Different methods have been analyzed before that might result in a better correction[Model and Burkhardt, 2001] [Tomaževič et al., 2002].Since the applied correction did improve the illumination, it was still used for the measurements. Also, the cells were positioned near the center of the image to minimize the effects of inhomogeneous illumination (the vignetting was negligible near the center of the image). Better correction should be determined, especially when multiple cells are present in a single image since not all cells can then be placed in the center of the image.

With the segmentation results, budding and polarization events can be automatically detected. An important step in this procedure is tracking of single cell over time. This is done applying constraints for the cell area, intensity and the relative location with respect to different time frames. By checking 138 cells, the software showed to be about 70% accurate. Most errors came from situations were multiple cells were close together and the cell tracker confused two cells with each other. This caused the segmentation to jump from one cell to the other between frames and therefore measuring wrong intensities and sizes. Those situations were ignored for measuring the cell volumes and concentrations. This could potentially be improved by also using neural networks for cell tracking instead of only using it for cell segmentation. Budding recognition proved to be relatively accurate, recognizing buds in almost all cases. But, also in this case, when two cells are close together, the software tend to assign budding events of one cell to another, nearby cell. This problem can partly be avoided during microscopy by selecting cells that are well separated from each other. However, this does not solve the problem for situations where the cell has produced daughter cells who typically remain close to the mother cell. By adding more/other constraints to the software for tracking cells, this error might be reduced and thereby increasing the accuracy and reliability of the software.

Polarization events are determined by taking the frame where the coefficient of variance for the summed intensity is maximum. This is in general a reliable method for recognizing polarity events which was also proven by other studies (for example [Lai et al., 2018]). However, it recognized polarization typically one to three frames (i.e. three to nine minutes) after initial onset could be visibly observed. For determining the Cdc42 concentration based on fluorescence intensity it is important to know when the cell polarizes to ensure all cells are measured during the same part of their cell cycle. Since a homogeneous Cdc42 distribution is required for accurately determining the concentration, a frame before onset of polarization is preferred. Due to the fluctuations in accuracy for recognizing the timepoint of polarization between measurements, up to the sixth frame before polarization is recognized is taken to determine the Cdc42 concentration. This is done to counterbalance fluctuations in recognition to ensure a frame is used where the cell has not established a polarity cap yet. This results in some spread in the timepoint of the cell cycle which is used for measuring the concentration and cell volume. It was shown that the difference in the summed intensity between subsequent frames is on average not more than 5%, so for the results that are discussed the fluctuations in the timepoints are ignored. But this could be improved by making the polarization recognition more robust that should result in better comparable results. This can be done by calculating more parameters besides the coefficient of variance. For example a kymograph can be made that shows the location(s) in the cell where a relative high intensity is measured (similar to [Lai et al., 2018] or [Kaksonen et al., 2003]). This

is discussed in more detail in the Future Work chapter.

The preparation for microscopy includes coating the imaging plate with the chemical ConA for immobilization of the cells. When the cells are added the imaging plate is centrifuged to spin down the cells, fixating them to the imaging plate. This ensures that the cells are all in the same focal plane and do not drift from their initial location. When the cells divide, the daughter cells are not necessarily stuck to the ConA and they can grow or drift out of focus of the objective. These cells should be ignored during analyzing since the measured intensity does not correspond to the actual intensity. With the constraints that are placed regarding the intensity (i.e. cells should have a minimum intensity in order to be analyzed), most of these cells were successfully ignored. When not successfully ignored, this is now done manually but this should be improved before applying the software to large datasets where manually checking the results is not feasible anymore. In a few occasions, budding is observed to be top or bottom of the mother cell. This has the disadvantage that volume and concentration calculation become unreliable and these situations were ignored as well. To prevent this, it might be possible of using Agar pads instead of ConA for immobilizing the cells (as used in for example [Wu et al., 2013]). This typically require microscopy slides with a thin groove where heated liquid agarose can be poured in. Once cooled down, the agarose becomes a polymer with a porous structure. Cells placed on the agar pads are not 'glued' to the imaging slide as with ConA but are still mostly immobilized as the cells cannot drift through the porous structure. This might prevent the buds to grow on top or bottom of the mother cell, making determining the concentration and volume easier.

Using the measured intensity and the estimated cell volume, the concentration and protein copy number can be determined. However, this requires a constant factor that relates the intensity to the actual protein copy number. This factor suggests what the intensity of a single fluorescent protein is as captured by the camera using specific settings of the microscope. Some measurements for determining this constant were attempted, but proved not to be successful (explained in more detail in the Future Work section). Therefore, the resulting concentrations and protein copy number that are shown are all divided by this constant factor and the actual numbers for the concentrations and copy numbers could not directly be compared with literature values. But, if this factor is really a constant, it only shifts the distributions but does not change the way the data is distributed. For this reason, the results could be compared with the simulation, but not to literature values.

Future Work

An important step in the development of software is the validation of the results. This step is not considered in detail in the work that is presented here and therefore the first priority should be performing validation steps. One step in validation could be measuring cells of the same strain as used for the results discussed here, but with different galactose concentrations. An increase in galactose concentration should increase the number of Cdc42 proteins and therefore a shift to higher values for the distribution for the concentration and Cdc42 copy number is expected.

Changes to the software for tracking a single cell (especially when two cells are close together) and for detecting budding and polarization events should be made to make it more reliable. This could mean adding constraints for assigning budding events to a cell or implementing new methods for cell tracking. Also, more measurements should be analyzed using the software to see if the histograms eventually follow the expected distributions. For the discussed results, typically 68 measurements were included which do not clearly show the patterns in the distributions. Based on the simulations, over 100 datapoints are needed to see the true distributions for the cell volume, protein concentration and copy number.

This report mainly focusses on the temporal information, but segmentation software allows for determining spatial information as well. An intensity kymograph plot can be made (similar to figure 4 in [Lai et al., 2018] or figure 3 in [Kaksonen et al., 2003]) which adds information about the location of Cdc42 localization. When measured as a function of time this shows the spatial dynamics of the Cdc42 localization. A possible method is by defining a thin line from the center of a cell to the segmented edge along which the intensity is determined. This line can then be rotated by a small angle after which the intensity along the line in this new position is determined. This step can be repeated until it made a full circle which yields a plot for the intensity as a function of angle. For example, for each angle the maximum intensity can be determined. This can be measured for a single cell during multiple cell cycles where the x-axis represents the time, the y-axis the angle of rotation and a color gradient can be used to represent the measured intensity. This shows the timepoint and location of the occurrence of a polarity cap which can be used for defining the onset of polarization in the recognition software.

After validation, different genetic backgrounds could be measured, for example Bem1Δ and Bem1ΔBem3Δ cells. The concentration distribution of Bem1Δ are expected to be similar to the distribution for the measured WT cells but with a higher average concentration. Since a Bem1Δ background requires a larger copy number of Cdc42 to survive, it is expected that a significant proportion of the cells do not survive as they do not have enough Cdc42 proteins. This would result in a distribution for the Cdc42 concentration in which the lower concentrations are absent. For the Bem1ΔBem3Δ cells the average concentration is expected to be in between that of WT and Bem1Δ cells. Also, lower Cdc42 concentrations, compared with the Bem1Δ cells, are expected to be present in the distribution of these cells.

As mentioned before, in order to get the actual concentrations from the measured fluorescence illumination, a constant scaling factor should be determined to relate the measured intensity to the number of fluorescent sources. If known, this potentially also allows for determining the production rate of Cdc42 using time lapse imaging, as is discussed in the section Fluorescence intensity changes during the cell cycle. A measurement is performed for determining this constant by using specific concentrations of purified mNG from which the number of mNG molecules can be estimated. When the concentrations are imaged in the microscope with the same settings as was used for imaging the cells (most importantly gain, exposure time and laser power), the intensity of a single mNG molecule can be calculated. It has been tried to determine this constant factor

using this approach, but the measurements did not prove to be reliable. Different concentrations were made by diluting 40 μM of mNG 5, 10, 50, 100 and 10^4 times in TAE buffer. Of each concentration, 10 μL was pipetted in separate wells of a 96-well plate and shaken to get an even distribution of liquid in the well. This was placed in 50°C for a few hours to let the TAE evaporate which should then result in a homogeneously distributed layer of mNG. However, when measured this never gave a homogeneous layer and therefore it is unknown how many proteins were actually being imaged. Different locations in a single well resulted in varying intensities that differed more than a factor 100. Either the protocol for this experiment has to be optimized to get an evenly distributed layer (i.e. the intensity of the measured proteins should be similar throughout a sample) or a different experiment needs to be designed.

If the discussed protocol can be optimized to give reliable results, a validation measurement could be performed, again using a homogeneously distributed layer of fluorescent proteins. The average intensity within an area of this layer needs be determined by imaging the sample with the same microscope settings as is used for imaging the cells. A small volume in this layer should then be bleached, causing a decrease in the average intensity. If the bleached volume is known and the fluorescent proteins are evenly distributed, the amount of bleached proteins can be calculated. The drop in intensity should then relate to the intensity of the amount of bleached proteins. Besides this validation, it is also possible to bleach individual proteins, rather than a small volume, where the loss of intensity directly relates to the intensity of a single fluorescent protein. However, this method requires a specialized setup and an accurate protocol optimized for the used fluorescent protein [Coffman and Wu, 2012] [Joglekar et al., 2008]. This would also add another problem as the measured intensity from this setup needs to be translated to the setup for the SDM.

Pseudocodes

A pseudocode is presented for the segmentation (Algorithm 1) and recognition (Algorithm 2 and 3) software. Lines that are shown in blue belong to preexisting code. Underlined words indicate variables and and italics indicate comments. Both the segmentation and the recognition algorithms use an options file which includes the path to the location of the images that need to be analyzed, paths to correction files (e.g. background noise and illumination), and some settings for showing and/or saving specific information from the code.

Figure 16 shows schematically the workflow of the most important part of the software (e.g. plotting of figures are not included in this figure). The input of the software consists of the images from the microscope where the intensities of the z-stack images are summed. The summing of intensities of the z-stack images is important to reduce the number of images that need to be analyzed. (For example, an 8-hour measurement with a time resolution of 3 minutes and 9 z-stack steps yields 1440 images. By summing the 9 z-stack images, this reduces to 160 images). The summed images are used for segmentation, tracking and determining the polarization and budding events of the cells. When a specific timepoint of interest is defined, for example onset of polarization, the software takes the corresponding z-stack image of that single timepoint (typically consisting of 9 or 11 images). These z-stack images then have to be segmented again after which the cell volume, protein concentration and protein copy number can be calculated. After recognition of the cells, some parameters are stored in text files. The most important parameters are the x-, y-coordinates of the location of the cell in the image, the area, mean and summed intensity, standard deviation in the intensity and the coefficient of variance.

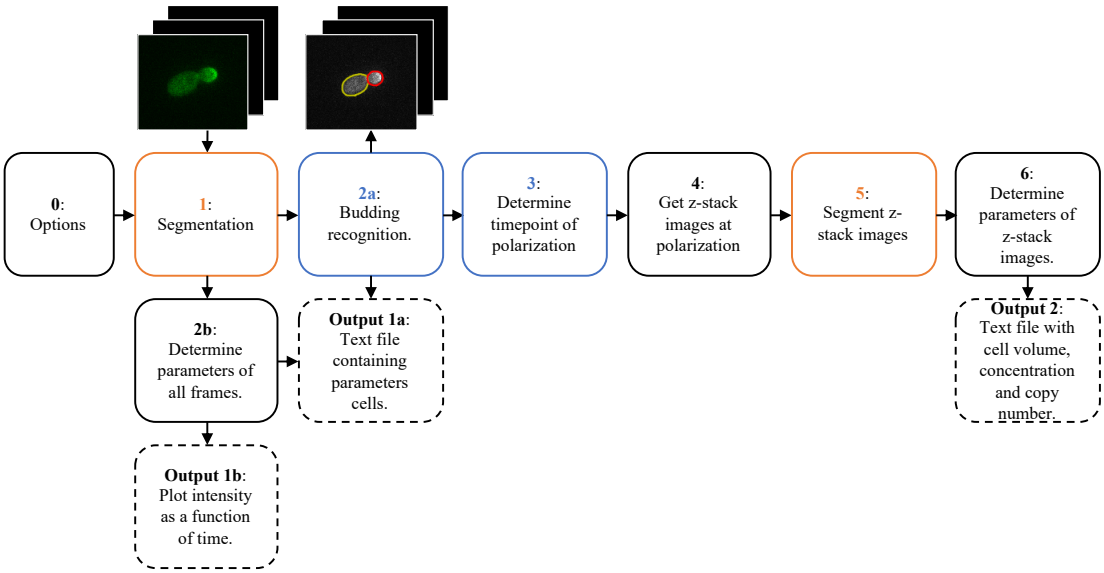

Figure 16: Schematic overview for the workflow of the software. The microscopy images and a file with options are the input of the software. Dashed outlined boxes are the output of the software and boxes that have the same color are integrated in the same part of the code. The code for the orange boxes is shown in algorithm 1 and the blue boxes are shown in algorithm 2 (which includes algorithm 3).

Algorithm 1 Cell Segmentation

Input:
Input directory containing the data from the microscope in the form of *.tif* movies.
Output:
For each frame in a movie in the input directory, a mask file is created that is stored in an output directory.

```
Options ⟵ open options file
InputDirectory ⟵ read path to input directory containing all movies
OutputDirectory ⟵ read path to output directory for storing the masked images

if OutputDirectory does not exist then
    Create output directory at location OutputDirectory
end if

for all Movie in InputDirectory do
    procedure READ FRAMES(FramesInputDirectory, Movie)
        if FramesInputDirectory does not exist then
            Create FramesInputDirectory in InputDirectory
        end if
        for all Frames in Movie do
            Save Frame as .tif image in FramesInputDirectory
        end for
    end procedure

    procedure PREPROCESS IMAGES(FramesInputDirectory, RgbOutputDirectory)
        for all Frames in FramesInputDirectory do
            if in Options MaxNumberFrames ≠ 0 then
                Consider only Frames 1 to MaxNumberFrames   ▷ If MaxNumberFrames = 0, then all Frames are considered
            end if
            RgbImage ⟵ Convert 16bit Frame image to rgb image
            if RgbOutputDirectory does not exist then
                Create RgbOutputDirectory in OuputDirectory
            end if
            Save preprocessed RgbImage to RgbOutputDirectory
        end for
    end procedure

    procedure NEURAL NETWORK(RgbOutputDirectory)
        for all RgbImages in RgbOutPutDirectory do
            Run RgbImage through pretrained neural network
            while new cell is found do
                PixelIndex ⟵ indices for all pixels in found cell
                Save PixelIndex in csvFile
            end while
            Append name of RgbImage to pixel indices in csvFile   ▷ Append name so that in the next function, the pixel indices are taken that correspond to the right image
        end for
    end procedure

    procedure CONVERT TO MASK(csvFile)
        LoopCounter = 1
        for all PixelIndex in csvFile do
            MaskImage ⟵ array with with same size as Frame where all entries have value 0
            for all indices in where MaskImage == PixelIndex do
                Set value equal to LoopCounter
                LoopCounter = LoopCounter + 1
            end for
            if MaskOutputDirectory does not exist then
                Create MaskOutputDirectory in OutputDirectory
            end if
            Save MaskImage to MaskOutputDirectory
        end for
        Remove RgbOutputDirectory
    end procedure
end for
```

Algorithm 2 Cell recognition until budding

Input:

Input directory containing the data from the microscope in the form of .tif movies.
Output directory containing a folder with the same name as the data and within this folder is a folder with all the mask images ▷ *This is generated by algorithm 1*

Output:

In the output directory, separate directories are created for each cell found in the first frame of the movie. In these directories, all the frames are stored and in these frames one cell is tracked until budding is detected. A text file is created for each cell to store some information like position, cell size and fluorescent intensity.

```
Options ⟵ open options file
InputDirectory ⟵ path to input directory containing all movies
OutputDirectory ⟵ read path to output directory for storing the masked images
MaskOutPutDirectory ⟵ path to output directory for masks

for all Movie in InputDirectory do
    procedure READ FRAMES(FramesInputDirectory, Movie)
        if FramesInputDirectory does not exist then
            Create FramesInputDirectory in InputDirectory
        end if
        for all Frames in Movie do
            Save Frame as .tif image in FramesInputDirectory
        end for
    end procedure

    procedure NUMBER OF CELLS(MaskOutputDirectory)
        for all MaskImage in MaskOutputDirectory do
            N ⟵ Count total number of cells in MaskImage
        end for
    end procedure

    for CellNumber in range 1 to N do
        procedure BUDDING RECOGNITION(FramesInputDirectory, MaskOutputDirectory, CellNumber)
                                                          ▷ See Algorithm 3
        end procedure
    end for

    if TextFile does not exist then
        Create TextFile in OutputDirectory                ▷ Store polarization information
    end if
    Save timestamp and name ImFluorescent to TextFile     ▷ ImFluorescent is a variable from procedure
BUDDING RECOGNITION
    if Daughter cell is found then
        Save frame where polarization is found to TextFile
        Save area and mean intensity to TextFile
    else
        Save area and mean intensity of FramePolarization to TextFile   ▷ FramePolarization is
a variable from procedure BUDDING RECOGNITION. Leave area and mean intensity empty so that it is clear
that this cell is calculated, but no bud is found
    end if
end for
```

Algorithm 3 Budding recognition

```
procedure BUDDING RECOGNITION(FramesInputDirectory, MaskOutputDirectory, CellNumber)
    for all MaskImage in MaskOutputDirectory do
        ImMask ⟵ open MaskImage
        ImFluorescent ⟵ open corresponding fluorescent image from FramesInputDirectory

        procedure IMAGE CORRECTIONS(ImFluorescent)
            Noise ⟵ open background noise image from path in Options
            Illumination ⟵ open background illumination image from path in Options
            IlluminationNormalized ⟵ Illumination / (max value Illumination)
            ImFluorescent = ImFluorescent - Noise
            ImFluorescent = ImFluorescent / IlluminationNormalized
        end procedure

        if ImFluorescent is first frame in FramesInputDirectory then
            if ContourOutputDirectory does not exist then
                Create ContourOutputDirectory at location OutputDirectory
            end if
            CellMask ⟵ get mask of cell represented by CellNumber
            CellFluorescent ⟵ get cell represented by CellNumber in ImFluorescent
            Determine pixels that have a neighbouring pixel that has the value 0 in CellMask   ▷ Determine contour by looking for pixels that have a neighbour that belongs to the background
            Draw yellow contour around CellFluorescent
            Save ImFluorescent with contour around CellFluorescent to ContourOutputDirectory
            PositionCellOldFrame ⟵ coordinates of center of CellMask
            Determine parameters of CellFluorescent ▷ parameters can be the area, mean intensity, coefficient of variance etc.
            Save center position and parameters to .txt file in ContourOuputDirectory
            NumberOfCellsOldFrame ⟵ get number of cells in ImFluorescent
        else
            NumberOfCellsCurrentFrame ⟵ get number of cells in ImFluorescent
            for all Cell in new frame do
                PositionCellNewFrame ⟵ get center coordinates Cell
                Determine Pythagorean distance between PositionCellNewFrame and PositionCellOldFrame
            end for
            CellNumber ⟵ get Cell with minimum distance   ▷ assume that minimum distance corresponds with the same cell as the previous frame
            CellMask ⟵ get mask of cell represented by CellMask
            CellFluorescent ⟵ get cell represented by CellMask in ImFluorescent
            PositionCellOldFrame ⟵ coordinates of center of CellMask
            Determine parameters of CellFluorescent
            Save center and parameters to .txt file in ContourOuputDirectory
            if NumberOfCellsCurrentFrame > NumberOfCellsOldFrame then
                for all Cell in ImFluorescent do
                    if Cell is not CellFluorescent then
                        Get center position and mean intensity of Cell
                        DifferencePosition ⟵ center position Cell - center position CellFluorescent
                        DifferenceIntensity ⟵ mean intensity Cell - mean intensity CellFluorescent
                        if DifferencePosition <= 30 and DifferenceIntensity >= 0.1· CellFluorescent then
                            DaughterCell ⟵ Cell   ▷ Cell is recognized as daughter cell
                            Save center position, area and mean intensity to .txt file in ContourOutputDirectory
                            FramePolarization ⟵ search in .txt file where coefficient of variance in CellFluorescent is highest
                            Draw red contour around DaughterCell
                            Draw yellow contour around CellFluorescent   ▷ CellFluorescent is assigned as mother cell
                            return FramePolarization, path to .txt file in ContourOutputDirectory, name ImFluorescent
                        else
                            Draw yellow contour around CellFluorescent
                        end if
                    end if
                end for
            else
                Draw yellow contour around CellFluorescent
            end if
        end if
        NumberOfCellsOldFrame ⟵ NumberOfCellsCurrentFrame   ▷ NumberOfCellsOldFrame is updated with the number of cells in current frame for the next for loop
    end for
end procedure
```

Fluorescence intensity changes during the cell cycle - figures

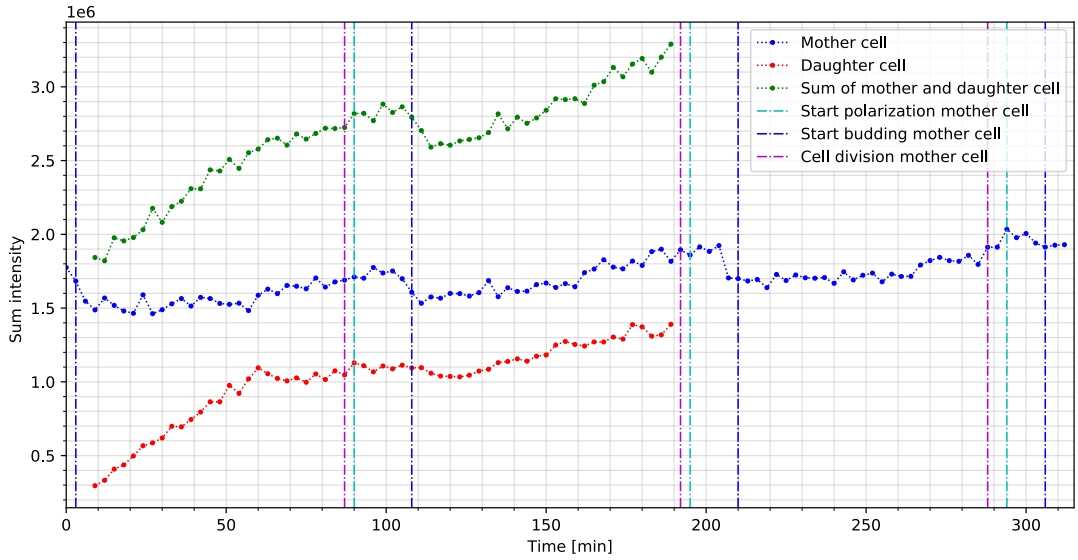

Figure 17: This graph is similar to figure 10. The blue line shows the summed intensity of the mother cell and the red line represents the daugther cell. The combined intensity of the mother and daughter cell is indicated by the green line. Vertical lines are shown to indicate distinctive events of the mother cell. Note that the mother was already polarized at the beginning of the measurement, thus the first event is budding instead of polarization.

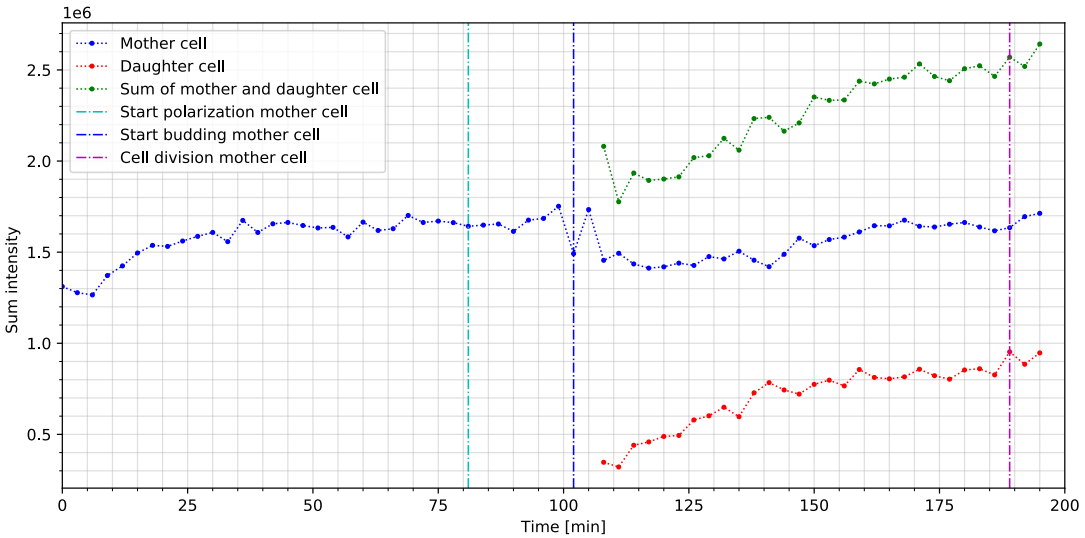

Figure 18: Similar to figure 10 and 17. In this case the mother cell needs over 80 minutes for its first polarization.

Distribution fits

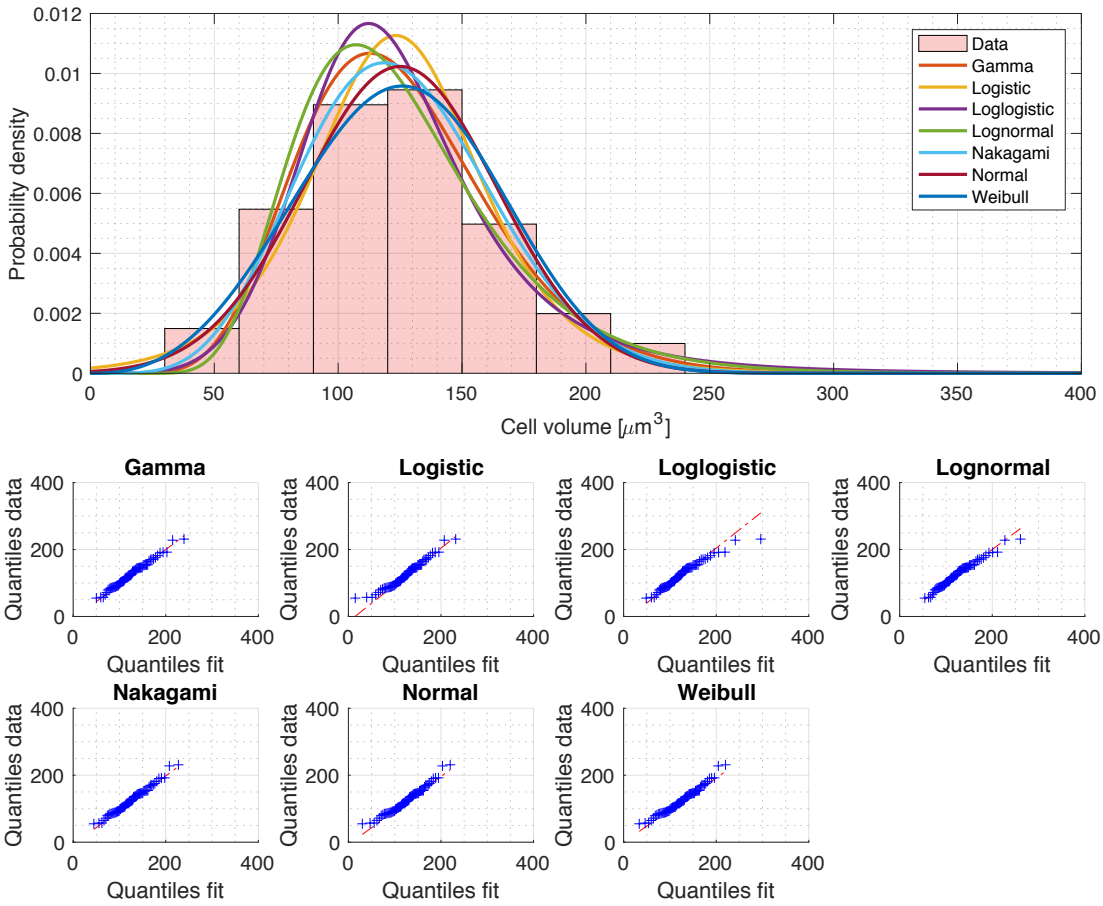

Figure 19: **Top**: Histogram for the cell volume with different distribution fits. **Bottom**: qq-plots for the distributions fitted in the histogram. The x-axis represents the quantiles of the distribution model and the y-axis represent the quantiles of the data. The red line follows the equation $y = x$ which indicates the ideal situation where the data fits the model perfectly. For the numerical data of the tests, see table 2.

Table 2: Values of the χ^2 and Anderson-Darling (AD) statistical test to determine the best fit for the cell volume histogram. With the Anderson-Darling test, not all distributions could be obtained, therefore only a limited number of tests are shown. The graphical representation of the distributions are shown in figure 19. There are 68 data points used. None of the distributions show a p-value that would indicate that the null hypothesis (i.e. the data is not statistically different from the distribution) should be rejected.

Concentration	χ^2			Anderson-Darling		
	Statistic value	p-value	DoF	Statistic value	p-value	cv
Gamma	3.7011	0.4480	4			
Logistic	5.7456	0.3318	5			
Loglogistic	5.4189	0.1436	3			
Lognormal	4.3747	0.2237	3	0.3393	0.4939	0.7430
Nakagami	3.5866	0.6103	5			
Normal	4.5923	0.4676	5	0.4050	0.3480	0.7430
Weibull	4.5959	0.4672	5	0.4306	0.3128	0.7506

Table 3: Values of the χ^2 and Anderson-Darling (AD) statistical test to determine the best fit for the Cdc42 concentration histogram. None of the of the distributions show a particularly high p-value in both the χ^2-test and AD-test. Only the loglogistic and lognormal distributions have a p-value that rejects the null hypothesis and therefore conclude that the data is statistically different from the distribution. The low p-values can partly be explained by the bimodal character of the histogram. Based on literature a gamma distribution is expected which might follow after more measurements.

Concentration	χ^2			Anderson-Darling		
	Statistic value	p-value	DoF	Statistic value	p-value	cv
Gamma	8.0196	0.0909	4			
Logistic	5.8720	0.1180	3			
Loglogistic	9.8881	0.0195	3			
Lognormal	9.5181	0.0231	3	1.2256	0.0031	0.7432
Nakagami	6.6203	0.0850	3			
Normal	5.3788	0.1461	3	0.7314	0.0535	0.7432
Weibull	6.0083	0.1985	4	0.7407	0.0530	0.7507

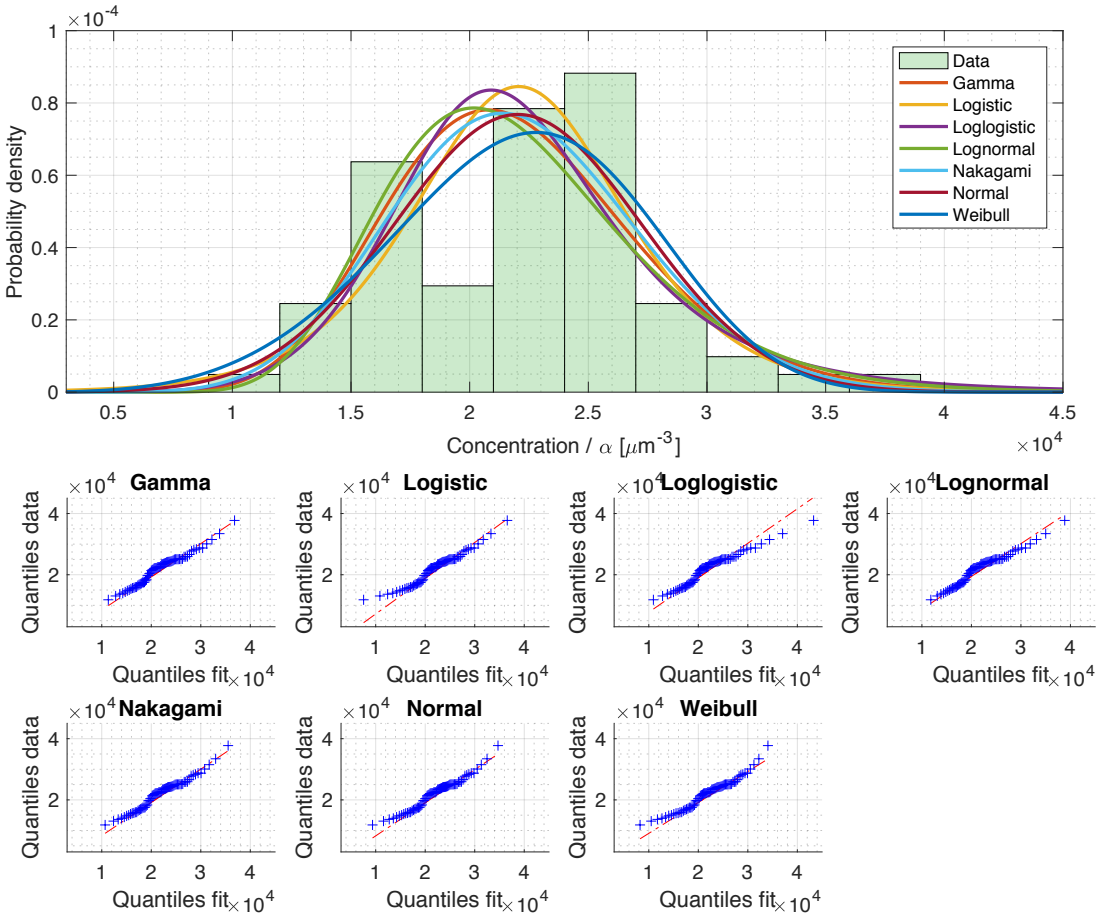

Figure 20: **Top**: Histogram for the Cdc42 concentration with different distribution fits. **Bottom**: qq-plots for the distributions fitted in the histogram. The x-axis represents the quantiles of the distribution model and the y-axis represent the quantiles of the data. The red line follows the equation $y = x$ which indicates the ideal situation where the data fits the model perfectly. In all plots a positive deviation from the red line can be observed that is due to the bimodal character of the histogram. For the numerical data of the tests, see table 3.

Table 4: Values of the χ^2 and Anderson-Darling (AD) statistical test to determine the best fit for the Cdc42 copy number histogram. The graphical representation of the distribution is shown in figure 21. Due to the positive skewness of the histogram, the null hypothesis of the normal distribution should be rejected according to the AD-test, but not according to the χ^2-test.

Concentration	χ^2			Anderson-Darling		
	Statistic value	p-value	DoF	Statistic value	p-value	cv
Gamma	2.8802	0.5781	4			
Logistic	2.2833	0.5157	3			
Loglogistic	4.4771	0.2143	3			
Lognormal	3.7995	0.2839	3	0.4143	0.3309	0.7432
Nakagami	1.9782	0.7398	4			
Normal	1.8083	0.7710	4	0.8974	0.0205	0.7432
Weibull	0.6019	0.9075	4	0.6019	0.1181	0.7507

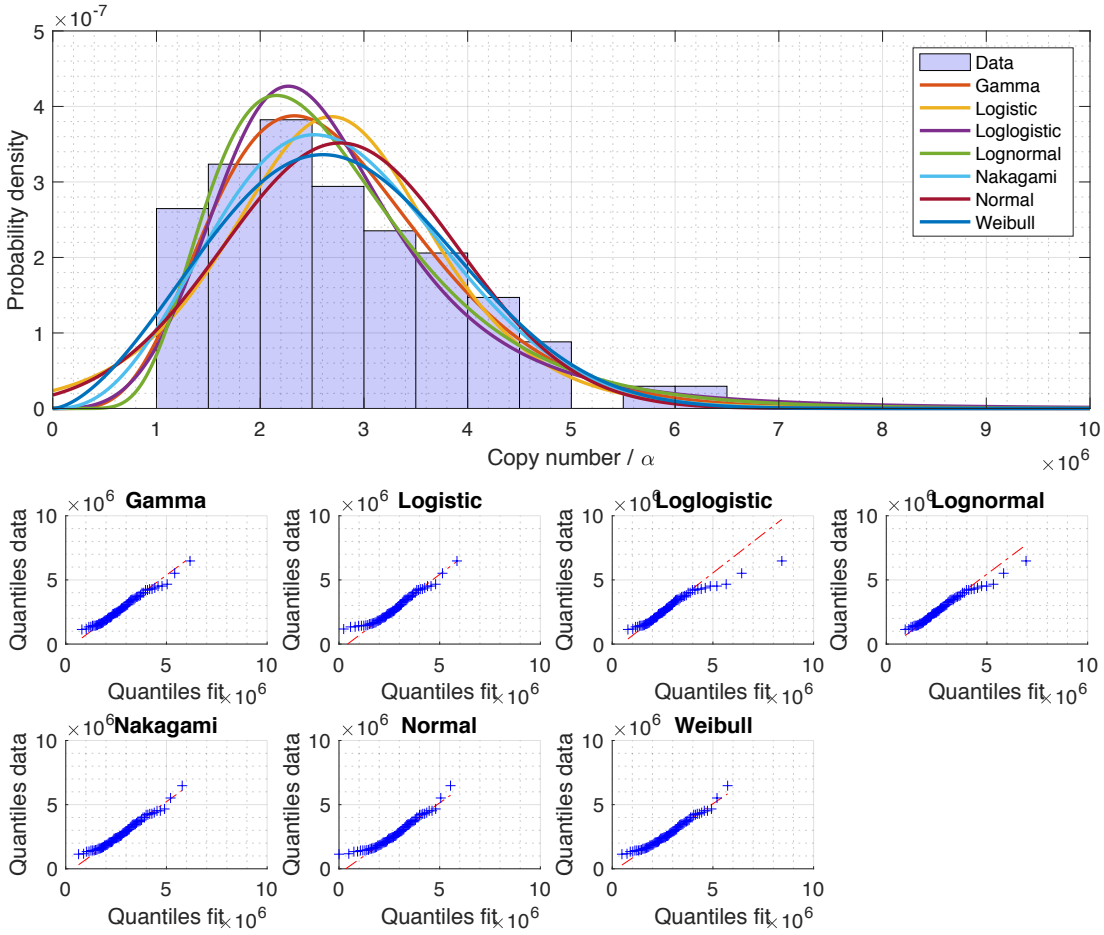

Figure 21: **Top**: Histogram for the Cdc42 copy number with different distribution fits. **Bottom**: qq-plots for the distributions fitted in the histogram. The x-axis represents the quantiles of the distribution model and the y-axis represent the quantiles of the data. The red line follows the equation $y = x$ which indicates the ideal situation where the data fits the model perfectly. For the numerical data of the tests, see table 4.

Bibliography

[Acar et al., 2008] Acar, M., Mettetal, J. T., and Van Oudenaarden, A. (2008). Stochastic switching as a survival strategy in fluctuating environments. *Nature genetics*, 40(4):471.

[Adams et al., 1990] Adams, A., Johnson, D. I., Longnecker, R. M., Sloat, B. F., and Pringle, J. R. (1990). Cdc42 and cdc43, two additional genes involved in budding and the establishment of cell polarity in the yeast saccharomyces cerevisiae. *The Journal of cell biology*, 111(1):131–142.

[Adams and Pringle, 1984] Adams, A. and Pringle, J. R. (1984). Relationship of actin and tubulin distribution to bud growth in wild-type and morphogenetic-mutant saccharomyces cerevisiae. *The Journal of cell biology*, 98(3):934–945.

[Ayscough et al., 1997] Ayscough, K. R., Stryker, J., Pokala, N., Sanders, M., Crews, P., and Drubin, D. G. (1997). High rates of actin filament turnover in budding yeast and roles for actin in establishment and maintenance of cell polarity revealed using the actin inhibitor latrunculin-a. *The Journal of cell biology*, 137(2):399–416.

[Baker et al., 2010] Baker, S. P., Phillips, J., Anderson, S., Qiu, Q., Shabanowitz, J., Smith, M. M., Yates 3rd, J. R., Hunt, D. F., and Grant, P. A. (2010). Histone h3 thr 45 phosphorylation is a replication-associated post-translational modification in s. cerevisiae. *Nature cell biology*, 12(3):294.

[Bar-Even et al., 2006] Bar-Even, A., Paulsson, J., Maheshri, N., Carmi, M., O'Shea, E., Pilpel, Y., and Barkai, N. (2006). Noise in protein expression scales with natural protein abundance. *Nature genetics*, 38(6):636.

[Barteneva et al., 2012] Barteneva, N. S., Fasler-Kan, E., and Vorobjev, I. A. (2012). Imaging flow cytometry: coping with heterogeneity in biological systems. *Journal of Histochemistry & Cytochemistry*, 60(10):723–733.

[Berger, 2002] Berger, S. L. (2002). Histone modifications in transcriptional regulation. *Current opinion in genetics & development*, 12(2):142–148.

[Berger et al., 2009] Berger, S. L., Kouzarides, T., Shiekhattar, R., and Shilatifard, A. (2009). An operational definition of epigenetics. *Genes & development*, 23(7):781–783.

[Bi and Park, 2012] Bi, E. and Park, H.-O. (2012). Cell polarization and cytokinesis in budding yeast. *Genetics*, 191(2):347–387.

[Bi and Pringle, 1996] Bi, E. and Pringle, J. R. (1996). Zds1 and zds2, genes whose products may regulate cdc42p in saccharomyces cerevisiae. *Molecular and Cellular Biology*, 16(10):5264–5275.

[Blake et al., 2003] Blake, W. J., Kærn, M., Cantor, C. R., and Collins, J. J. (2003). Noise in eukaryotic gene expression. *Nature*, 422(6932):633.

[Bose et al., 2001] Bose, I., Irazoqui, J. E., Moskow, J. J., Bardes, E. S., Zyla, T. R., and Lew, D. J. (2001). Assembly of scaffold-mediated complexes containing cdc42p, the exchange factor cdc24p, and the effector cla4p required for cell cycle-regulated phosphorylation of cdc24p. *Journal of Biological Chemistry*, 276(10):7176–7186.

[Bryan et al., 2010] Bryan, A. K., Goranov, A., Amon, A., and Manalis, S. R. (2010). Measurement of mass, density, and volume during the cell cycle of yeast. *Proceedings of the National Academy of Sciences*, 107(3):999–1004.

[Capuano et al., 2014] Capuano, F., Mulleder, M., Kok, R., Blom, H. J., and Ralser, M. (2014). Cytosine dna methylation is found in drosophila melanogaster but absent in saccharomyces cerevisiae, schizosaccharomyces pombe, and other yeast species. *Analytical chemistry*, 86(8):3697–3702.

[Caviston et al., 2002] Caviston, J. P., Tcheperegine, S. E., and Bi, E. (2002). Singularity in budding: a role for the evolutionarily conserved small gtpase cdc42p. *Proceedings of the National Academy of Sciences*, 99(19):12185–12190.

[Chant and Pringle, 1995] Chant, J. and Pringle, J. R. (1995). Patterns of bud-site selection in the yeast saccharomyces cerevisiae. *The Journal of cell biology*, 129(3):751–765.

[Cheffings et al., 2016] Cheffings, T. H., Burroughs, N. J., and Balasubramanian, M. K. (2016). Actomyosin ring formation and tension generation in eukaryotic cytokinesis. *Current Biology*, 26(15):R719–R737.

[Chen et al., 1997] Chen, G.-C., Kim, Y.-J., and Chan, C. S. (1997). The cdc42 gtpase-associated proteins gic1 and gic2 are required for polarized cell growth in saccharomyces cerevisiae. *Genes & Development*, 11(22):2958–2971.

[Chen et al., 2012] Chen, H., Kuo, C.-C., Kang, H., Howell, A. S., Zyla, T. R., Jin, M., and Lew, D. J. (2012). Cdc42p regulation of the yeast formin bni1p mediated by the effector gic2p. *Molecular biology of the cell*, 23(19):3814–3826.

[Chiou et al., 2017] Chiou, J.-g., Balasubramanian, M. K., and Lew, D. J. (2017). Cell polarity in yeast. *Annual review of cell and developmental biology*, 33:77–101.

[Christiano et al., 2014] Christiano, R., Nagaraj, N., Fröhlich, F., and Walther, T. C. (2014). Global proteome turnover analyses of the yeasts s. cerevisiae and s. pombe. *Cell reports*, 9(5):1959–1965.

[Coffman and Wu, 2012] Coffman, V. C. and Wu, J.-Q. (2012). Counting protein molecules using quantitative fluorescence microscopy. *Trends in biochemical sciences*, 37(11):499–506.

[Cookson et al., 2009] Cookson, N. A., Cookson, S. W., Tsimring, L. S., and Hasty, J. (2009). Cell cycle-dependent variations in protein concentration. *Nucleic acids research*, 38(8):2676–2681.

[Cvrckova et al., 1995] Cvrckova, F., De Virgilio, C., Manser, E., Pringle, J. R., and Nasmyth, K. (1995). Ste20-like protein kinases are required for normal localization of cell growth and for cytokinesis in budding yeast. *Genes & development*, 9(15):1817–1830.

[Drees et al., 1995] Drees, B., Brown, C., Barrell, B. G., and Bretscher, A. (1995). Tropomyosin is essential in yeast, yet the tpm1 and tpm2 products perform distinct functions. *The Journal of cell biology*, 128(3):383–392.

[Elowitz et al., 2002] Elowitz, M. B., Levine, A. J., Siggia, E. D., and Swain, P. S. (2002). Stochastic gene expression in a single cell. *Science*, 297(5584):1183–1186.

[Evangelista et al., 1997] Evangelista, M., Blundell, K., Longtine, M. S., Chow, C. J., Adames, N., Pringle, J. R., Peter, M., and Boone, C. (1997). Bni1p, a yeast formin linking cdc42p and the actin cytoskeleton during polarized morphogenesis. *Science*, 276(5309):118–122.

[Evangelista et al., 2002] Evangelista, M., Pruyne, D., Amberg, D. C., Boone, C., and Bretscher, A. (2002). Formins direct arp2/3-independent actin filament assembly to polarize cell growth in yeast. *Nature cell biology*, 4(1):32.

[Florian et al., 2012] Florian, M. C., Dörr, K., Niebel, A., Daria, D., Schrezenmeier, H., Rojewski, M., Filippi, M.-D., Hasenberg, A., Gunzer, M., Scharffetter-Kochanek, K., et al. (2012). Cdc42 activity regulates hematopoietic stem cell aging and rejuvenation. *Cell stem cell*, 10(5):520–530.

[France et al., 2006] France, Y. E., Boyd, C., Coleman, J., and Novick, P. J. (2006). The polarity-establishment component bem1p interacts with the exocyst complex through the sec15p subunit. *Journal of cell science*, 119(5):876–888.

[Freisinger et al., 2013] Freisinger, T., Klünder, B., Johnson, J., Müller, N., Pichler, G., Beck, G., Costanzo, M., Boone, C., Cerione, R. A., Frey, E., et al. (2013). Establishment of a robust single axis of cell polarity by coupling multiple positive feedback loops. *Nature communications*, 4:1807.

[Friedman et al., 2006] Friedman, N., Cai, L., and Xie, X. S. (2006). Linking stochastic dynamics to population distribution: an analytical framework of gene expression. *Physical review letters*, 97(16):168302.

[Geiger and Zheng, 2013] Geiger, H. and Zheng, Y. (2013). Cdc42 and aging of hematopoietic stem cells. *Current opinion in hematology*, 20(4):295.

[Ghaemmaghami et al., 2003] Ghaemmaghami, S., Huh, W.-K., Bower, K., Howson, R. W., Belle, A., Dephoure, N., O'shea, E. K., and Weissman, J. S. (2003). Global analysis of protein expression in yeast. *Nature*, 425(6959):737.

[Glock and Schwille, 2018] Glock, P. and Schwille, P. (2018). Switching protein patterns on membranes. *Current Opinion in Colloid & Interface Science*.

[Goode et al., 2015] Goode, B. L., Eskin, J. A., and Wendland, B. (2015). Actin and endocytosis in budding yeast. *Genetics*, 199(2):315–358.

[Goryachev and Leda, 2017] Goryachev, A. B. and Leda, M. (2017). Many roads to symmetry breaking: molecular mechanisms and theoretical models of yeast cell polarity. *Molecular biology of the cell*, 28(3):370–380.

[Gruenert and Cozens, 1991] Gruenert, D. C. and Cozens, A. L. (1991). Inheritance of phenotype in mammalian cells: genetic vs. epigenetic mechanisms. *American Journal of Physiology-Lung Cellular and Molecular Physiology*, 260(6):L386–L394.

[Grunstein, 1997] Grunstein, M. (1997). Histone acetylation in chromatin structure and transcription. *Nature*, 389(6649):349.

[Gulli et al., 2000] Gulli, M.-P., Jaquenoud, M., Shimada, Y., Niederhäuser, G., Wiget, P., and Peter, M. (2000). Phosphorylation of the cdc42 exchange factor cdc24 by the pak-like kinase cla4 may regulate polarized growth in yeast. *Molecular cell*, 6(5):1155–1167.

[Han et al., 2016] Han, Y., Gu, Y., Zhang, A. C., and Lo, Y.-H. (2016). Imaging technologies for flow cytometry. *Lab on a Chip*, 16(24):4639–4647.

[Harris and Tepass, 2010] Harris, K. P. and Tepass, U. (2010). Cdc42 and vesicle trafficking in polarized cells. *Traffic*, 11(10):1272–1279.

[Heard and Martienssen, 2014] Heard, E. and Martienssen, R. A. (2014). Transgenerational epigenetic inheritance: myths and mechanisms. *Cell*, 157(1):95–109.

[Hirsch et al., 2001] Hirsch, D. S., Pirone, D. M., and Burbelo, P. D. (2001). A new family of cdc42 effector proteins, ceps, function in fibroblast and epithelial cell shape changes. *Journal of Biological Chemistry*, 276(2):875–883.

[Ho et al., 2018] Ho, B., Baryshnikova, A., and Brown, G. W. (2018). Unification of protein abundance datasets yields a quantitative saccharomyces cerevisiae proteome. *Cell systems*, 6(2):192–205.

[Howell et al., 2012] Howell, A. S., Jin, M., Wu, C.-F., Zyla, T. R., Elston, T. C., and Lew, D. J. (2012). Negative feedback enhances robustness in the yeast polarity establishment circuit. *Cell*, 149(2):322–333.

[Howell and Lew, 2012] Howell, A. S. and Lew, D. J. (2012). Morphogenesis and the cell cycle. *Genetics*, 190(1):51–77.

[Huang et al., 2013] Huang, C., Xu, M., and Zhu, B. (2013). Epigenetic inheritance mediated by histone lysine methylation: maintaining transcriptional states without the precise restoration of marks? *Philosophical Transactions of the Royal Society B: Biological Sciences*, 368(1609):20110332.

[Huckaba et al., 2004] Huckaba, T. M., Gay, A. C., Pantalena, L. F., Yang, H.-C., and Pon, L. A. (2004). Live cell imaging of the assembly, disassembly, and actin cable–dependent movement of endosomes and actin patches in the budding yeast, saccharomyces cerevisiae. *J Cell Biol*, 167(3):519–530.

[Irazoqui et al., 2005] Irazoqui, J. E., Howell, A. S., Theesfeld, C. L., and Lew, D. J. (2005). Opposing roles for actin in cdc42p polarization. *Molecular biology of the cell*, 16(3):1296–1304.

[Joglekar et al., 2008] Joglekar, A. P., Salmon, E., and Bloom, K. S. (2008). Counting kinetochore protein numbers in budding yeast using genetically encoded fluorescent proteins. *Methods in cell biology*, 85:127–151.

[Johnson, 1999] Johnson, D. I. (1999). Cdc42: an essential rho-type gtpase controlling eukaryotic cell polarity. *Microbiol. Mol. Biol. Rev.*, 63(1):54–105.

[Johnson and Pringle, 1990] Johnson, D. I. and Pringle, J. R. (1990). Molecular characterization of cdc42, a saccharomyces cerevisiae gene involved in the development of cell polarity. *The Journal of cell biology*, 111(1):143–152.

[Johnson et al., 2009] Johnson, J. L., Erickson, J. W., and Cerione, R. A. (2009). New insights into how the rho guanine nucleotide dissociation inhibitor regulates the interaction of cdc42 with membranes. *Journal of biological chemistry*, 284(35):23860–23871.

[Johnston et al., 1979] Johnston, G., Ehrhardt, C., Lorincz, A., and Carter, B. (1979). Regulation of cell size in the yeast saccharomyces cerevisiae. *Journal of bacteriology*, 137(1):1–5.

[Kaeberlein et al., 2005] Kaeberlein, M., Powers, R. W., Steffen, K. K., Westman, E. A., Hu, D., Dang, N., Kerr, E. O., Kirkland, K. T., Fields, S., and Kennedy, B. K. (2005). Regulation of yeast replicative life span by tor and sch9 in response to nutrients. *Science*, 310(5751):1193–1196.

[Kaksonen et al., 2003] Kaksonen, M., Sun, Y., and Drubin, D. G. (2003). A pathway for association of receptors, adaptors, and actin during endocytic internalization. *Cell*, 115(4):475–487.

[Kamei et al., 1998] Kamei, T., Tanaka, K., Hihara, T., Umikawa, M., Imamura, H., Kikyo, M., Ozaki, K., and Takai, Y. (1998). Interaction of bnr1p with a novel src homology 3 domain-containing hof1p implication in cytokinesis in saccharomyces cerevisiae. *Journal of Biological Chemistry*, 273(43):28341–28345.

[Kang et al., 2014] Kang, P. J., Lee, M. E., and Park, H.-O. (2014). Bud3 activates cdc42 to establish a proper growth site in budding yeast. *J Cell Biol*, 206(1):19–28.

[Kang et al., 2018] Kang, P. J., Miller, K. E., Guegueniat, J., Beven, L., and Park, H.-O. (2018). The shared role of the rsr1 gtpase and gic1/gic2 in cdc42 polarization. *Molecular biology of the cell*, 29(20):2359–2369.

[Karpova et al., 1998] Karpova, T. S., McNally, J. G., Moltz, S. L., and Cooper, J. A. (1998). Assembly and function of the actin cytoskeleton of yeast: relationships between cables and patches. *The Journal of cell biology*, 142(6):1501–1517.

[Kerber et al., 2009] Kerber, R. A., O'Brien, E., and Cawthon, R. M. (2009). Gene expression profiles associated with aging and mortality in humans. *Aging cell*, 8(3):239–250.

[Klünder et al., 2013] Klünder, B., Freisinger, T., Wedlich-Söldner, R., and Frey, E. (2013). Gdi-mediated cell polarization in yeast provides precise spatial and temporal control of cdc42 signaling. *PLoS computational biology*, 9(12):e1003396.

[Knaus et al., 2007] Knaus, M., Pelli-Gulli, M.-P., Van Drogen, F., Springer, S., Jaquenoud, M., and Peter, M. (2007). Phosphorylation of bem2p and bem3p may contribute to local activation of cdc42p at bud emergence. *The EMBO journal*, 26(21):4501–4513.

[Koch et al., 1997] Koch, G., Tanaka, K., Masuda, T., Yamochi, W., Nonaka, H., and Takai, Y. (1997). Association of the rho family small gtp-binding proteins with rho gdp dissociation inhibitor (rho gdi) in saccharomyces cerevisiae. *Oncogene*, 15(4):417.

[Kozminski and Park, 2010] Kozminski, K. G. and Park, H.-O. (2010). Yeast small g-protein function: Molecular basis of cell polarity in yeast. In *Handbook of Cell Signaling*, pages 1813–1817. Elsevier.

[Kozubowski et al., 2008] Kozubowski, L., Saito, K., Johnson, J. M., Howell, A. S., Zyla, T. R., and Lew, D. J. (2008). Symmetry-breaking polarization driven by a cdc42p gef-pak complex. *Current Biology*, 18(22):1719–1726.

[Krogan et al., 2003] Krogan, N. J., Kim, M., Tong, A., Golshani, A., Cagney, G., Canadien, V., Richards, D. P., Beattie, B. K., Emili, A., Boone, C., et al. (2003). Methylation of histone h3 by set2 in saccharomyces cerevisiae is linked to transcriptional elongation by rna polymerase ii. *Molecular and cellular biology*, 23(12):4207–4218.

[Kulak et al., 2014] Kulak, N. A., Pichler, G., Paron, I., Nagaraj, N., and Mann, M. (2014). Minimal, encapsulated proteomic-sample processing applied to copy-number estimation in eukaryotic cells. *Nature methods*, 11(3):319.

[Kuo et al., 2014] Kuo, C.-C., Savage, N. S., Chen, H., Wu, C.-F., Zyla, T. R., and Lew, D. J. (2014). Inhibitory gef phosphorylation provides negative feedback in the yeast polarity circuit. *Current Biology*, 24(7):753–759.

[Kussell and Leibler, 2005] Kussell, E. and Leibler, S. (2005). Phenotypic diversity, population growth, and information in fluctuating environments. *Science*, 309(5743):2075–2078.

[Laan et al., 2015] Laan, L., Koschwanez, J. H., and Murray, A. W. (2015). Evolutionary adaptation after crippling cell polarization follows reproducible trajectories. *Elife*, 4:e09638.

[Lahtvee et al., 2017] Lahtvee, P.-J., Sánchez, B. J., Smialowska, A., Kasvandik, S., Elsemman, I. E., Gatto, F., and Nielsen, J. (2017). Absolute quantification of protein and mrna abundances demonstrate variability in gene-specific translation efficiency in yeast. *Cell systems*, 4(5):495–504.

[Lai et al., 2018] Lai, H., Chiou, J.-G., Zhurikhina, A., Zyla, T. R., Tsygankov, D., and Lew, D. J. (2018). Temporal regulation of morphogenetic events in saccharomyces cerevisiae. *Molecular biology of the cell*, 29(17):2069–2083.

[Lawless et al., 2016] Lawless, C., Holman, S. W., Brownridge, P., Lanthaler, K., Harman, V. M., Watkins, R., Hammond, D. E., Miller, R. L., Sims, P. F., Grant, C. M., et al. (2016). Direct and absolute quantification of over 1800 yeast proteins via selected reaction monitoring. *Molecular & Cellular Proteomics*, 15(4):1309–1322.

[Lee et al., 2015] Lee, M. E., Lo, W.-C., Miller, K. E., Chou, C.-S., and Park, H.-O. (2015). Regulation of cdc42 polarization by the rsr1 gtpase and rga1, a cdc42 gtpase-activating protein, in budding yeast. *J Cell Sci*, 128(11):2106–2117.

[Levy et al., 2012] Levy, S. F., Ziv, N., and Siegal, M. L. (2012). Bet hedging in yeast by heterogeneous, age-correlated expression of a stress protectant. *PLoS biology*, 10(5):e1001325.

[Li and Wedlich-Soldner, 2009] Li, R. and Wedlich-Soldner, R. (2009). Bem1 complexes and the complexity of yeast cell polarization. *Current Biology*, 19(5):R194–R195.

[Liu and Novick, 2014] Liu, D. and Novick, P. (2014). Bem1p contributes to secretory pathway polarization through a direct interaction with exo70p. *J Cell Biol*, 207(1):59–72.

[Liu and Bretscher, 1992] Liu, H. and Bretscher, A. (1992). Characterization of tpm1 disrupted yeast cells indicates an involvement of tropomyosin in directed vesicular transport. *The Journal of cell biology*, 118(2):285–299.

[Marco et al., 2007] Marco, E., Wedlich-Soldner, R., Li, R., Altschuler, S. J., and Wu, L. F. (2007). Endocytosis optimizes the dynamic localization of membrane proteins that regulate cortical polarity. *Cell*, 129(2):411–422.

[Martin, 2015] Martin, S. G. (2015). Spontaneous cell polarization: feedback control of cdc42 gtpase breaks cellular symmetry. *Bioessays*, 37(11):1193–1201.

[Miller and Park, 2019] Miller, K. E. and Park, H.-O. (2019). Temporal regulation of cell polarity via the interaction of the ras gtpase rsr1 and the scaffold protein bem1. *bioRxiv*, page 554105.

[Miller and Johnson, 1997] Miller, P. J. and Johnson, D. I. (1997). Characterization of the saccharomyces cerevisiae cdc42-1ts allele and new temperature-conditional-lethal cdc42 alleles. *Yeast*, 13(6):561–572.

[Milo, 2013] Milo, R. (2013). What is the total number of protein molecules per cell volume? a call to rethink some published values. *Bioessays*, 35(12):1050–1055.

[Mishra et al., 2014] Mishra, M., Huang, J., and Balasubramanian, M. K. (2014). The yeast actin cytoskeleton. *FEMS microbiology reviews*, 38(2):213–227.

[Model and Burkhardt, 2001] Model, M. A. and Burkhardt, J. K. (2001). A standard for calibration and shading correction of a fluorescence microscope. *Cytometry: The Journal of the International Society for Analytical Cytology*, 44(4):309–316.

[Moran et al., 2019] Moran, K. D., Kang, H., Araujo, A. V., Zyla, T. R., Saito, K., Tsygankov, D., and Lew, D. J. (2019). Cell-cycle control of cell polarity in yeast. *J Cell Biol*, 218(1):171–189.

[Moran et al., 2010] Moran, U., Phillips, R., and Milo, R. (2010). Snapshot: key numbers in biology. *Cell*, 141(7):1262–1262.

[Moseley and Goode, 2006] Moseley, J. B. and Goode, B. L. (2006). The yeast actin cytoskeleton: from cellular function to biochemical mechanism. *Microbiol. Mol. Biol. Rev.*, 70(3):605–645.

[Munemitsu et al., 1990] Munemitsu, S., Innis, M., Clark, R., McCormick, F., Ullrich, A., and Polakis, P. (1990). Molecular cloning and expression of a g25k cdna, the human homolog of the yeast cell cycle gene cdc42. *Molecular and cellular biology*, 10(11):5977–5982.

[Murray et al., 2007] Murray, J. M., Appleton, P. L., Swedlow, J. R., and Waters, J. C. (2007). Evaluating performance in three-dimensional fluorescence microscopy. *Journal of microscopy*, 228(3):390–405.

[Nagy et al., 2002] Nagy, P. L., Griesenbeck, J., Kornberg, R. D., and Cleary, M. L. (2002). A trithorax-group complex purified from saccharomyces cerevisiae is required for methylation of histone h3. *Proceedings of the national academy of sciences*, 99(1):90–94.

[Newman et al., 2006] Newman, J. R., Ghaemmaghami, S., Ihmels, J., Breslow, D. K., Noble, M., DeRisi, J. L., and Weissman, J. S. (2006). Single-cell proteomic analysis of s. cerevisiae reveals the architecture of biological noise. *Nature*, 441(7095):840.

[Norden et al., 2004] Norden, C., Liakopoulos, D., and Barral, Y. (2004). Dissection of septin actin interactions using actin overexpression in saccharomyces cerevisiae. *Molecular microbiology*, 53(2):469–483.

[Okada et al., 2013] Okada, S., Leda, M., Hanna, J., Savage, N. S., Bi, E., and Goryachev, A. B. (2013). Daughter cell identity emerges from the interplay of cdc42, septins, and exocytosis. *Developmental cell*, 26(2):148–161.

[O'Shea and Herskowitz, 2000] O'Shea, E. K. and Herskowitz, I. (2000). The ins and outs of cell-polarity decisions. *Nature cell biology*, 2(3):E39.

[Ozbudak et al., 2005] Ozbudak, E. M., Becskei, A., and van Oudenaarden, A. (2005). A system of counteracting feedback loops regulates cdc42p activity during spontaneous cell polarization. *Developmental cell*, 9(4):565–571.

[Ozbudak et al., 2002] Ozbudak, E. M., Thattai, M., Kurtser, I., Grossman, A. D., and Van Oudenaarden, A. (2002). Regulation of noise in the expression of a single gene. *Nature genetics*, 31(1):69.

[Perez and Rincón, 2010] Perez, P. and Rincón, S. A. (2010). Rho gtpases: regulation of cell polarity and growth in yeasts. *Biochemical Journal*, 426(3):243–253.

[Pillus and Rine, 1989] Pillus, L. and Rine, J. (1989). Epigenetic inheritance of transcriptional states in s. cerevisiae. *Cell*, 59(4):637–647.

[Pruyne and Bretscher, 2000] Pruyne, D. and Bretscher, A. (2000). Polarization of cell growth in yeast. *J Cell Sci*, 113(4):571–585.

[Pruyne et al., 2004] Pruyne, D., Gao, L., Bi, E., and Bretscher, A. (2004). Stable and dynamic axes of polarity use distinct formin isoforms in budding yeast. *Molecular biology of the cell*, 15(11):4971–4989.

[Pruyne et al., 1998] Pruyne, D. W., Schott, D. H., and Bretscher, A. (1998). Tropomyosin-containing actin cables direct the myo2p-dependent polarized delivery of secretory vesicles in budding yeast. *J Cell Biol*, 143(7):1931–1945.

[Rodrıguez-Pachón et al., 2002] Rodrıguez-Pachón, J. M., Martın, H., North, G., Rotger, R., Nombela, C., and Molina, M. (2002). A novel connection between the yeast cdc42 gtpase and the slt2-mediated cell integrity pathway identified through the effect of secreted salmonella gtpase modulators. *Journal of Biological Chemistry*, 277(30):27094–27102.

[Sanders and Herskowitz, 1996] Sanders, S. L. and Herskowitz, I. (1996). The bud4 protein of yeast, required for axial budding, is localized to the mother/bud neck in a cell cycle-dependent manner. *The Journal of Cell Biology*, 134(2):413–427.

[Schenkman et al., 2002] Schenkman, L. R., Caruso, C., Pagé, N., and Pringle, J. R. (2002). The role of cell cycle–regulated expression in the localization of spatial landmark proteins in yeast. *The Journal of cell biology*, 156(5):829–841.

[Schulz et al., 2013] Schulz, O., Pieper, C., Clever, M., Pfaff, J., Ruhlandt, A., Kehlenbach, R. H., Wouters, F. S., Großhans, J., Bunt, G., and Enderlein, J. (2013). Resolution doubling in fluorescence microscopy with confocal spinning-disk image scanning microscopy. *Proceedings of the National Academy of Sciences*, 110(52):21000–21005.

[Shahrezaei and Swain, 2008] Shahrezaei, V. and Swain, P. S. (2008). Analytical distributions for stochastic gene expression. *Proceedings of the National Academy of Sciences*, 105(45):17256–17261.

[Shaw, 2006] Shaw, P. J. (2006). Comparison of widefield/deconvolution and confocal microscopy for three-dimensional imaging. In *Handbook of biological confocal microscopy*, pages 453–467. Springer.

[Sherman, 2002] Sherman, F. (2002). Getting started with yeast. In *Methods in enzymology*, volume 350, pages 3–41. Elsevier.

[Sibarita, 2005] Sibarita, J.-B. (2005). Deconvolution microscopy. In *Microscopy Techniques*, pages 201–243. Springer.

[Slaughter et al., 2009] Slaughter, B. D., Das, A., Schwartz, J. W., Rubinstein, B., and Li, R. (2009). Dual modes of cdc42 recycling fine-tune polarized morphogenesis. *Developmental cell*, 17(6):823–835.

[Slaughter et al., 2013] Slaughter, B. D., Unruh, J. R., Das, A., Smith, S. E., Rubinstein, B., and Li, R. (2013). Non-uniform membrane diffusion enables steady-state cell polarization via vesicular trafficking. *Nature communications*, 4:1380.

[Smith et al., 2013] Smith, S. E., Rubinstein, B., Pinto, I. M., Slaughter, B. D., Unruh, J. R., and Li, R. (2013). Independence of symmetry breaking on bem1-mediated autocatalytic activation of cdc42. *J Cell Biol*, 202(7):1091–1106.

[Stengel and Zheng, 2011] Stengel, K. and Zheng, Y. (2011). Cdc42 in oncogenic transformation, invasion, and tumorigenesis. *Cellular signalling*, 23(9):1415–1423.

[Stevenson et al., 1995] Stevenson, B. J., Ferguson, B., De Virgilio, C., Bi, E., Pringle, J. R., Ammerer, G., and Sprague, G. F. (1995). Mutation of rga1, which encodes a putative gtpase-activating protein for the polarity-establishment protein cdc42p, activates the pheromone-response pathway in the yeast saccharomyces cerevisiae. *Genes & development*, 9(23):2949–2963.

[Sun and Allis, 2002] Sun, Z.-W. and Allis, C. D. (2002). Ubiquitination of histone h2b regulates h3 methylation and gene silencing in yeast. *Nature*, 418(6893):104.

[Tcheperegine et al., 2005] Tcheperegine, S. E., Gao, X.-D., and Bi, E. (2005). Regulation of cell polarity by interactions of msb3 and msb4 with cdc42 and polarisome components. *Molecular and cellular biology*, 25(19):8567–8580.

[Thorn, 2010] Thorn, K. (2010). Spinning-disk confocal microscopy of yeast. In *Methods in enzymology*, volume 470, pages 581–602. Elsevier.

[Toenjes et al., 1999] Toenjes, K. A., Sawyer, M. M., and Johnson, D. I. (1999). The guanine-nucleotide-exchange factor cdc24p is targeted to the nucleus and polarized growth sites. *Current biology*, 9(20):1183–S1.

[Tomaževič et al., 2002] Tomaževič, D., Likar, B., and Pernuš, F. (2002). Comparative evaluation of retrospective shading correction methods. *Journal of microscopy*, 208(3):212–223.

[Tong et al., 2007] Tong, Z., Gao, X.-D., Howell, A. S., Bose, I., Lew, D. J., and Bi, E. (2007). Adjacent positioning of cellular structures enabled by a cdc42 gtpase-activating protein–mediated zone of inhibition. *J Cell Biol*, 179(7):1375–1384.

[Vega and Ridley, 2008] Vega, F. M. and Ridley, A. J. (2008). Rho gtpases in cancer cell biology. *FEBS letters*, 582(14):2093–2101.

[Wai et al., 2009] Wai, S. C., Gerber, S. A., and Li, R. (2009). Multisite phosphorylation of the guanine nucleotide exchange factor cdc24 during yeast cell polarization. *PloS one*, 4(8):e6563.

[Walworth et al., 1992] Walworth, N. C., Brennwald, P., Kabcenell, A., Garrett, M., and Novick, P. (1992). Hydrolysis of gtp by sec4 protein plays an important role in vesicular transport and is stimulated by a gtpase-activating protein in saccharomyces cerevisiae. *Molecular and Cellular Biology*, 12(5):2017–2028.

[Watson et al., 2014] Watson, L. J., Rossi, G., and Brennwald, P. (2014). Quantitative analysis of membrane trafficking in regulation of cdc42 polarity. *Traffic*, 15(12):1330–1343.

[Wedlich-Soldner et al., 2003] Wedlich-Soldner, R., Altschuler, S., Wu, L., and Li, R. (2003). Spontaneous cell polarization through actomyosin-based delivery of the cdc42 gtpase. *Science*, 299(5610):1231–1235.

[Wedlich-Soldner and Li, 2003] Wedlich-Soldner, R. and Li, R. (2003). Spontaneous cell polarization: undermining determinism. *Nature cell biology*, 5(4):267.

[Wedlich-Soldner et al., 2004] Wedlich-Soldner, R., Wai, S. C., Schmidt, T., and Li, R. (2004). Robust cell polarity is a dynamic state established by coupling transport and gtpase signaling. *J Cell Biol*, 166(6):889–900.

[Weinert et al., 2014] Weinert, B. T., Iesmantavicius, V., Moustafa, T., Schölz, C., Wagner, S. A., Magnes, C., Zechner, R., and Choudhary, C. (2014). Acetylation dynamics and stoichiometry in saccharomyces cerevisiae. *Molecular systems biology*, 10(1).

[Weiss et al., 2000] Weiss, E. L., Bishop, A. C., Shokat, K. M., and Drubin, D. G. (2000). Chemical genetic analysis of the budding-yeast p21-activated kinase cla4p. *Nature cell biology*, 2(10):677.

[Witte et al., 2017] Witte, K., Strickland, D., and Glotzer, M. (2017). Cell cycle entry triggers a switch between two modes of cdc42 activation during yeast polarization. *Elife*, 6:e26722.

[Woods et al., 2016] Woods, B., Lai, H., Wu, C.-F., Zyla, T. R., Savage, N. S., and Lew, D. J. (2016). Parallel actin-independent recycling pathways polarize cdc42 in budding yeast. *Current Biology*, 26(16):2114–2126.

[Wu et al., 2013] Wu, C.-F., Savage, N. S., and Lew, D. J. (2013). Interaction between bud-site selection and polarity-establishment machineries in budding yeast. *Philosophical Transactions of the Royal Society B: Biological Sciences*, 368(1629):20130006.

[Xue and Leibler, 2016] Xue, B. and Leibler, S. (2016). Evolutionary learning of adaptation to varying environments through a transgenerational feedback. *Proceedings of the National Academy of Sciences*, 113(40):11266–11271.

[Yamamoto et al., 2010] Yamamoto, T., Mochida, J., Kadota, J., Takeda, M., Bi, E., and Tanaka, K. (2010). Initial polarized bud growth by endocytic recycling in the absence of actin cable–dependent vesicle transport in yeast. *Molecular biology of the cell*, 21(7):1237–1252.

[Yang et al., 2007] Yang, L., Wang, L., Geiger, H., Cancelas, J. A., Mo, J., and Zheng, Y. (2007). Rho gtpase cdc42 coordinates hematopoietic stem cell quiescence and niche interaction in the bone marrow. *Proceedings of the National Academy of Sciences*, 104(12):5091–5096.

[Young et al., 1993] Young, I., Zagers, R., Van Vliet, L., Mullikin, J., Boddeke, F., and Netten, H. (1993). Depth-of-focus in microscopy. In *8th Scandinavian Conference on Image Analysis, Tromso, Norway*. Citeseer.

[Zheng et al., 1995] Zheng, Y., Bender, A., and Cerione, R. A. (1995). Interactions among proteins involved in bud-site selection and bud-site assembly in saccharomyces cerevisiae. *Journal of Biological Chemistry*, 270(2):626–630.

[Ziman and Johnson, 1994] Ziman, M. and Johnson, D. I. (1994). Genetic evidence for a functional interaction between saccharomyces cerevisiae cdc24 and cdc42. *Yeast*, 10(4):463–474.